This document was prepared for the ETI by third parties under contract to the ETI. The ETI is making these documents and data available to the public to inform the debate on low carbon energy innovation and deployment.

Programme Area: Marine

Project: PerAWAT

Title: Influence of Free Surface Waves on the Performance and Wake Structure of a Horizontal Axis Tidal Turbine

Abstract:

This deliverable presents the simulation and analysis of the influence of surface waves on the performance, loading and wake of a marine turbine. A full scale rotor is simulated using three-dimensional Computational Fluid Dynamics (Ansys Fluent) in which the blade resolved rotor is embedded within a rotating sliding mesh. The turbine is subjected to a sheared flow profile, together with waves of varying wave length, wave height and yaw angle. Performance is assessed over a range of tip-speed-ratios.

Context:

The Performance Assessment of Wave and Tidal Array Systems (PerAWaT) project, launched in October 2009 with £8m of ETI investment. The project delivered validated, commercial software tools capable of significantly reducing the levels of uncertainty associated with predicting the energy yield of major wave and tidal stream energy arrays. It also produced information that will help reduce commercial risk of future large scale wave and tidal array developments.

Disclaimer:

The Energy Technologies Institute is making this document available to use under the Energy Technologies Institute Open Licence for Materials. Please refer to the Energy Technologies Institute website for the terms and conditions of this licence. The Information is licensed 'as is' and the Energy Technologies Institute excludes all representations, warranties, obligations and liabilities in relation to the Information to the maximum extent permitted by law. The Energy Technologies Institute is not liable for any errors or omissions in the Information and shall not be liable for any loss, injury or damage of any kind caused by its use. This exclusion of liability includes, but is not limited to, any direct, indirect, special, incidental, consequential, punitive, or exemplary damages in each case such as loss of revenue, data, anticipated profits, and lost business. The Energy Technologies Institute does not guarantee the continued supply of the Information. Notwithstanding any statement to the contrary contained on the face of this document, the Energy Technologies Institute confirms that the authors of the document have consented to its publication by the Energy Technologies Institute.

Energy Technologies Institute

PerAWaT

WG3 WP1 D6: Influence of free surface waves on the performance and wake structure of a horizontal axis tidal turbine

Authors	C. F. Fleming, R. H. J. Willden
Version	1.0
Date	08/12/13

Revision History		
Issue / Version	**Issue Date**	**Summary**
0.1	23/10/13	First draft for review by GH
0.2	25/10/13	Update to first draft
1.0	08/12/13	Final version following review by GH

Executive Summary

This deliverable presents the simulation and analysis of the influence of surface waves on the performance, loading and wake of a marine turbine. A full scale rotor is simulated using three-dimensional Computational Fluid Dynamics (Ansys Fluent) in which the blade resolved rotor is embedded within a rotating sliding mesh. The turbine is subjected to a sheared flow profile, together with waves of varying wave length, wave height and yaw angle. Performance is assessed over a range of tip-speed-ratios. It is found that surface waves have a detrimental effect on the mean power of the turbine, which is reduced by c. 15-20% for the waves considered. Mean thrust is also reduced but to a lesser extent. Blade thrust and power are observed to fluctuate with significant amplitude as the blades rotate (far more so than for the case of shear flow with no waves reported in D4). Blade thrust fluctuates by c. ± 10-20% about its mean value, whilst blade power fluctuates by c. ± 100-200% about its mean value, with blade torque (and thus power) reaching negative values through the rotation cycle depending on the relative phasing of the passing wave to the blade rotation. Surface waves are seen to accelerate the wake recovery process as might be expected due to the wave kinematics increasing the mixing between through-turbine and bypass flows.

Table of Contents

1 Introduction

The objective of this work is to investigate the effect of free surface waves on the performance of a tidal turbine in sheared flow. Certain wave parameters, such as height, length and alignment, are varied in order that their effects may be identified independently.

Relevant details of the D4 model, such as blockage and boundary conditions, are given in section 3. Alterations to this model, some of which have been described already in deliverable D5, are also discussed. Additionally, changes to the wave model used in D5 are also described. These changes were necessary in order to enable simulation of wave motion in combination with sheared flow, and wave propogation at an angle to the streamwise direction.

Subsets of the simulated cases are discussed, highlighting the effects of wave height, length and alignment respectively.

Finally, a standardized presentation of the results for the full set of simulated cases is given in the Appendix.

2 Deliverable objectives

The aim of this deliverable is to examine the influence of free surface waves on the performance, loading and wake structure of a tidal turbine. The computational model developed in deliverables D1 - D4 has been extended in D5 to include a linear wave model. This model is now developed further in D6 to allow combined free surface waves and a sheared velocity profile.

The case of waves aligned with the current direction is then investigated and compared to the case with no waves (Rigid lid base case from D4). A parametric study is then carried out to examine the effect of perturbations on wavelength, wave height and wave alignment on tidal turbine performance.

The near wake model developed in D4 is again used to compare against the present results including the influence of surface waves.

3 Computational model

The Reynolds averaged Navier-Stokes (RANS) equation model presented in D5 had the capacity to model linear free surface waves using an open channel wave boundary condition, which is a built-in feature of ANSYS Fluent v14.5 and is based on the volume of fluid (VOF) method. However, this wave model was found to be incompatible with a sheared velocity profile.

3.1 D4 Model - reference case without waves

The current model is based on case 'C' from deliverable WG3 WP1 D4. This case is a simulation of the D = 18 m diameter PerAWaT turbine in a numerical channel measuring 4D in width and 2D in height. The resulting area blockage is B = 9.8%. Symmetry conditions at the lateral boundaries represent an infinite fence of such turbines with a centre-to-centre spacing of 4D. A symmetry condition is applied at the upper boundary, approximating the free surface as a rigid lid. A bed roughness coefficient of c_f = 0.0035 (corresponding to the lower shear case 'S1' in deliverable D4) is prescribed at the lower boundary of the domain. The effect of this condition is to maintain the sheared velocity profile which is applied at the inlet to the domain.

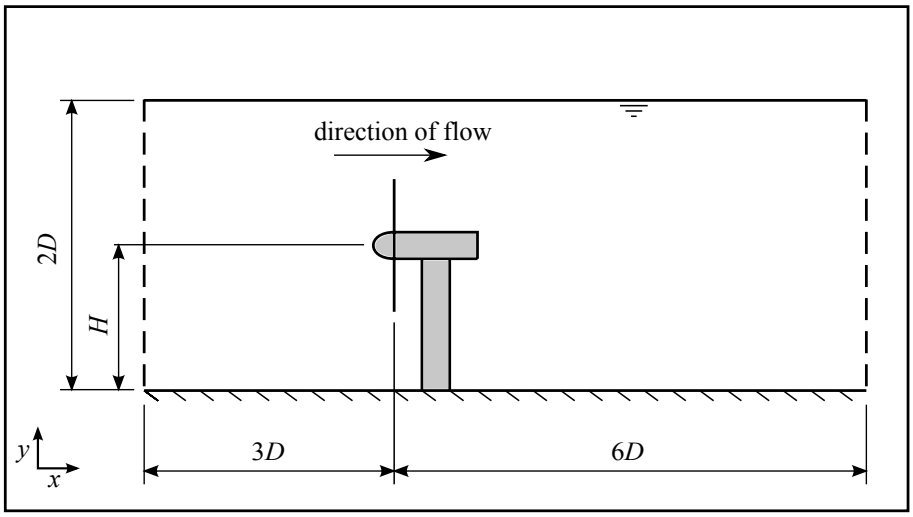

(a)

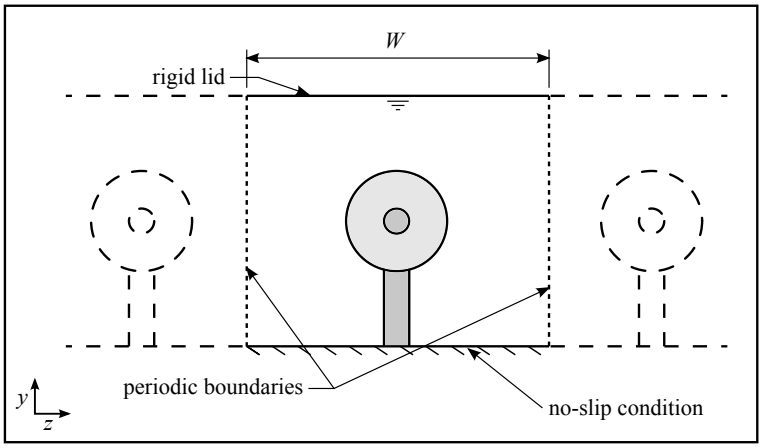

(b)

Figure 1: (a) Elevation and (b) end views of the rigid lid model from deliverable D4.

3.2 Alterations to D4 rigid lid model

The rigid lid model domain has been altered in two ways. Firstly, the domain height has been increased to include a passage for the air above the free surface. Secondly, the domain length has been increased from 6*D* to 14*D* downstream, with the final 4*D* used as a wave absorption zone.

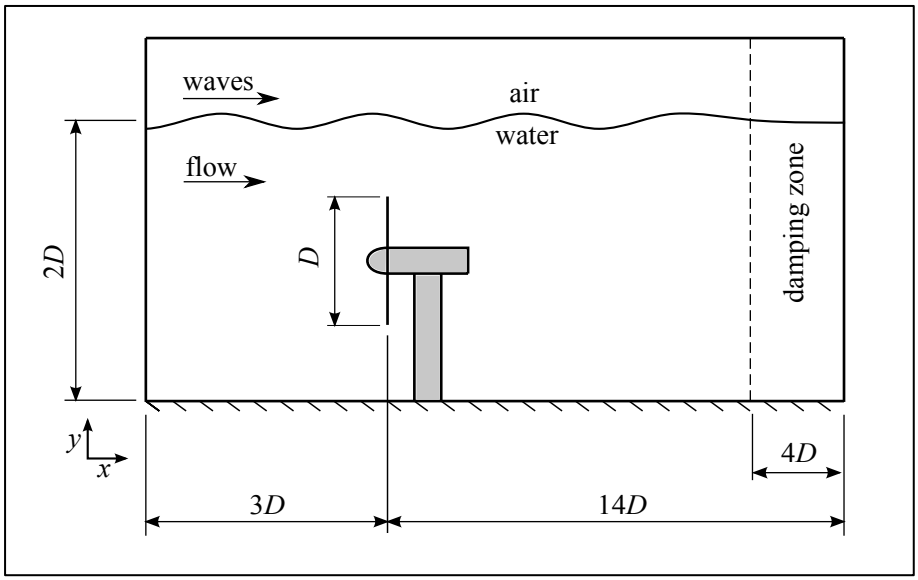

Figure 2: Elevation view of the current computational model.

3.3 Alterations to D5 wave model

To date, the RANS model has been re-worked to combine linear free surface waves with a sheared inlet velocity profile. This is achieved via a user-defined function (UDF) that specifies the following conditions at the inlet:

$$u = \frac{\sigma H}{2}\frac{\cosh(k(y+h))}{\sinh kh}\cos\theta \quad (1)$$

$$v = \frac{\sigma H}{2}\frac{\sinh(k(y+h)}{\sinh kh}\sin\theta \quad (2)$$

where x, z, and y are the streamwise, transverse and vertical directions respectively (with $y = 0$ corresponding to the mean surface elevation), u and v are the streamwise and vertical components of velocity, g is acceleration due to gravity, h is mean water depth, H is wave height, and k is the wave number, defined by $k = 2\pi/\lambda$. The phase angle θ is defined as

$$\theta = kx - \omega t \quad (3)$$

where t is time. ω is the wave frequency with respect to the turbine,

$$\omega = ku_h + \sigma \tag{4}$$

and σ is the wave frequency with respect to the mean flow,

$$\sigma = \sqrt{kg \tanh kh}\,. \tag{5}$$

For accuracy and numerical stability of the wave model, wave motion must be aligned with the computational domain. The relative angle of wave motion to the rotor and current axis is achieved by adjusting the orientation of the rotor within the computational domain as shown in the figure below. Periodicity is applied at the lateral boundaries to enable a mean flow aligned with the turbine axis. Thus the effect of waves aligned at a different angle to the mean flow and turbine axis can be examined.

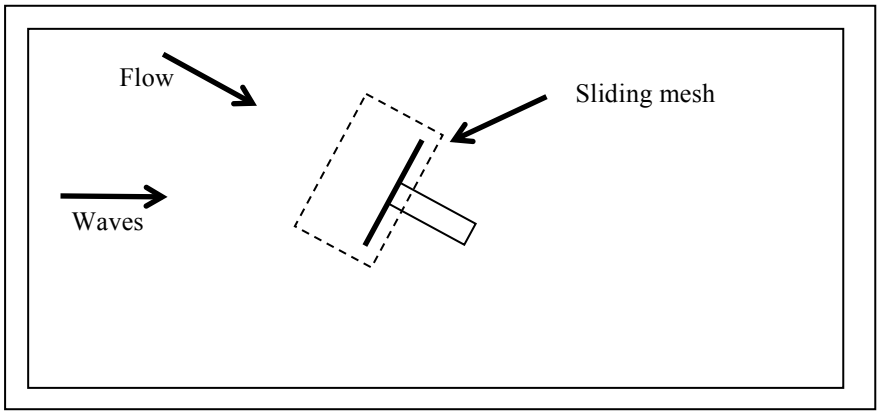

Figure 3: The wave heading angle is adjusted by rotating the turbine geometry within the computational domain. The flow angle is altered to remain aligned with the turbine axis, while the wave direction is aligned with the domain.

4 Parametric Study

A series of simulation cases are chosen to isolate the effects of wavelength, wave height and wave heading. Each case (except the yawed flow case) is run at three tip speed ratios, in order to capture the peak power operating point of the turbine. Details of the simulation cases for this deliverable are tabulated below.

Table 1: Simulation matrix for deliverable D6.

Case	Wavelength, λ_w [m]	Height, H_w [m]	Heading, ϕ_w [˚]	Tip speed ratio, λ
1	55	1	0	3.5
2	55	1	0	4.5
3	55	1	0	5.5
4	100	1	0	3.5
5	100	1	0	4.5
6	100	1	0	5.5
7	55	2	0	3.5
8	55	2	0	4.5
9	55	2	0	5.5
10	55	1	30	4.5

Simulation results for each case are presented in the Appendix. The effect of waves, wave height, wave length and wave direction are examined in the following four sections.

5 Influence of waves

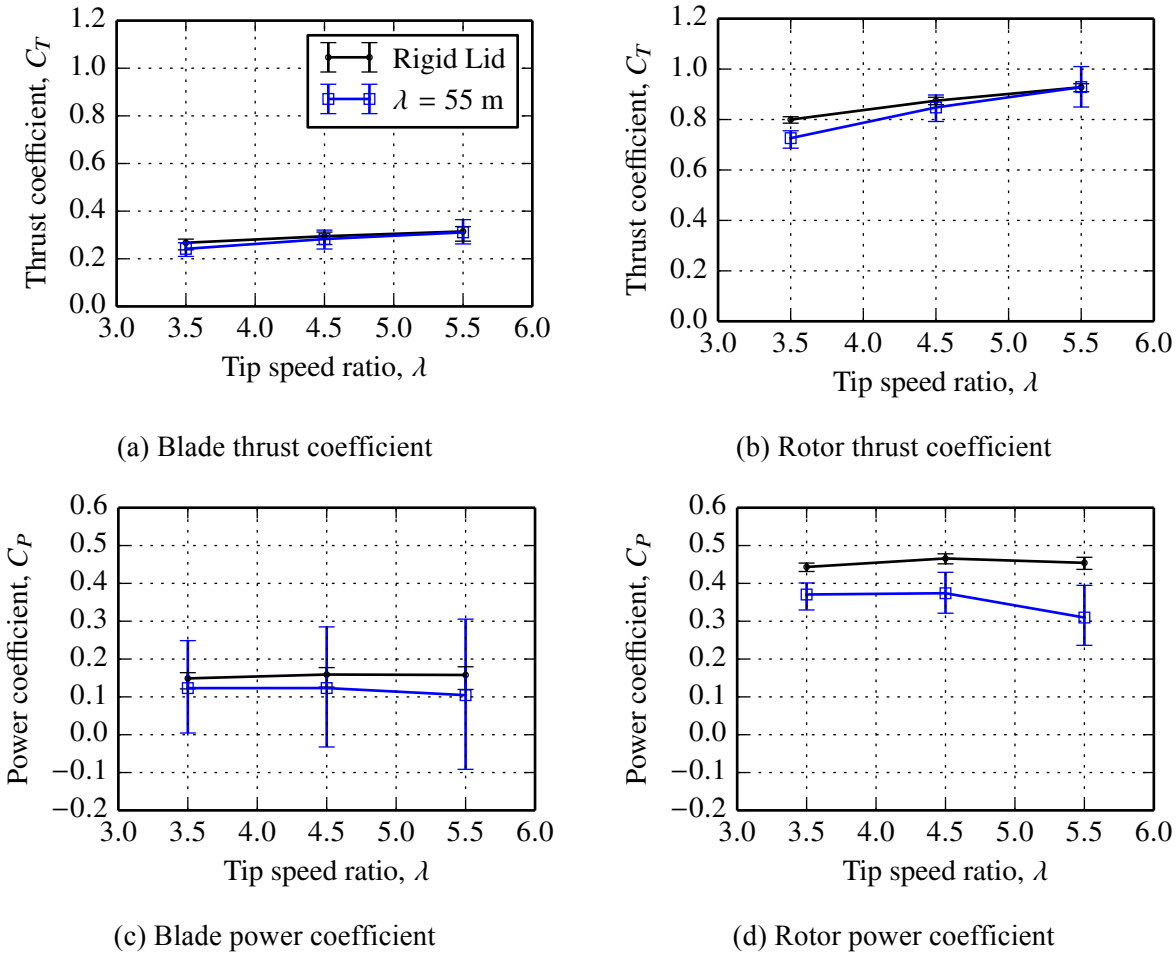

(a) Blade thrust coefficient

(b) Rotor thrust coefficient

(c) Blade power coefficient

(d) Rotor power coefficient

Figure 4: Comparison of thrust and power with and without waves.

We start by recalling from deliverable WG3 WP1 D4 the nature of the loading and performance of the turbine when placed in a sheared onset flow with no surface waves (rigid lid condition). The detailed performance of the turbine is reproduced in section 9 and the turbine's overall performance characteristics are shown in

Figure 4.

The rotor's power curve,
Figure 4(d), takes on the conventional bell shape and we note that, due to the design of the rotor, the power curve is particularly flat across the range of tip-speed-ratios simulated; 3.5 to 5.5. Rotor thrust,

Figure 4(b), increases monotonically with tip-speed-ratio taking a value of $C_T = 0.875$ at the peak power point, $C_P = 0.465$ at $\lambda = 4.5$.

In section 9 we report the thrust and power histories of each rotor blade and for the overall rotor (blade thrust and power coefficients are normalized with the same denominators as overall rotor coefficients and hence can be directly summed to recover the rotor coefficients).

As expected the shear in the flow causes a fluctuation in blade thrust and power at the rotor's rotation frequency; see accompanying spectra. Further the shape of the time fluctuations are such that they have broader crests and sharper troughs. This is due to the nature of the shear profile, $\partial u/\partial y > 0$ but $\partial^2 u/\partial y^2 < 0$, such that the change in the onset flow condition through the blade's upper passage is small (leading to the broad crest), whilst the change in flow condition through the lower passage is large (leading to the deeper and sharper trough). Once the forces on the three blades are summed to give total thrust and torque the resulting thrust and torque ripples are of lower amplitude than those experienced by individual blades. Note also that the frequency of the resulting rotor thrust and power variations is three times the rotor's rotational frequency (see spectra).

The performance, thrust and power coefficient of each rotor blade are also report in

Figure 4(a) & (c). Note that the vertical bars in all subplots of this figure indicate the limits of the fluctuations in the indicated quantity about its mean. The fluctuations in thrust and power are seen to be greater at blade level than at rotor level.

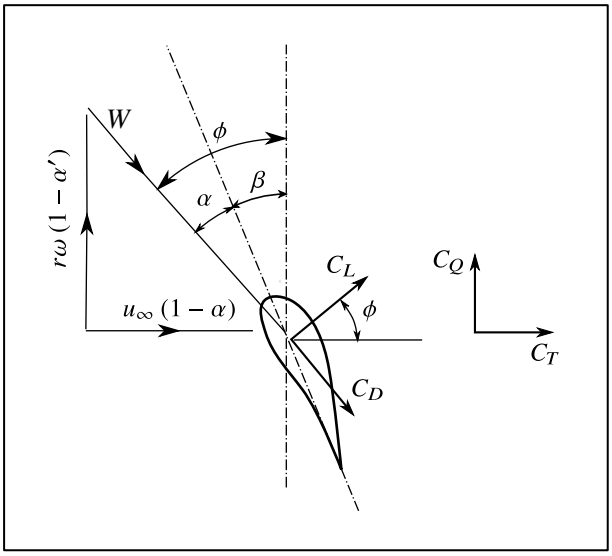

Figure 5: Definition of angles for Blade Element Theory.

Of note is that power fluctuations are greater than thrust fluctuations. This follows from Blade Element Theory (see

Figure 5) in which the sectional circumferential torque, C'_Q, and thrust, C'_T, coefficients are given by:

$$C'_Q = r(C_L \sin\phi - C_D \cos\phi)$$

$$C'_T = C_L \cos\phi + C_D \sin\phi$$

in which C_L and C_D are the hydrofoil's sectional lift and drag coefficients, $\phi = \alpha + \beta$ is the flow angle and α and β the angle of incidence and geometric twist respectively. We wish to consider how the torque and thrust vary as the inflow condition changes as the blade moves

through the shear profile (or as waves passes overhead). The rotor blades will see a changing flow angle, ϕ, as they rotate. We take ϕ to be small and approximate;

$$C_L \approx \frac{\partial C_L}{\partial \alpha}\alpha + C_{L0}$$

$$C_D \approx \bar{C}_D$$

such that;

$$C'_Q \approx r\left(\frac{\partial C_L}{\partial \alpha}[\phi - \beta]\phi + C_{L0}\phi - \bar{C}_D\right)$$

$$C'_T \approx \frac{\partial C_L}{\partial \alpha}[\phi - \beta] + C_{L0} + \bar{C}_D\phi$$

As torque is quadratic in ϕ, whilst thrust is linear in ϕ, we expect fluctuations in ϕ caused by passing through a shear profile (or through the passing of surface waves) to result in larger fluctuations in blade power than in blade thrust.

Figure 4 also includes the performance metrics for the turbine when subjected to the same shear profile as in the rigid lid base case, but with the addition of passing surface waves. The surface waves are of wavelength, $\lambda_w = 55$ m, wave height, $H_w = 1$ m, and are aligned with the current direction, $\phi_w = 0°$. This case is referred to as the wave base case. Additional blade and rotor thrust and power histories and spectra and given in section 10.1.

The addition of waves is seen to have a modest effect on blade and rotor thrust coefficient, reducing the mean value of each by a small amount. Blade and rotor power is more significantly affected with mean rotor power at the peak power operating point, $\lambda = 4.5$, being reduced from $C_P = 0.465$ to $C_P = 0.374$. The most significant change is however the increase in range of fluctuations experienced by the blade and rotor in both thrust and particularly power. Rotor power is seen to fluctuate by up to $\pm 30\%$ of mean rotor power, whilst blade power is seen to fluctuate by up to $\pm 200\%$ of mean blade power, resulting in instantaneous blade powers that can be negative.

Observing the blade power and thrust histories and their spectra (see section 10.1), it is evident that the blade traces contain two principal frequency components, one at the rotation frequency and the other at the wave frequency. This results in a complex waveform typified by a modulated amplitude oscillation. The period of the modulation, T_B, is given by the inverse of the difference in frequency between the two underlying components, and hence where the wave and rotation frequencies are close the beating period is long. Instead of the three blade traces being phase shifted by $120°$ as occurs for the turbine in shear with no waves, the three blade traces are now phase shifted by $T_B/3$.

The fluctuations in total rotor thrust are of similar magnitude to fluctuations in individual blade thrust, which is contrary to the no wave case in which thrust and torque ripple are substantially reduced through the phase offset that occurs with multiple blades. Analysis of the rotor thrust reveals that the significant frequency components are at three times the rotation frequency and at the wave frequency, with the latter being the dominant. This is unexpected given the complex waveform of the blade thrust histories. Consequently the magnitude of the fluctuations in blade and rotor thrust are of similar magnitude (see vertical bars in

Figure 4(a) & (b).

The fluctuations in blade power exhibit the multi-frequency content with beating of period T_B but are clearly more dominated by a single frequency component (at the rotation frequency) and consequently have a less modulated wave form that is closer to a single sine wave. On summing the three blade power contributions, the resulting rotor power trace is found to have similar frequency content to the rotor thrust trace; two dominant frequency peaks at the wave and three times the rotation frequencies. As the underlying blade power traces are closer in form to sinusoids and their amplitude less modulated, their sum, the rotor power trace, exhibits lower amplitude fluctuations as some "phase cancellation" occurs. The fluctuation amplitude bars in

Figure 4 (d), rotor, and consequently much reduced from those seen for the individual blades,

Figure 4 (c).

Wake recovery in the presence of surface waves is seen to be more rapid than for the no waves case. Centre-line velocities recover more rapidly, see Figures 31, 38 and 45, compared to those experienced with the rigid lid condition (see Figure 39 of report D4). This is to be expected as the wave motion acts to accelerate the wake and bypass flow mixing process so as to promote accelerated recovery.

The wake model developed in D4 has again been applied to the turbine simulations in the presence of overhead waves. Recall that this model is valid at the streamwise point of pressure recovery and develops a profile at this point based on thrust, blockage and linear momentum actuator disk theory; for further details see D4. In Figures 32, 39 and 46 the lines marked "fit" are a numerical fit to the CFD data to aide comparison to the wake model profiles. It can be seen that the CFD data at 2D downstream of the rotor plane is in reasonable agreement with the wake model data, in contrast to agreement found at 5D downstream in the absence of waves (see D4). We therefore conclude that that waves act to accelerate the wake mixing process leading to enhanced wake recovery.

6 Influence of wave height

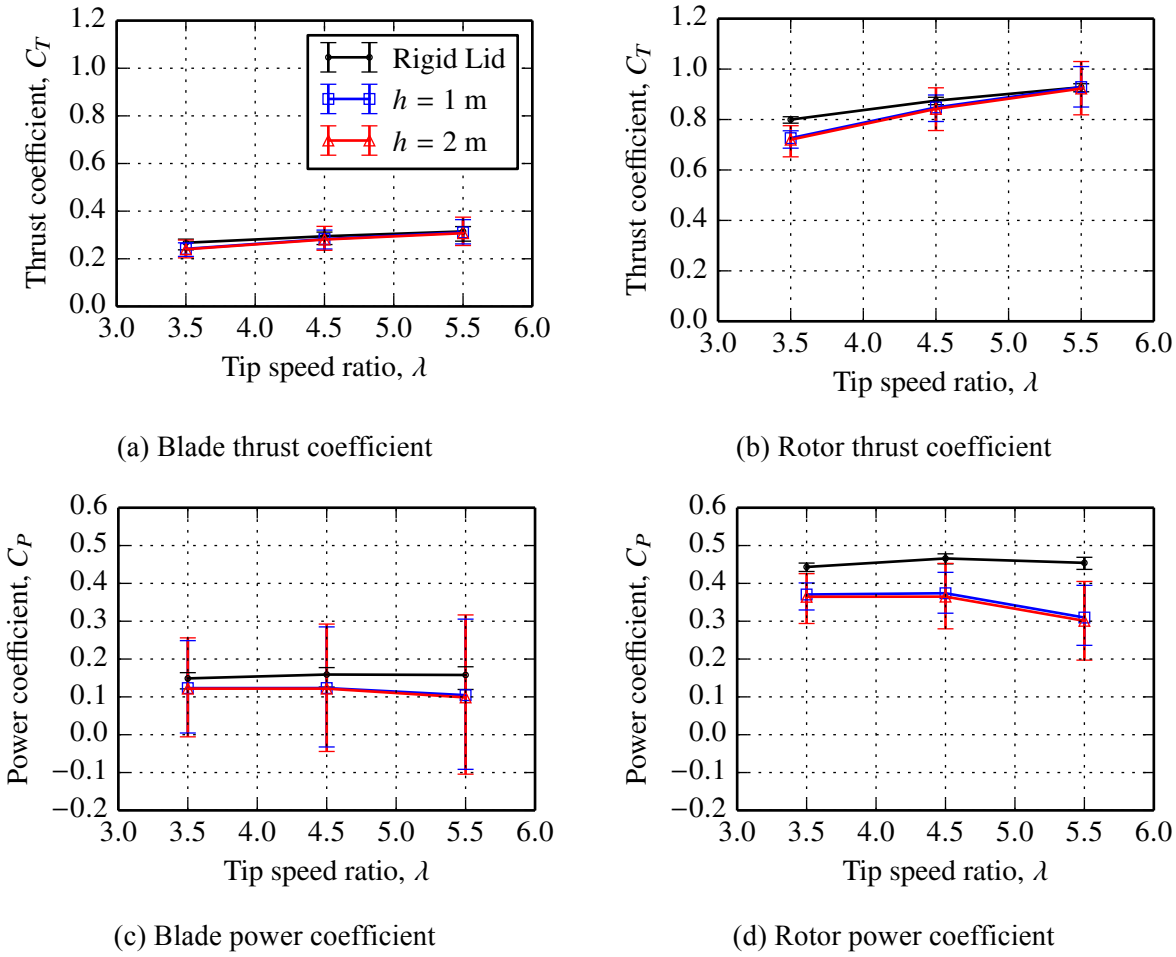

(a) Blade thrust coefficient

(b) Rotor thrust coefficient

(c) Blade power coefficient

(d) Rotor power coefficient

Figure 6: Comparison of thrust and power for various wave heights.

We now compare a third case with those discussed previously in section 5. Here the wave height has been increased to $H_W = 2\ m$, resulting in an increase in the magnitude of the fluctuations in thrust and power experienced by both blade and rotor. This is clearly due to an increase in the wave kinematic velocities experienced beneath the higher amplitude waves. This results in a greater fluctuation in flow angle, ϕ, and with it greater fluctuations in blade power and thrust. The frequency content of blade thrust and power traces (see section 10.3) shows greater energy at the wave frequency with consequence that the overall rotor thrust and power spectra are more dominated by the wave frequency over the three times rotation frequency. The associated rotor thrust and power traces are then closer to sinusoids.

Time mean thrust and power, for both blade and rotor, are seen to decrease as the wave amplitude increases. The peak power coefficient reduces to, $C_P = 0.365$ (a reduction of 22% relative to the rigid lid case), with an associated (marginally) reduced thrust coefficient, $C_T = 0.842$. The effect of wave height on peak power coefficient is noted in the table below.

Table 2: The influence of wave height on peak power.

Case	$C_{P\,max}$	$C_T\ at\ C_{P\,max}$
Rigid lid	0.466	0.875
$H_W = 1\text{m}$	0.374	0.849
$H_W = 2\text{m}$	0.365	0.842

Wave height is seen to have a modest influence on wake recovery with centreline velocity recovering slightly faster in the high wave case; see Figures 75, 82 and 89.

7 Influence of wave length

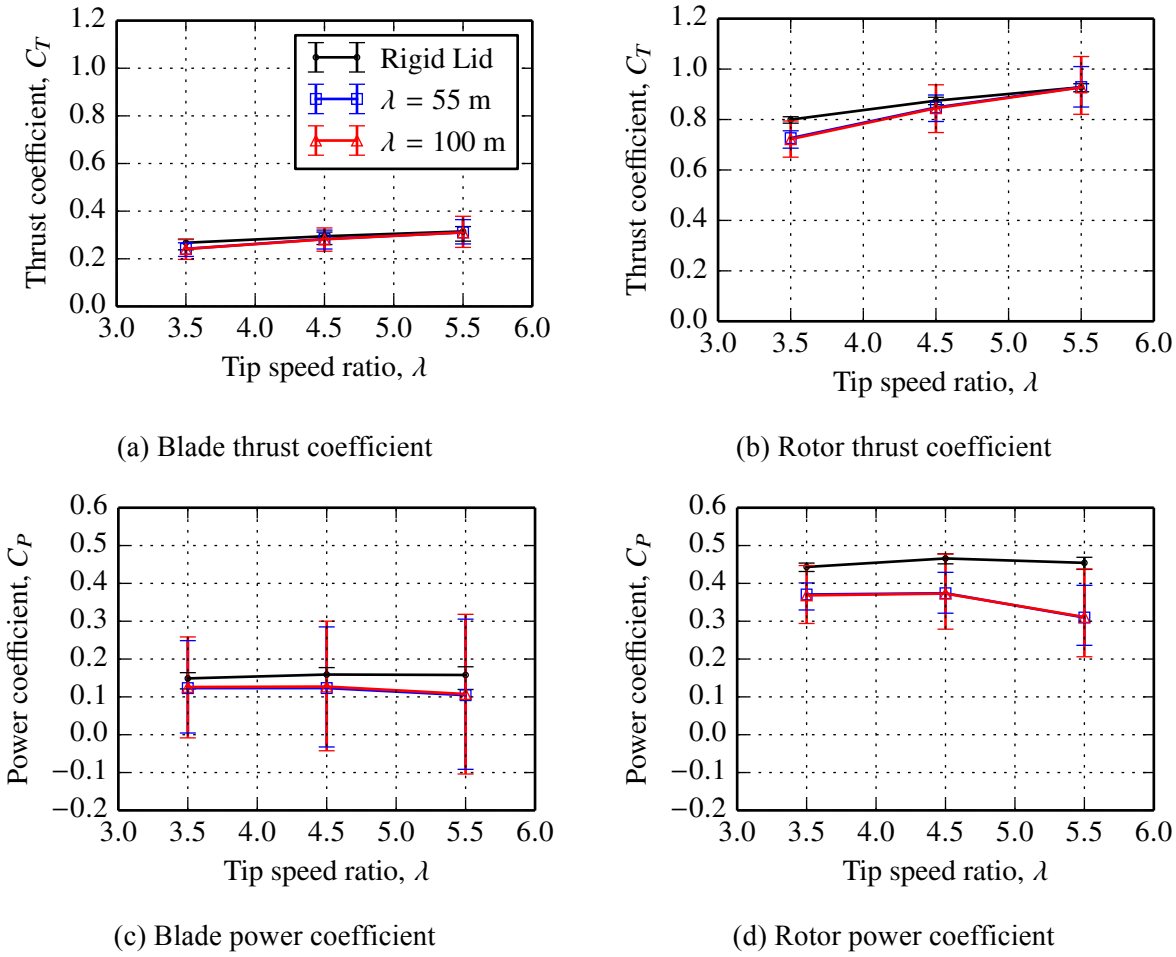

(a) Blade thrust coefficient

(b) Rotor thrust coefficient

(c) Blade power coefficient

(d) Rotor power coefficient

Figure 7: Comparison of thrust and power for various wave lengths.

Both blade and rotor mean power and thrust are relatively unaffected by wavelength; see Figure 7 and Table 3. However, fluctuating thrust and power components are seen to increase with wavelength as might be expected from wave kinematics (fluctuating velocity components increasing with λ at given depth) and blade element theory (see sections 3.3 and 5). The wave forms of individual blade thrust and power follow a similar form to those for shorter waves with the modulated wave forms taking on different beating periods dependent on the difference in frequency between the propagating wave and blade rotational frequencies.

Table 3: The influence of wavelength on peak power.

Case	$C_{P\,max}$	$C_T\ at\ C_{P\,max}$
Rigid lid	0.466	0.875
$\lambda_W = 55$m	0.374	0.848
$\lambda_W = 100$m	0.373	0.845

8 Influence of wave alignment

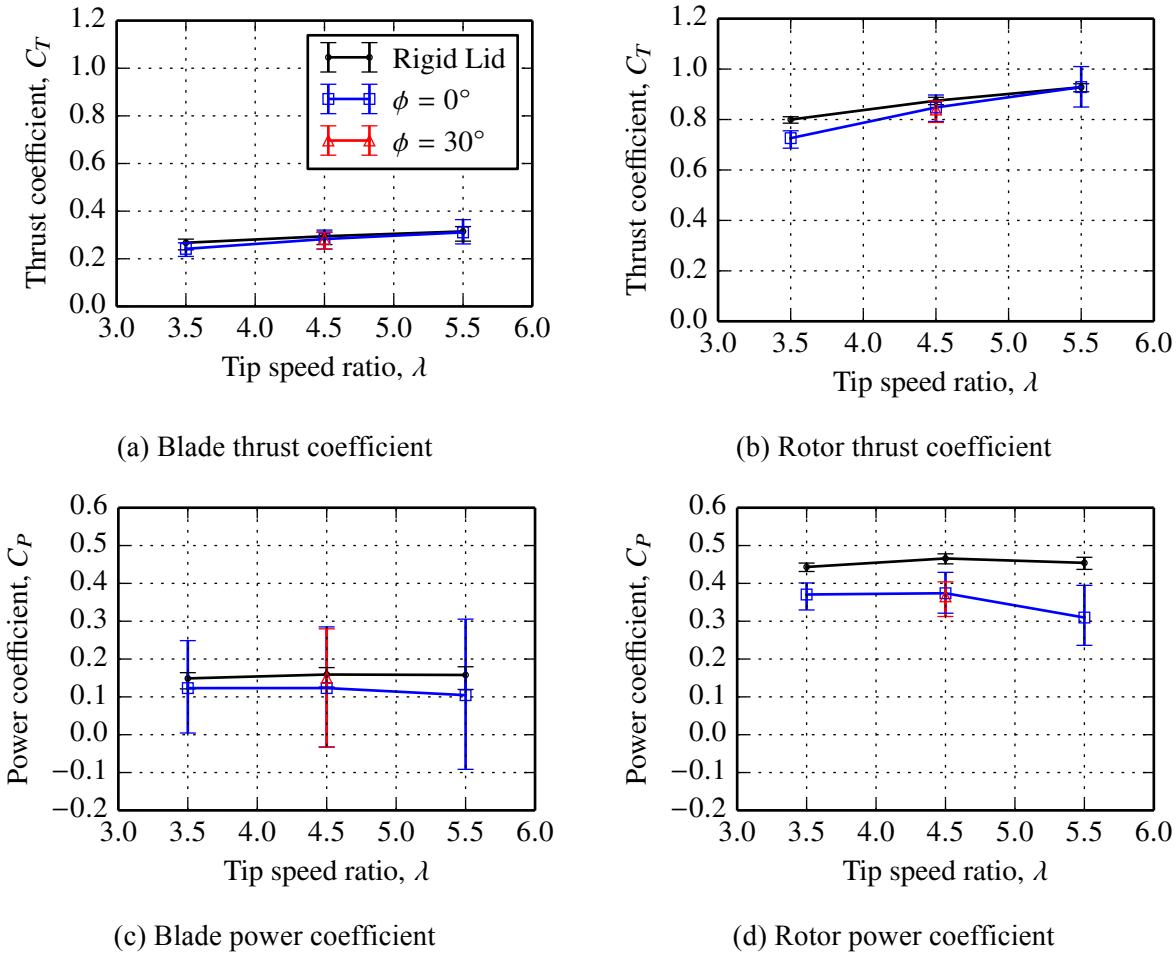

(a) Blade thrust coefficient

(b) Rotor thrust coefficient

(c) Blade power coefficient

(d) Rotor power coefficient

Figure 8: Comparison of thrust and power for cases with no waves ('Rigid Lid'), waves aligned with the streamwise direction ($\phi_w = 0^\circ$), and waves at an angle of 30° to the streamwise direction ($\phi_w = 30^\circ$).

Wave direction is seen to have little influence on the performance, power or thrust, of the turbine; see Figure 8 and Table 4. Even for a large wave yaw angle of 30° both mean and fluctuating components are largely unaffected; peak power being reduced by only 2%. Time traces for the 0° and 30° wave yaw cases are also similar. The point of streamwise pressure recovery is still seen to be at about 2D; see Figure 98.

Table 4: The influence of wave direction on peak power.

Case	$C_{P\,max}$	$C_T\ at\ C_{P\,max}$
Rigid lid	0.466	0.875
$\phi_w = 0^\circ$	0.374	0.848
$\phi_w = 30^\circ$	0.366	0.840

9 Reference case - Rigid Lid

9.1.1 Details

This “no wave” case corresponds to case ‘C’ from deliverable WG3 WP1 D4. The bed roughness coefficient, which governs the level of velocity shear, is $c_f = 0.0035$.

9.1.2 Performance

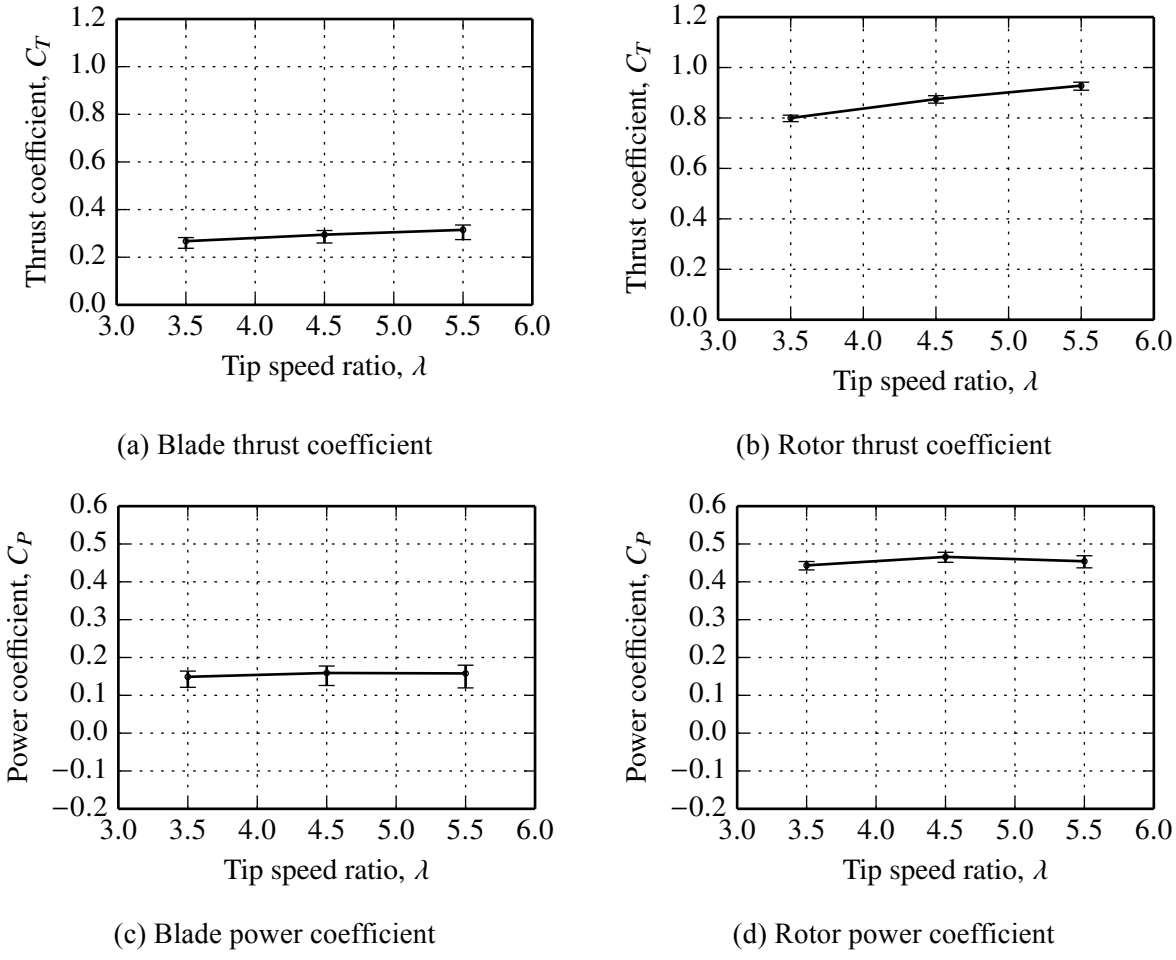

(a) Blade thrust coefficient

(b) Rotor thrust coefficient

(c) Blade power coefficient

(d) Rotor power coefficient

Figure 9: Blade and rotor thrust and power coefficients for the “no wave” reference case. Time mean values are displayed as points and vertical bars represent the range (min to max) of the computed quantity.

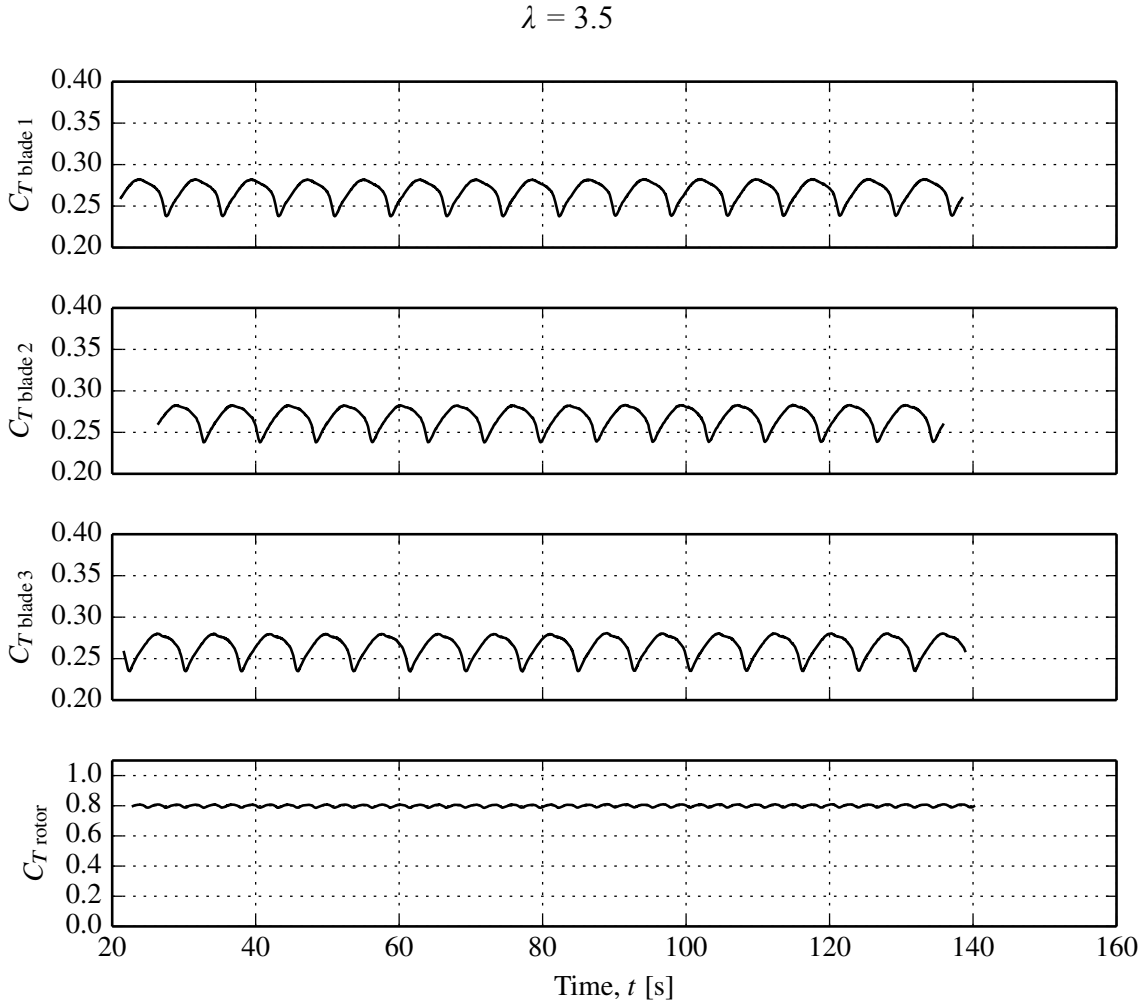

Figure 10: Blade and rotor load histories. Rigid lid case, λ = 3.5.

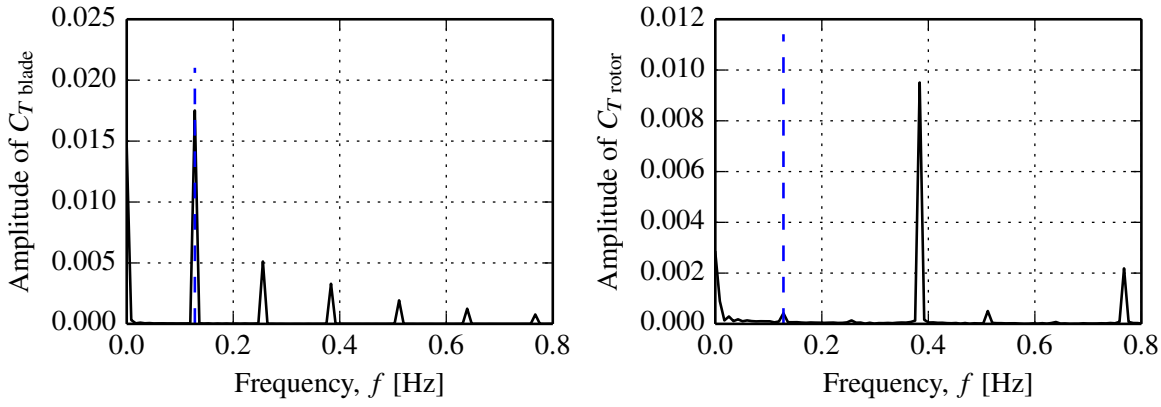

(a) (b)

Figure 11: Thrust spectra; (a) blade, (b) rotor. Blue - rotor frequency. Rigid lid case, λ = 3.5.

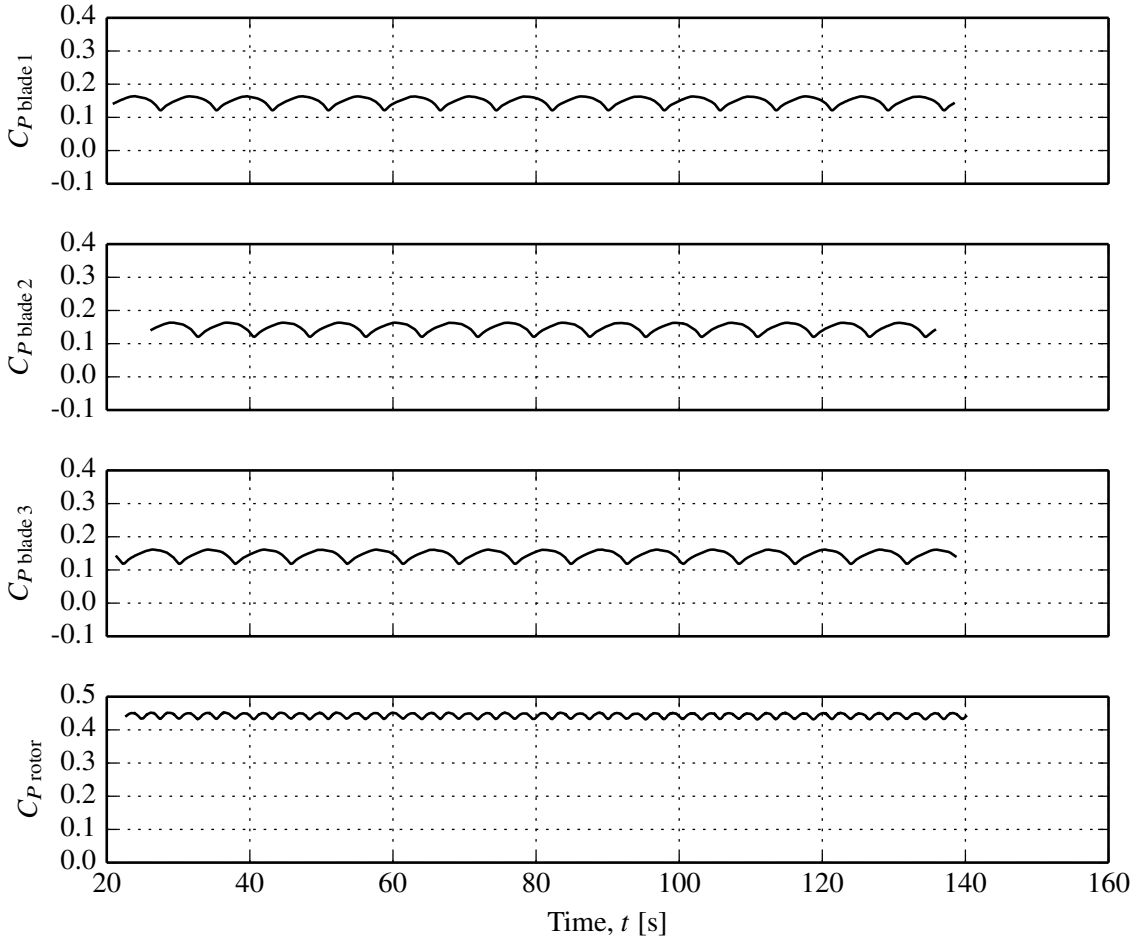

Figure 12: Blade and rotor power histories. Rigid lid case, λ = 3.5.

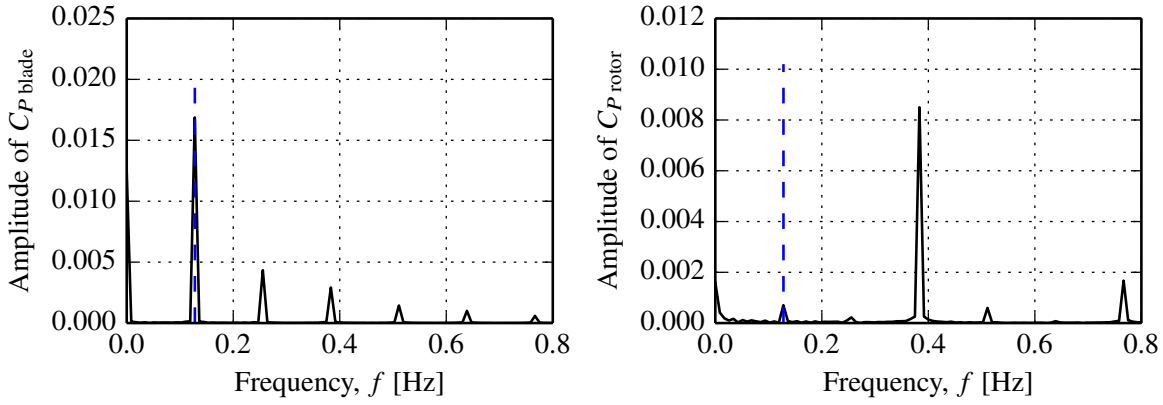

(a) (b)

Figure 13: Power spectra; (a) blade, (b) rotor. Blue - rotor frequency. Rigid lid case, λ = 3.5.

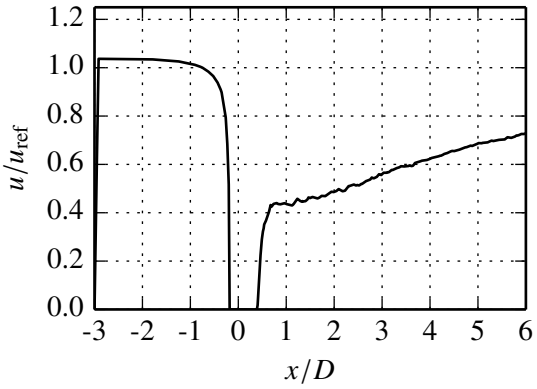

Figure 14: Centre-line streamwise velocity component. Rigid lid case, $\lambda = 3.5$.

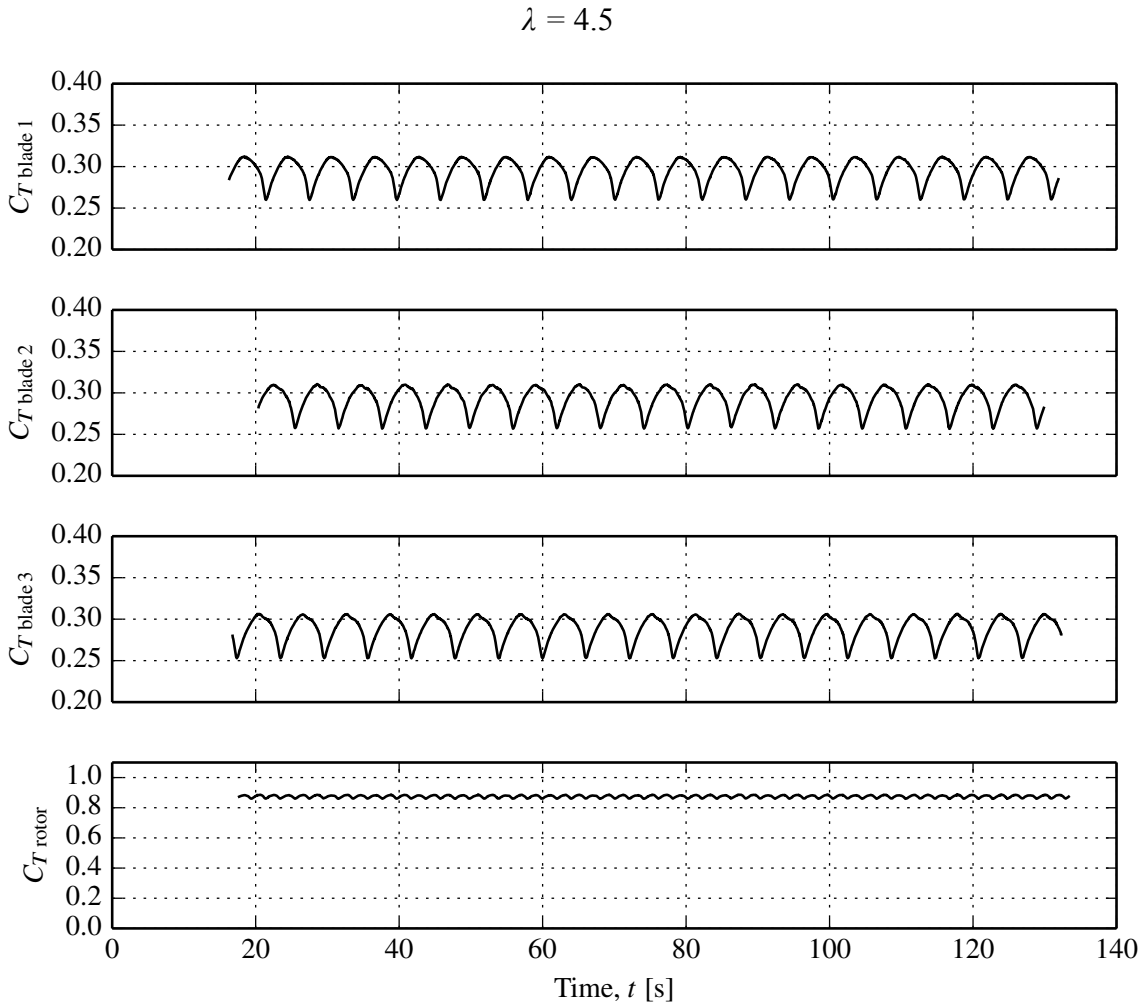

Figure 15: Blade and rotor load histories. Rigid lid case, λ = 4.5.

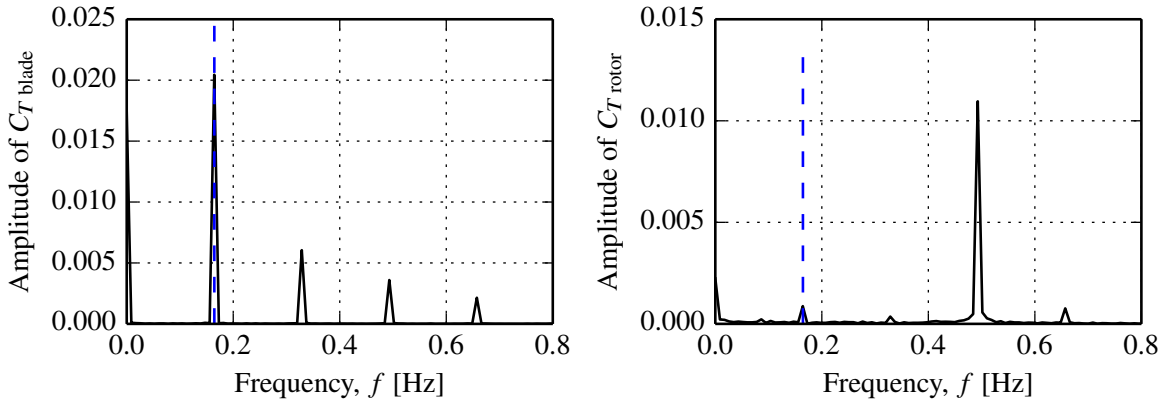

(a) (b)

Figure 16: Thrust spectra; (a) blade, (b) rotor. Blue - rotor frequency. Rigid lid case, λ = 4.5. The largest frequency component in (b) is due to the blade-tower interaction.

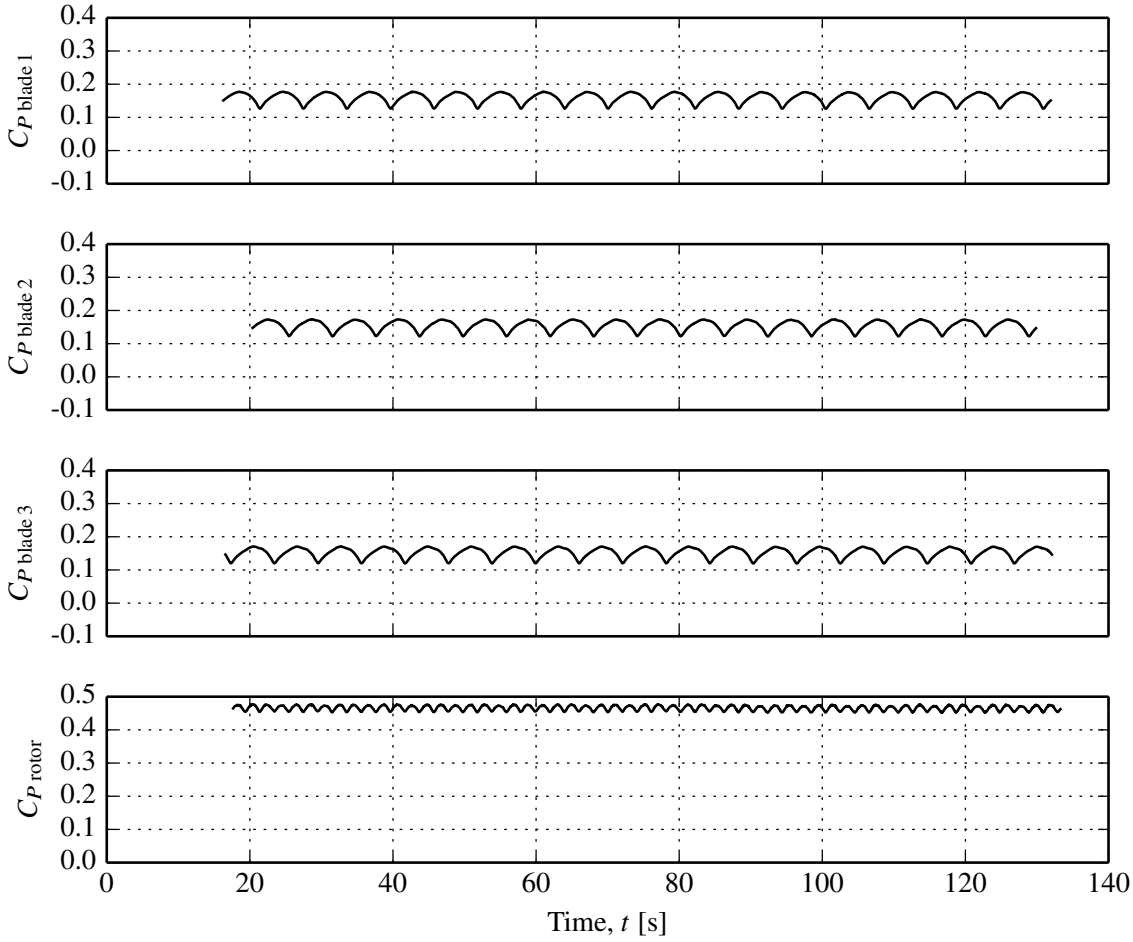

Figure 17: Blade and rotor power histories. Rigid lid case, λ = 4.5.

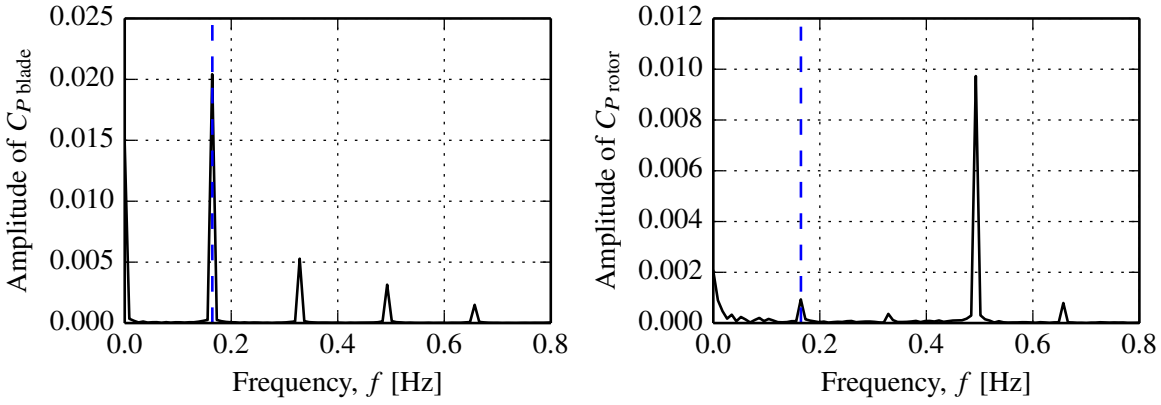

(a) (b)

Figure 18: Power spectra; (a) blade, (b) rotor. Blue - rotor frequency. Rigid lid case, λ = 4.5.

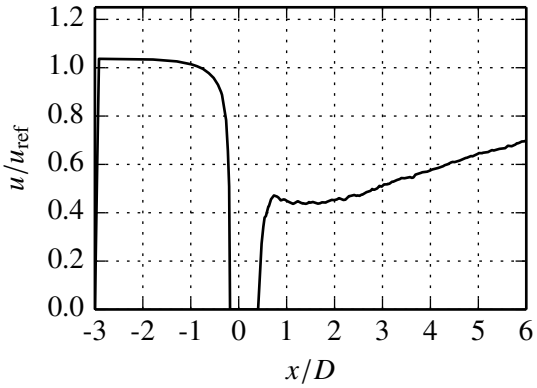

Figure 19: Centre-line streamwise velocity component. Rigid lid case, λ = 4.5.

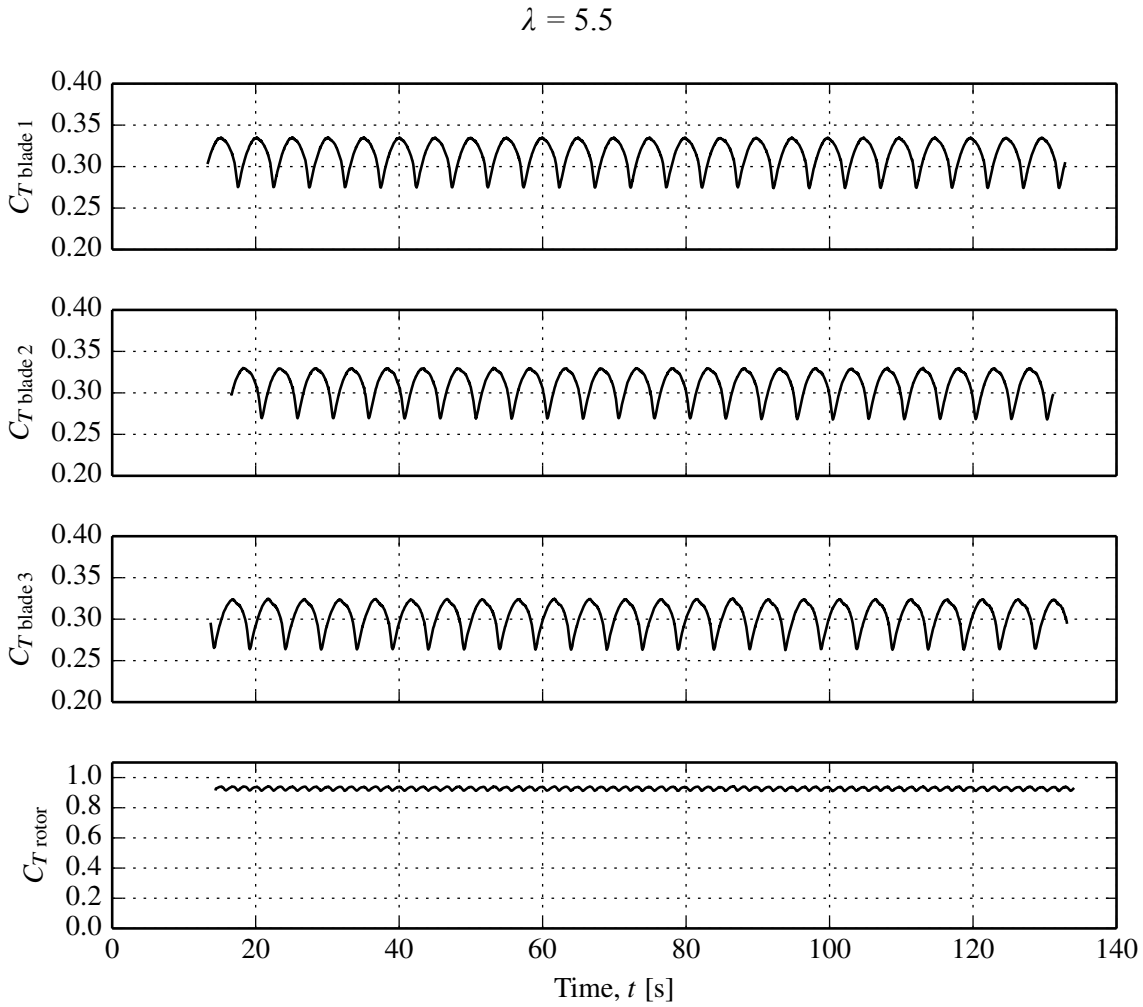

Figure 20: Blade and rotor load histories. Rigid lid case, λ = 5.5.

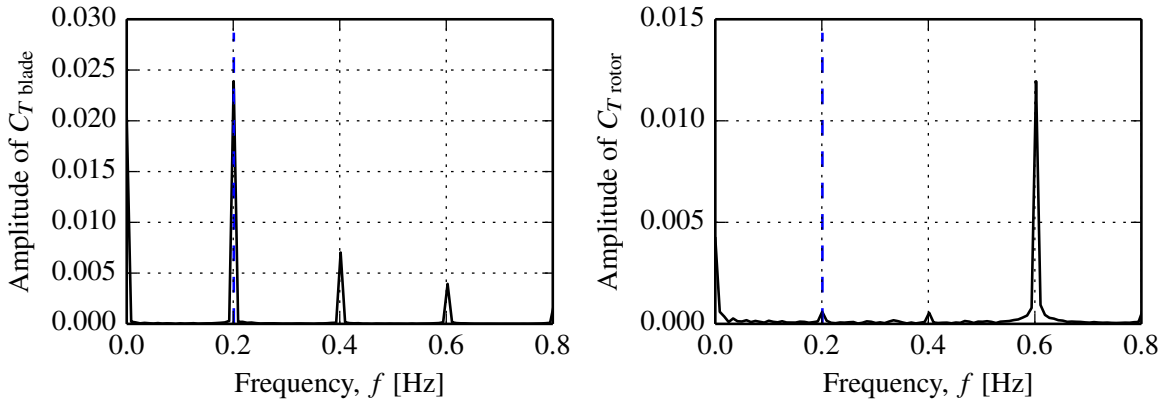

(a) (b)

Figure 21: Thrust spectra; (a) blade, (b) rotor. Blue - rotor frequency. Rigid lid case, λ = 5.5.

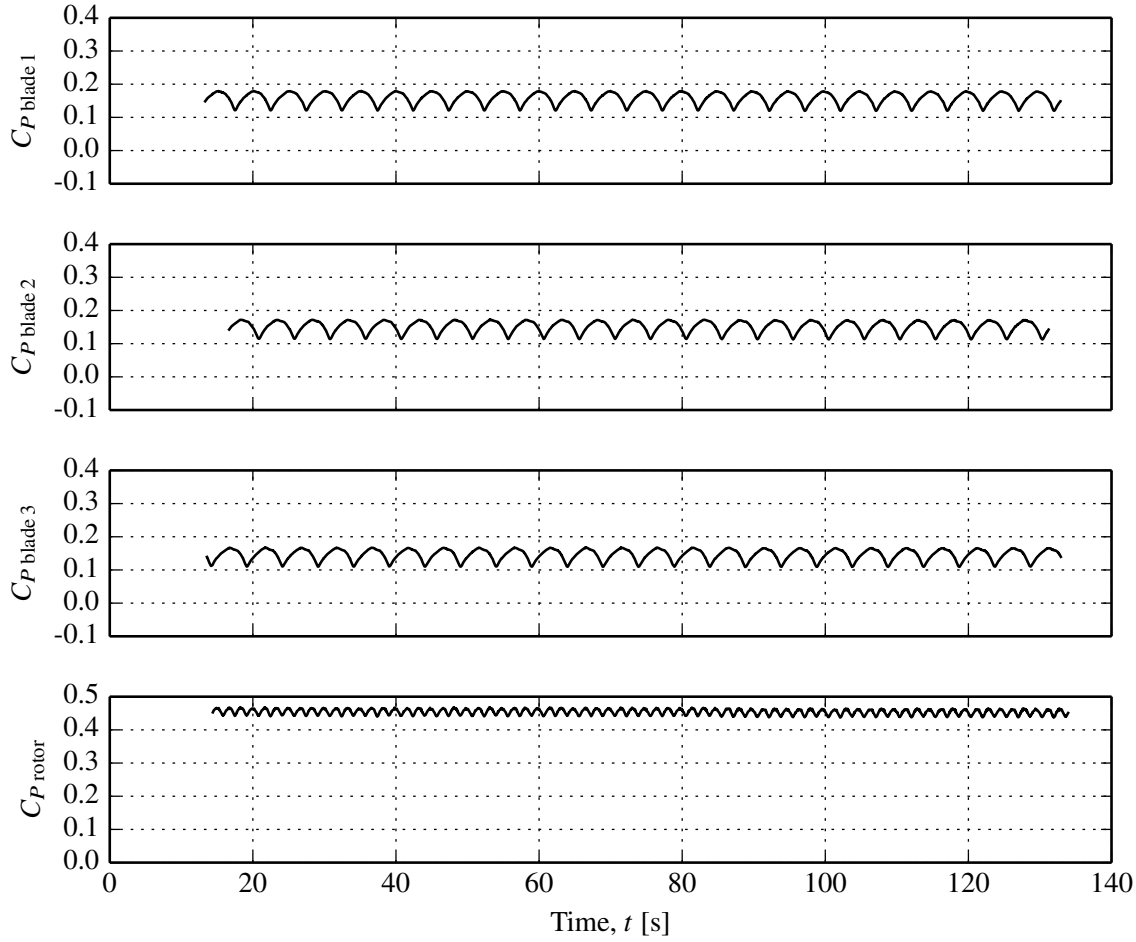

Figure 22: Blade and rotor power histories. Rigid lid case, λ = 5.5.

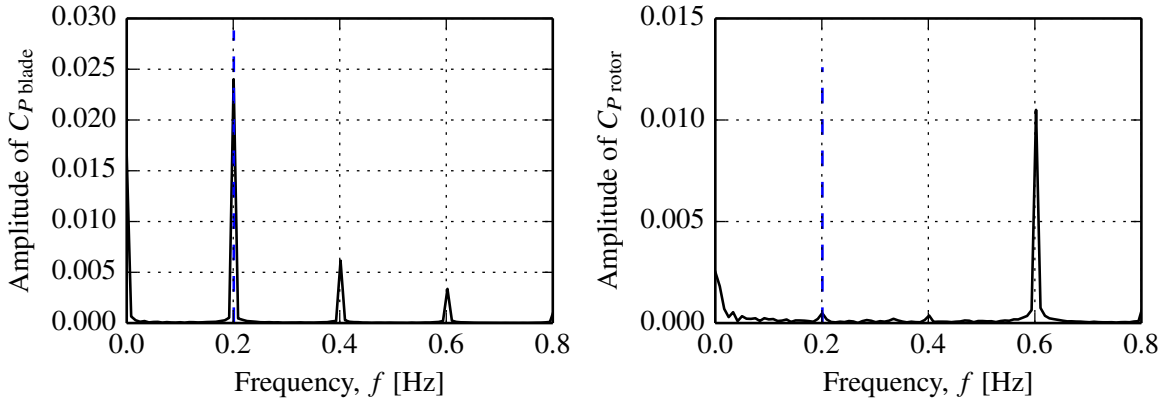

(a) (b)

Figure 23: Power spectra; (a) blade, (b) rotor. Blue - rotor frequency. Rigid lid case, λ = 5.5.

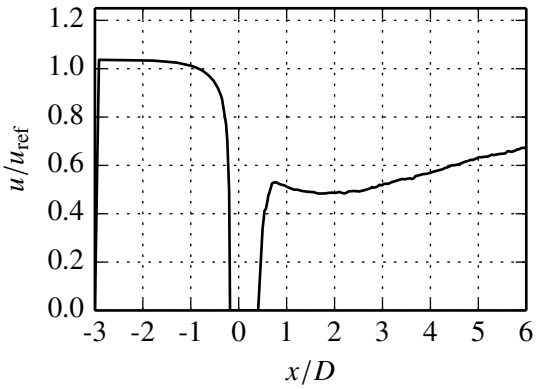

Figure 24: Centre-line streamwise velocity component. Rigid lid case, λ = 5.5.

10 Appendix

10.1 Case 1 - Base case

10.1.1 Details

λ_w	55 m
H_w	1 m
ϕ_w	0˚

10.1.2 Performance

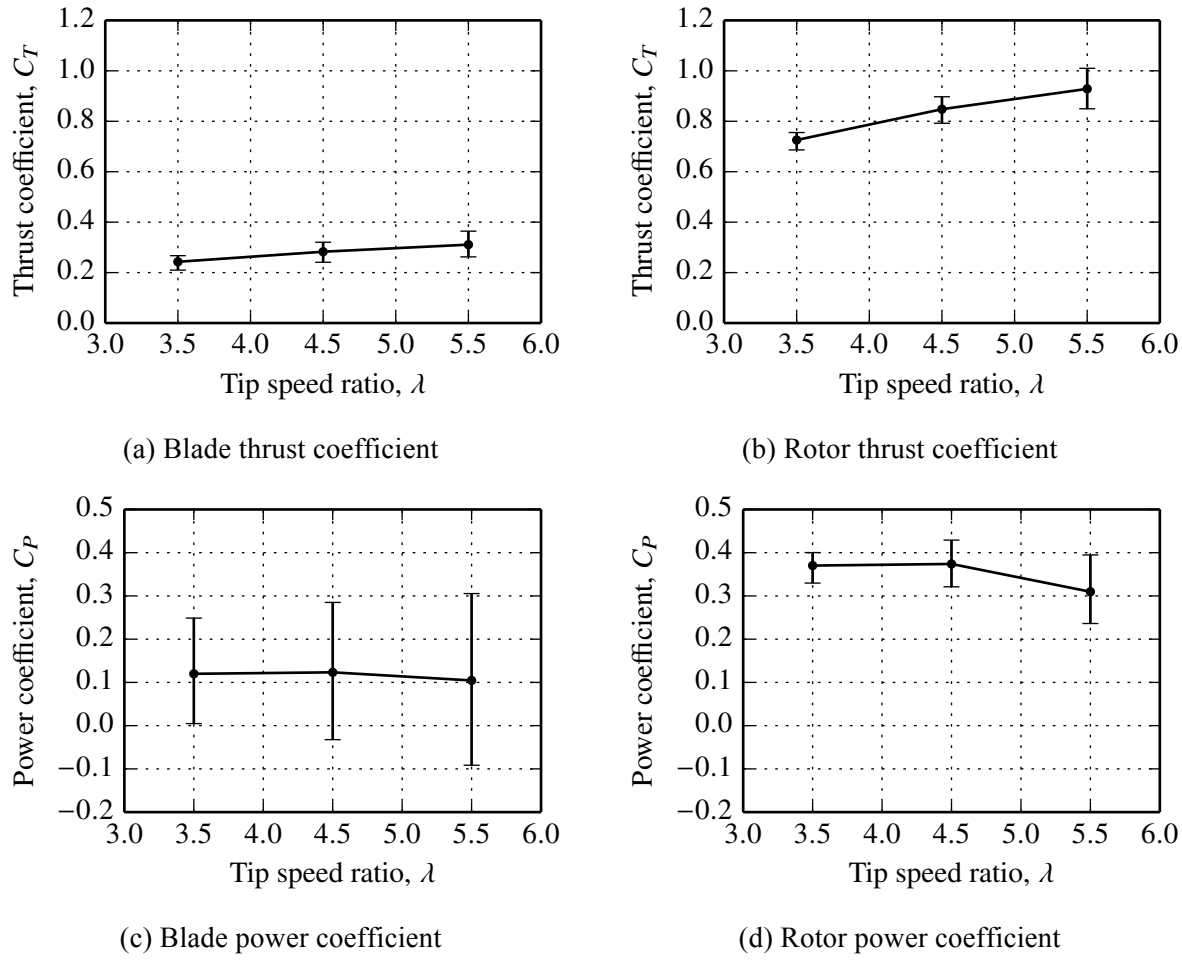

(a) Blade thrust coefficient

(b) Rotor thrust coefficient

(c) Blade power coefficient

(d) Rotor power coefficient

Figure 25: Blade and rotor thrust and power coefficients for the base case. Time mean values are displayed as points and vertical bars represent the range of the computed quantity.

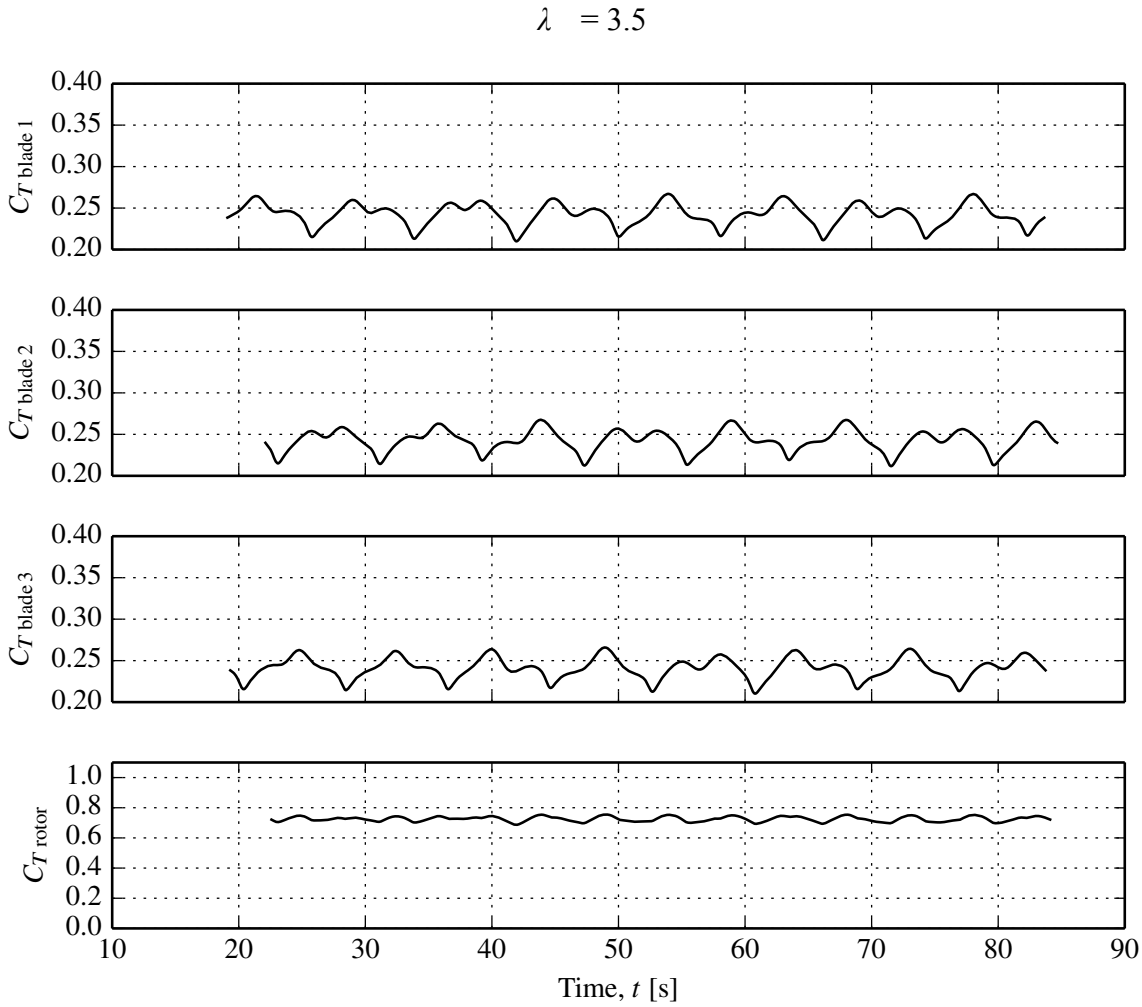

Figure 26: Blade and rotor load histories. Base case, λ = 3.5.

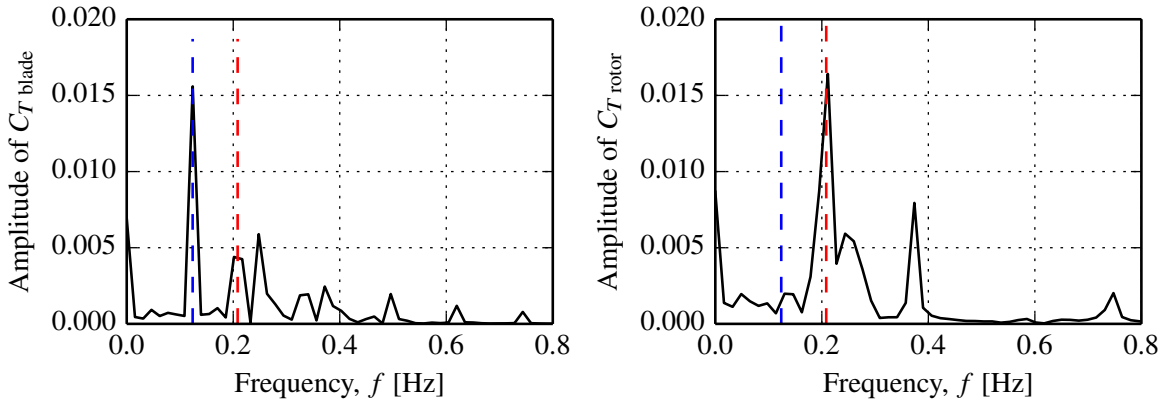

(a) (b)

Figure 27: Thrust spectra; (a) blade, (b) rotor. Blue - rotor frequency, red - wave frequency. Base case, λ = 3.5.

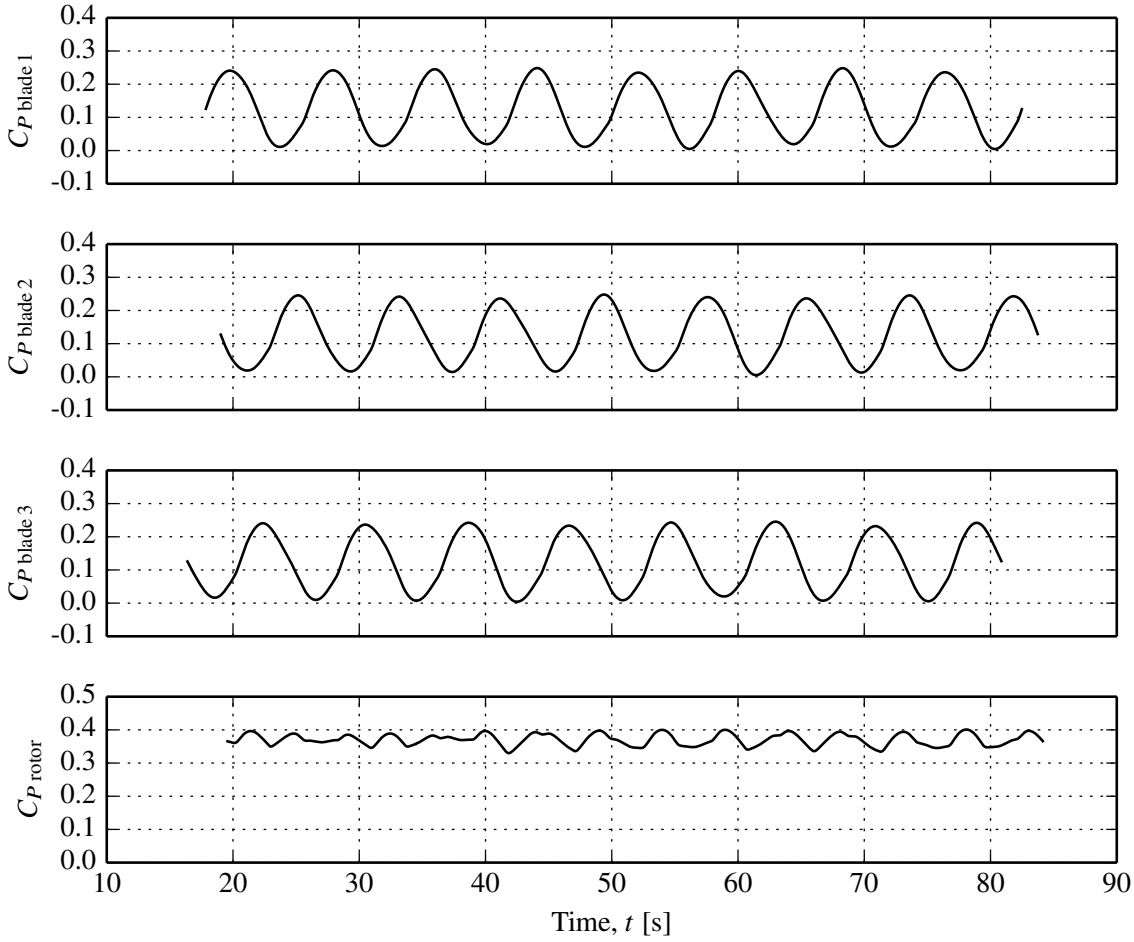

Figure 28: Blade and rotor power histories. Base case, λ = 3.5.

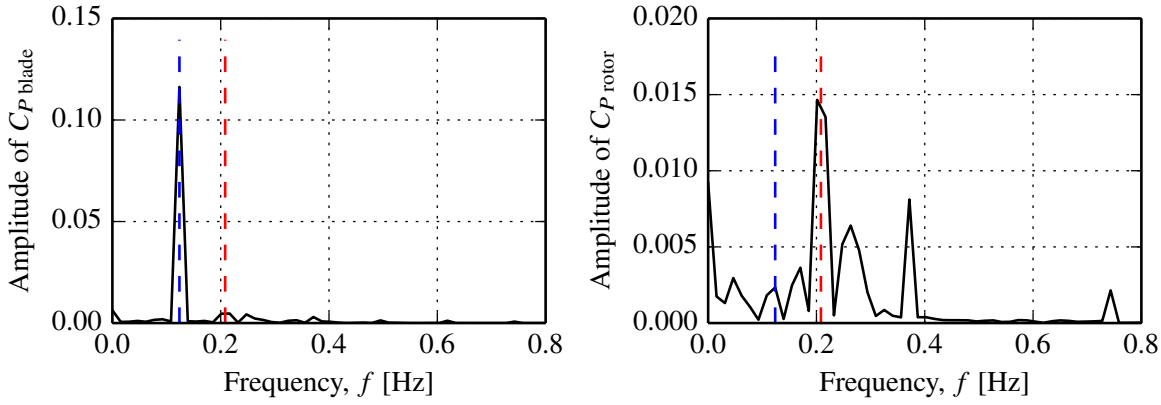

(a) (b)

Figure 29: Power spectra; (a) blade, (b) rotor. Blue - rotor frequency, red - wave frequency. Base case, λ = 3.5.

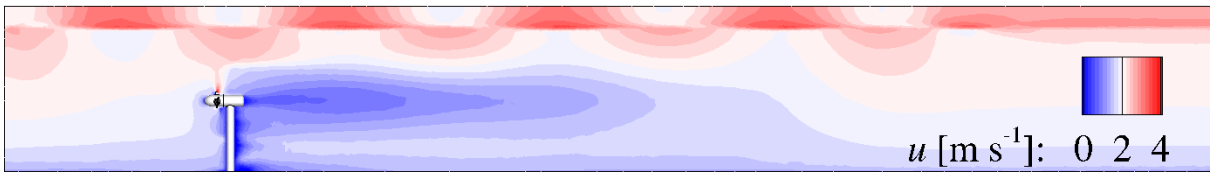

Figure 30: Centre plane velocity field. Base case, λ = 3.5.

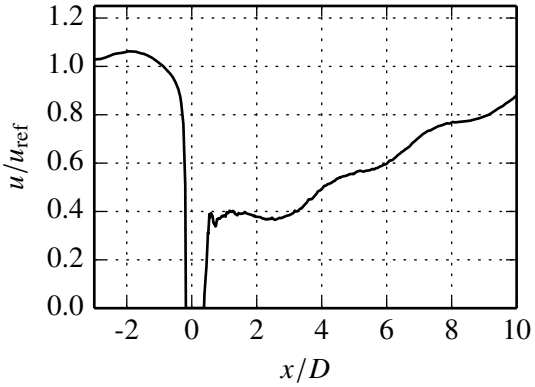

Figure 31: Centre-line streamwise velocity component. Base case, λ = 3.5.

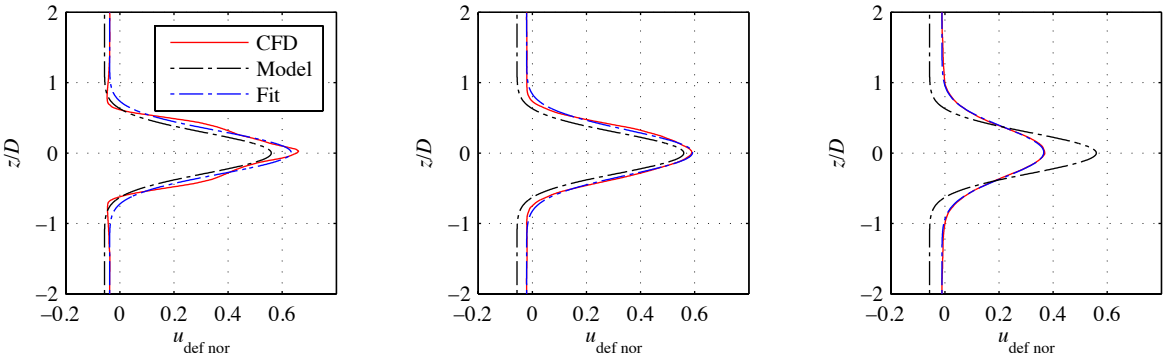

Figure 32: Parametric model of wake velocity deficit (Left to right, x =1D, 2D, 5D). Base case, λ = 3.5.

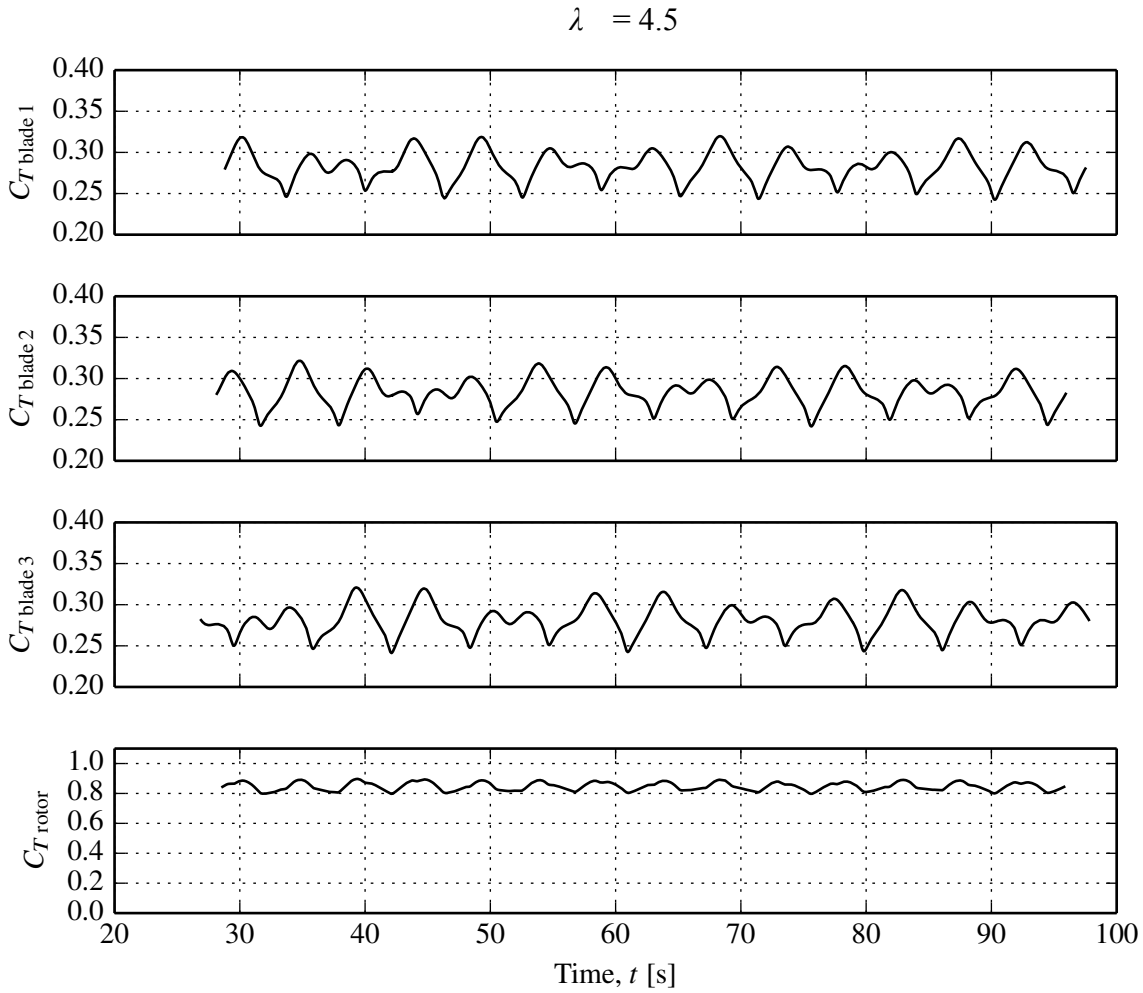

Figure 33: Blade and rotor load histories. Base case, λ = 4.5.

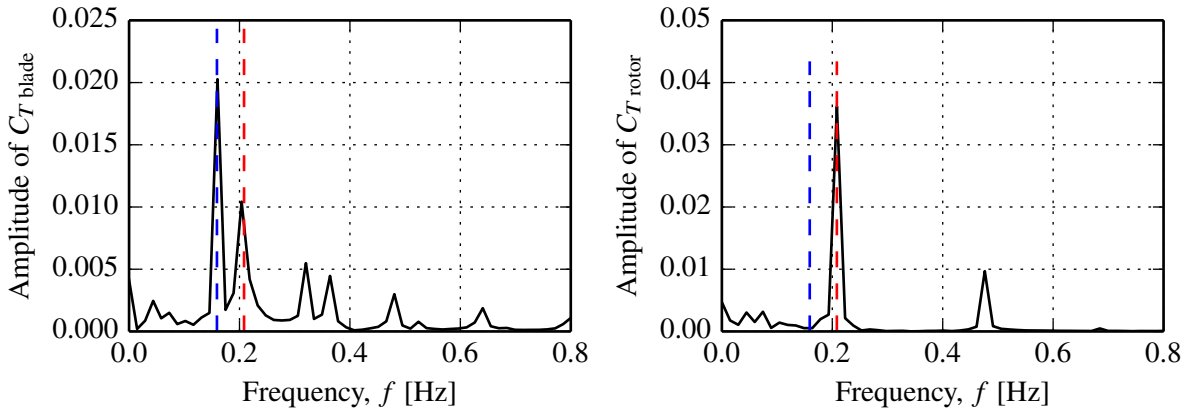

(a) (b)

Figure 34: Thrust spectra; (a) blade, (b) rotor. Blue - rotor frequency, red - wave frequency. Base case, λ = 4.5.

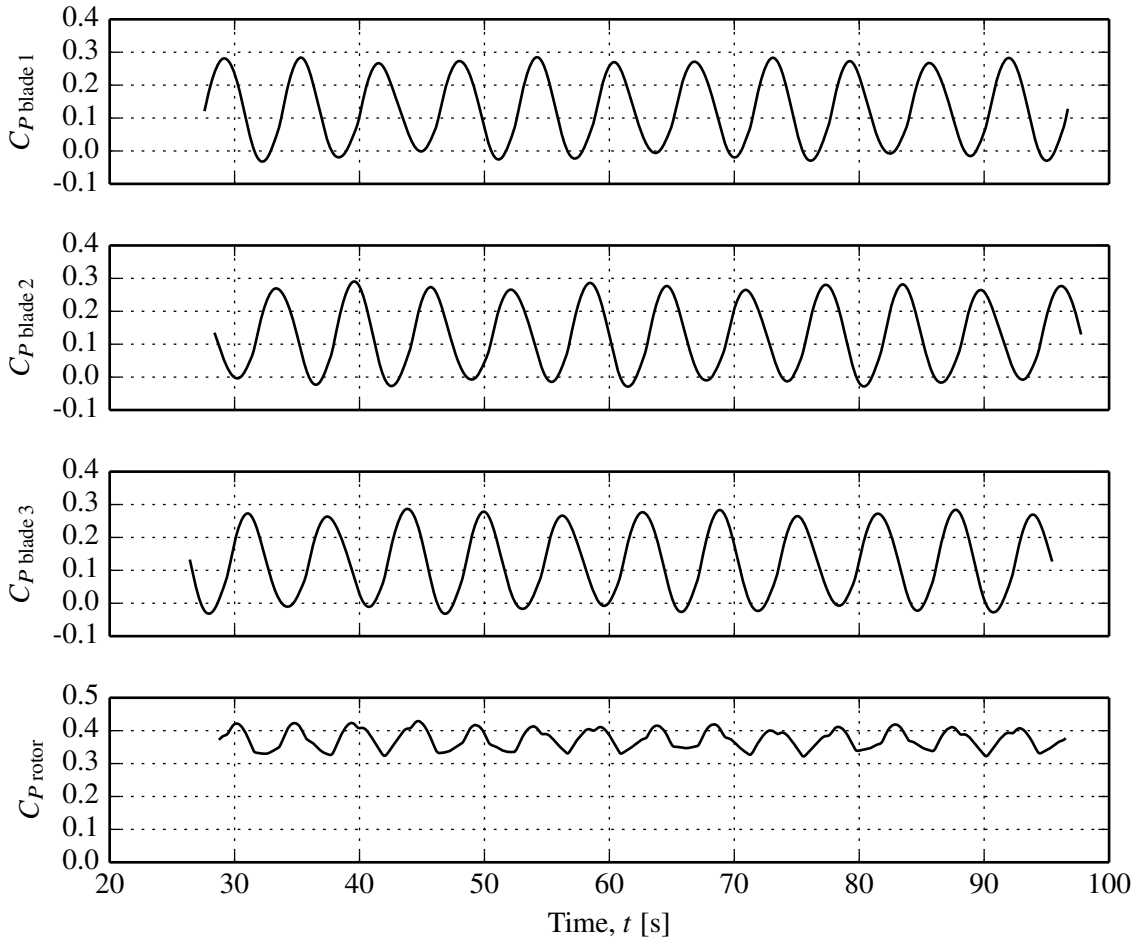

Figure 35: Blade and rotor power histories. Base case, λ = 4.5.

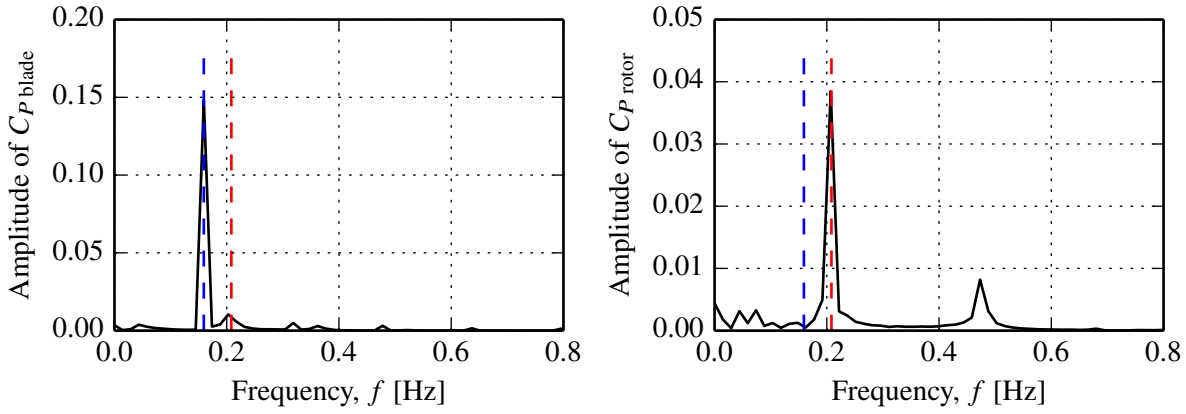

(a) (b)

Figure 36: Power spectra; (a) blade, (b) rotor. Blue - rotor frequency, red - wave frequency. Base case, λ = 4.5.

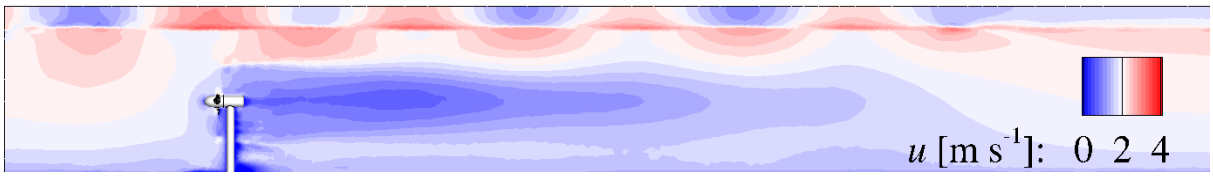

Figure 37: Centre plane velocity field. Base case, λ = 4.5.

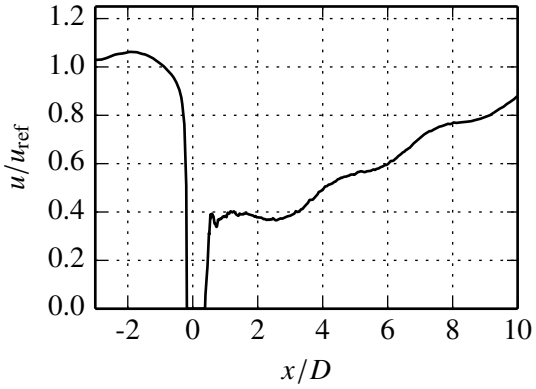

Figure 38: Centre-line streamwise velocity component. Base case, λ = 4.5.

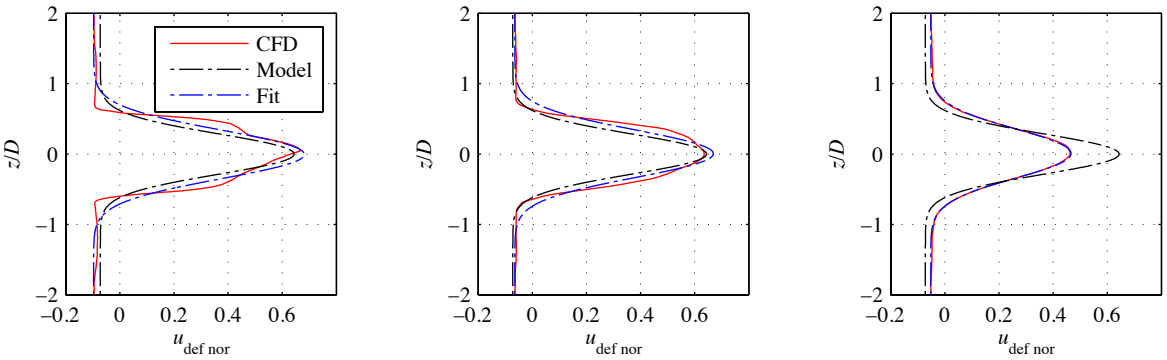

Figure 39: Parametric model of wake velocity deficit (Left to right, x =1D, 2D, 5D). Base case, λ = 4.5.

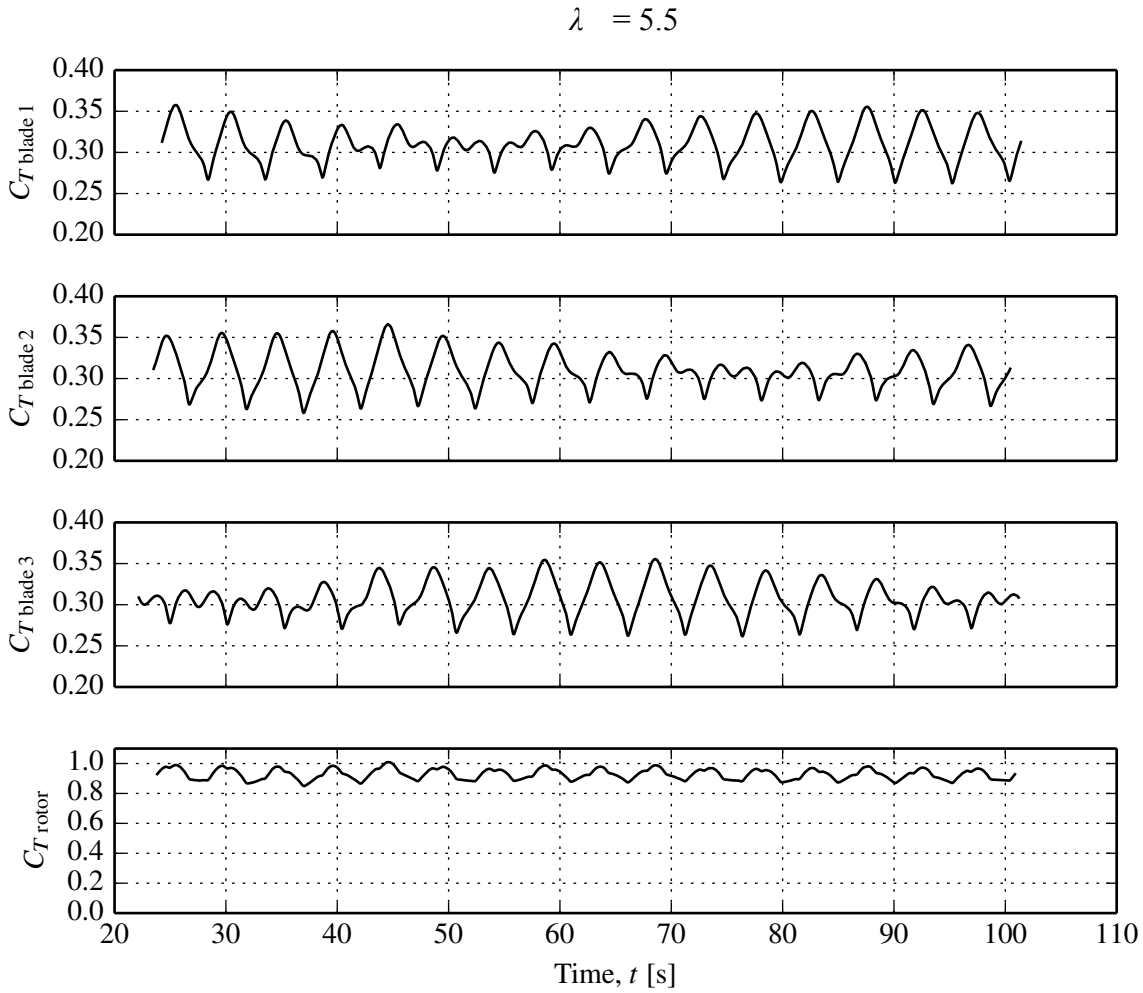

Figure 40: Blade and rotor load histories. Base case, λ = 5.5.

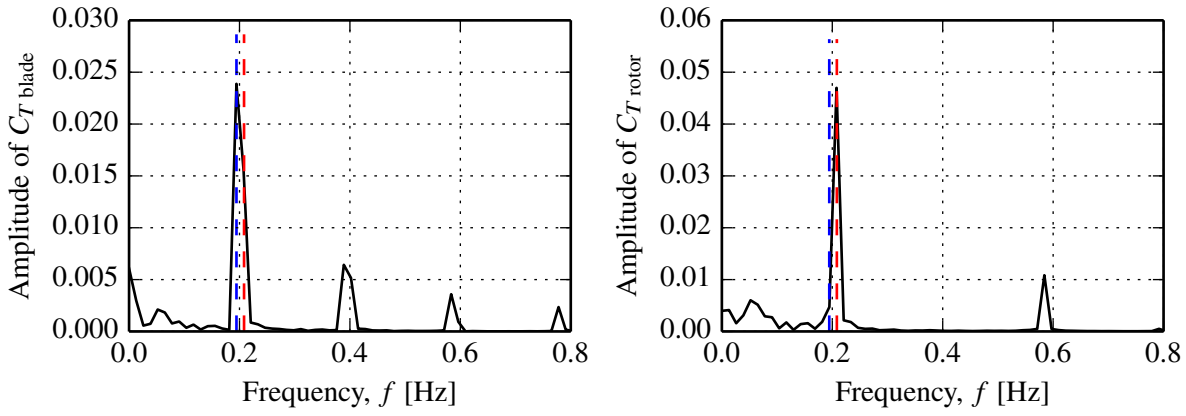

(a) (b)

Figure 41: Thrust spectra; (a) blade, (b) rotor. Blue - rotor frequency, red - wave frequency. Base case, λ = 5.5.

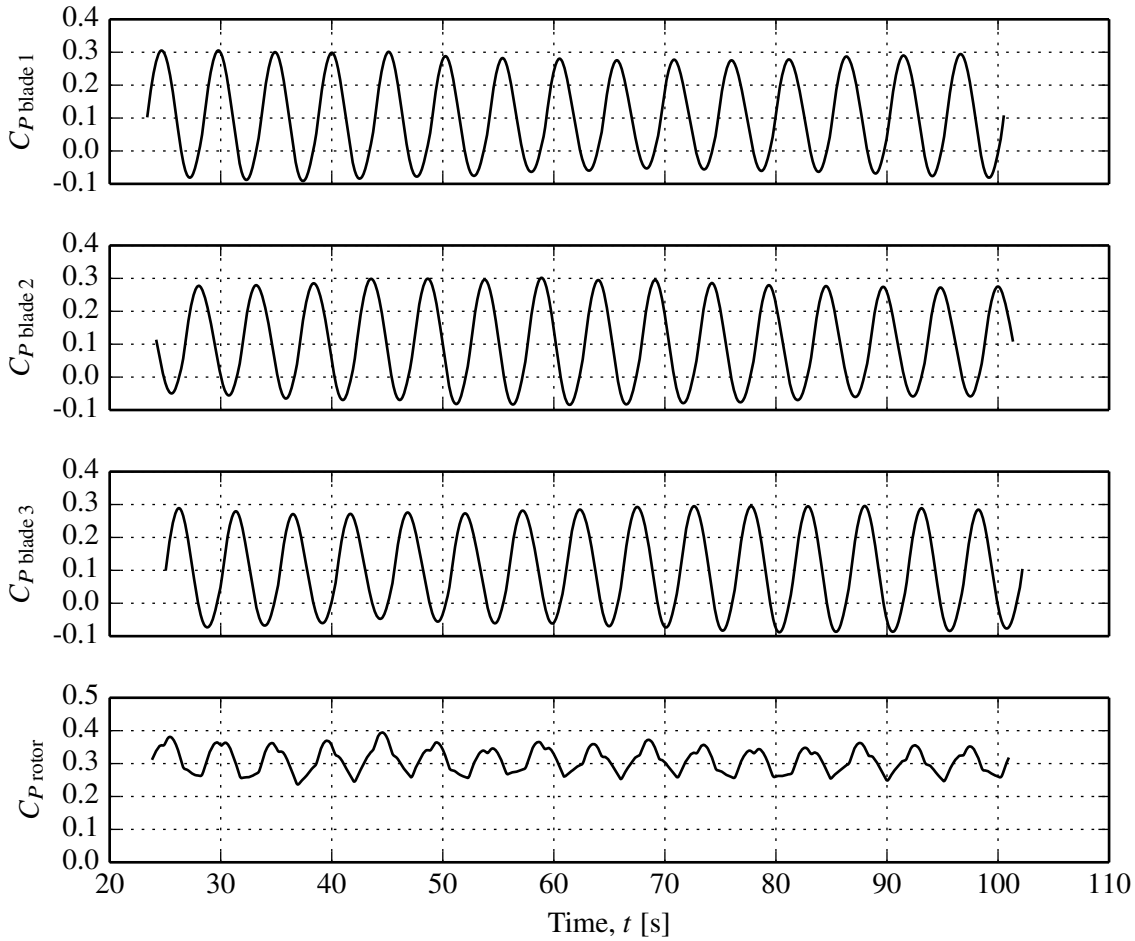

Figure 42: Blade and rotor power histories. Base case, λ = 5.5.

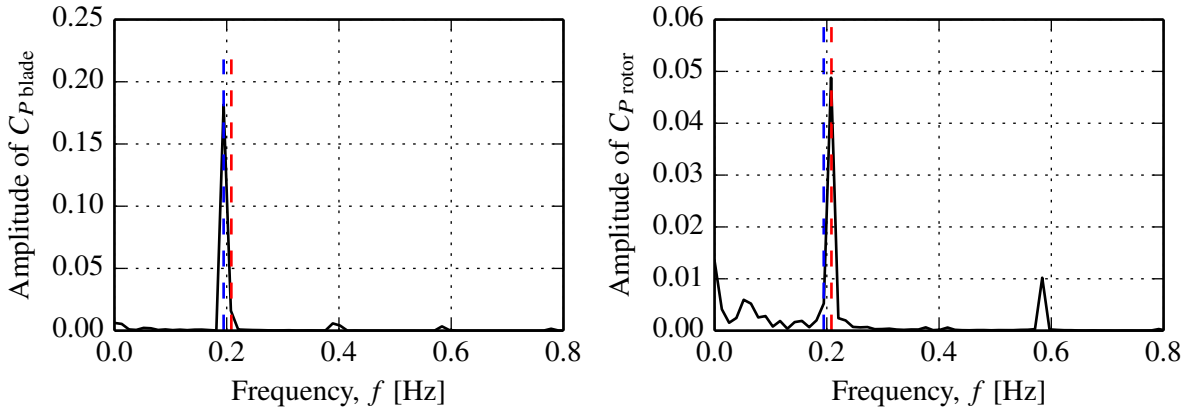

(a) (b)

Figure 43: Power spectra; (a) blade, (b) rotor. Blue - rotor frequency, red - wave frequency. Base case, λ = 5.5.

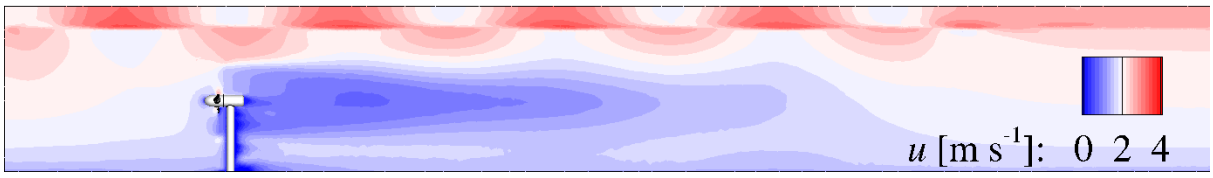

Figure 44: Centre plane velocity field. Base case, λ = 5.5.

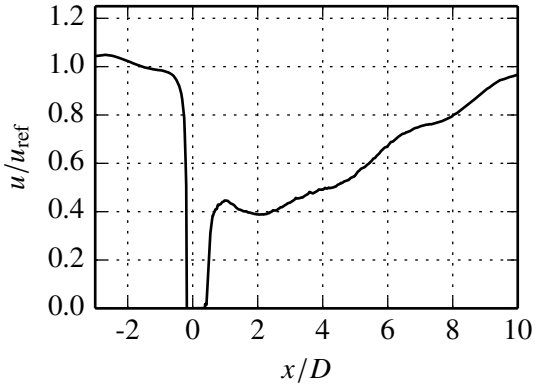

Figure 45: Centre-line streamwise velocity component. Base case, λ = 5.5.

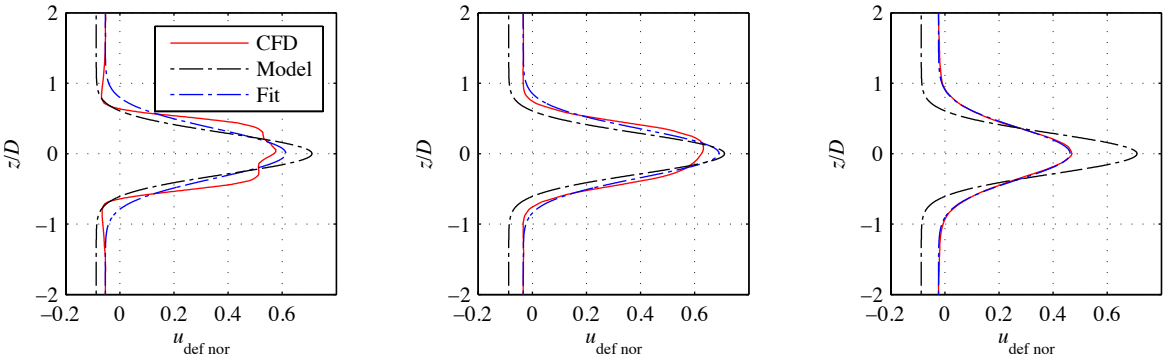

Figure 46: Parametric model of wake velocity deficit (Left to right, x =1D, 2D, 5D). Base case, λ = 5.5.

10.2 Case 2 - Long wave case

10.2.1 Details

λ_w	100 m
H_w	1 m
ϕ_w	0°

10.2.2 Performance

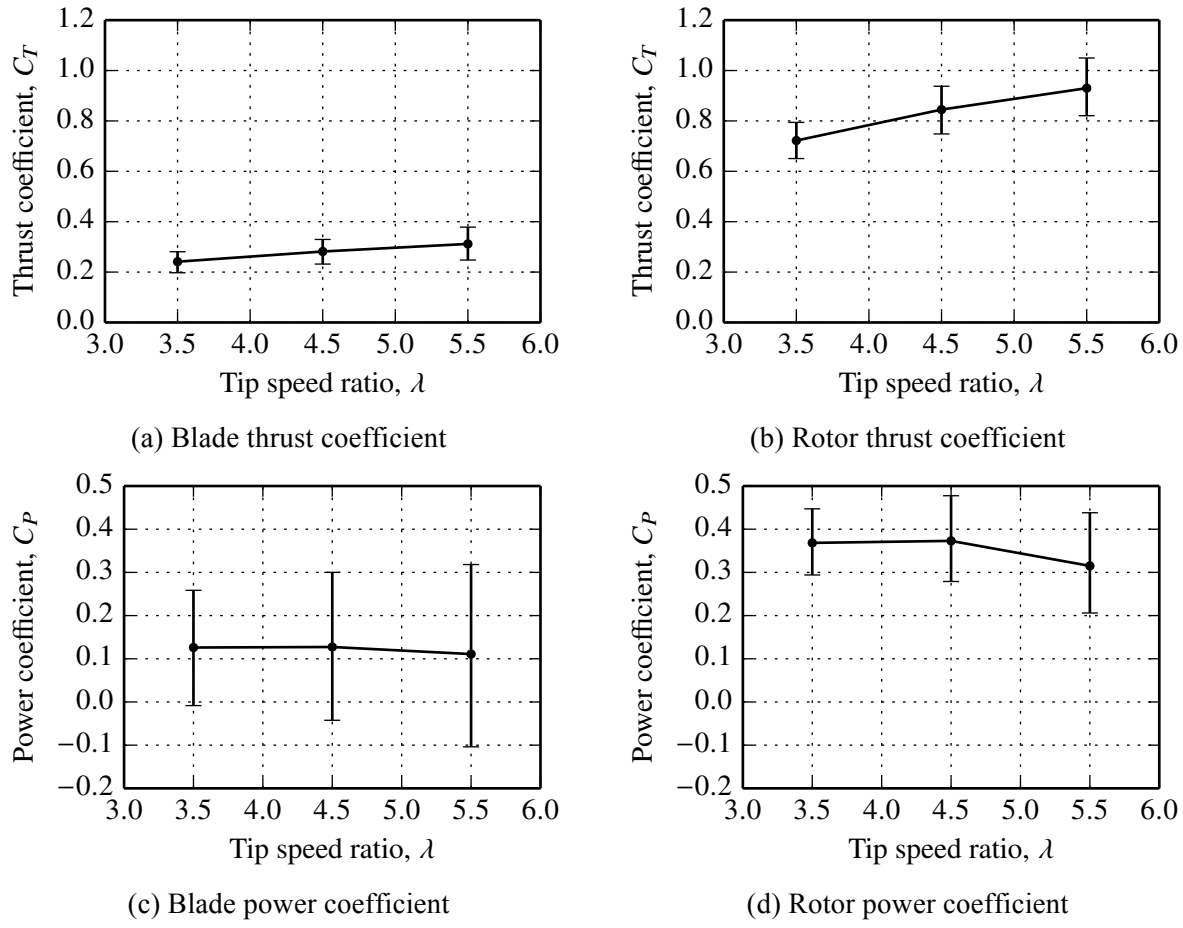

(a) Blade thrust coefficient

(b) Rotor thrust coefficient

(c) Blade power coefficient

(d) Rotor power coefficient

Figure 47: Blade and rotor thrust and power coefficients for the long wave case. Time mean values are displayed as points and vertical bars represent the range of the computed quantity.

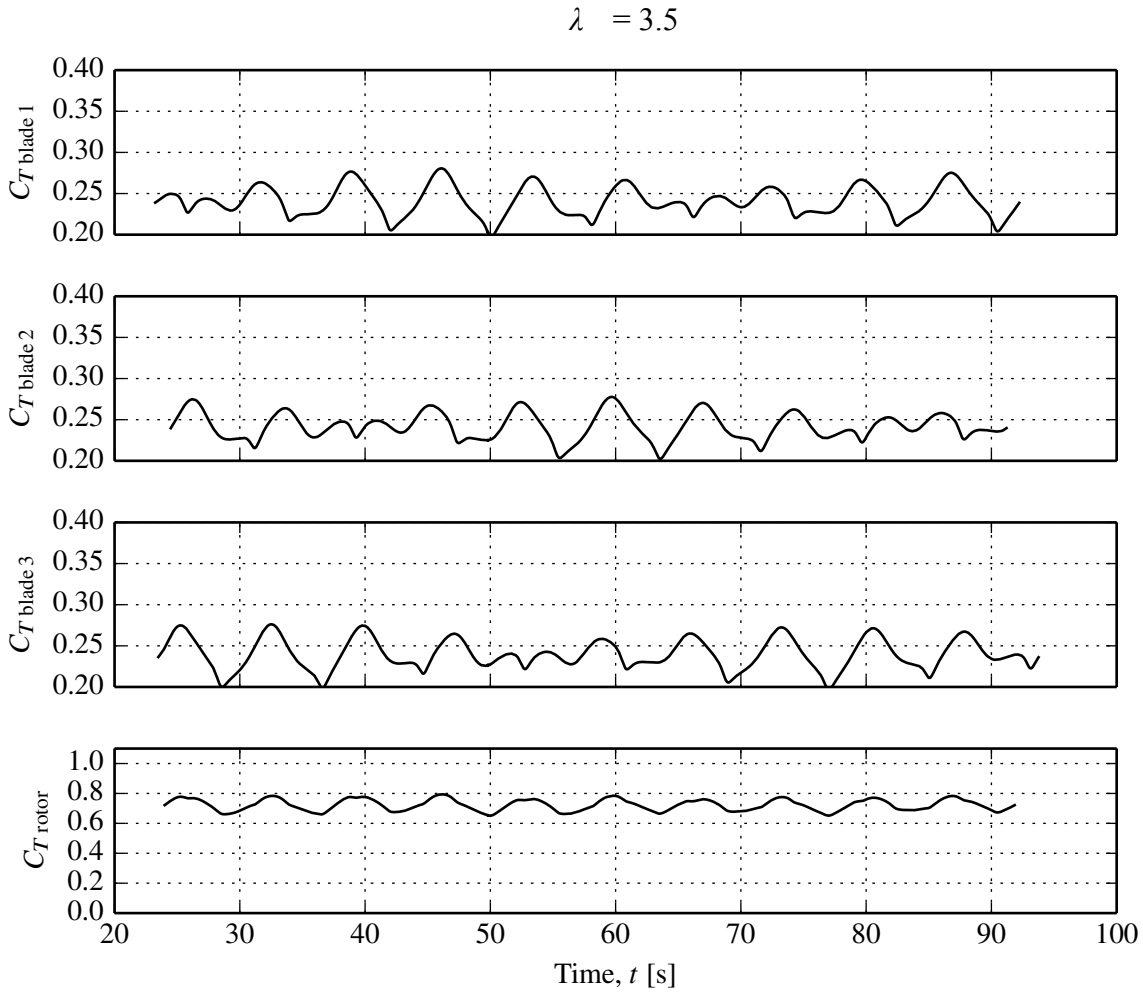

Figure 48: Blade and rotor load histories. Long wave case, λ = 3.5.

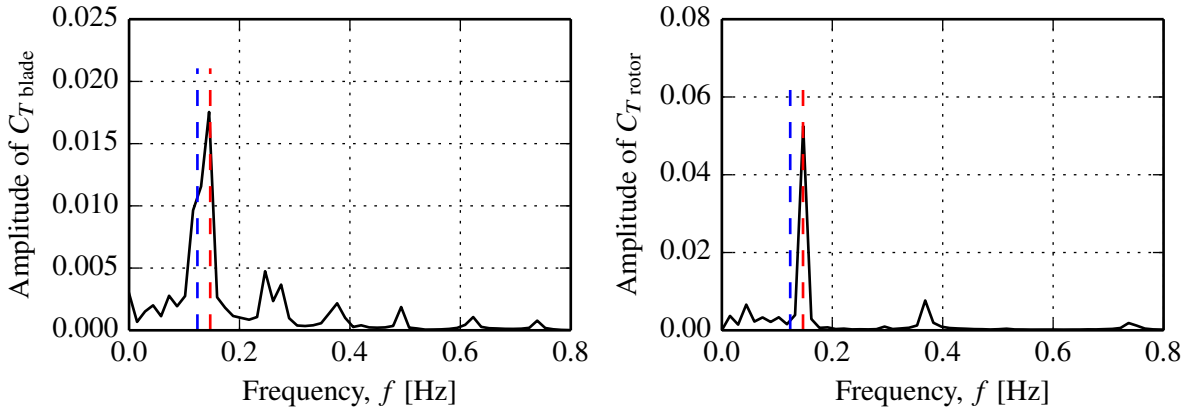

(a) (b)

Figure 49: Thrust spectra; (a) blade, (b) rotor. Blue - rotor frequency, red - wave frequency. Long wave case, λ = 3.5.

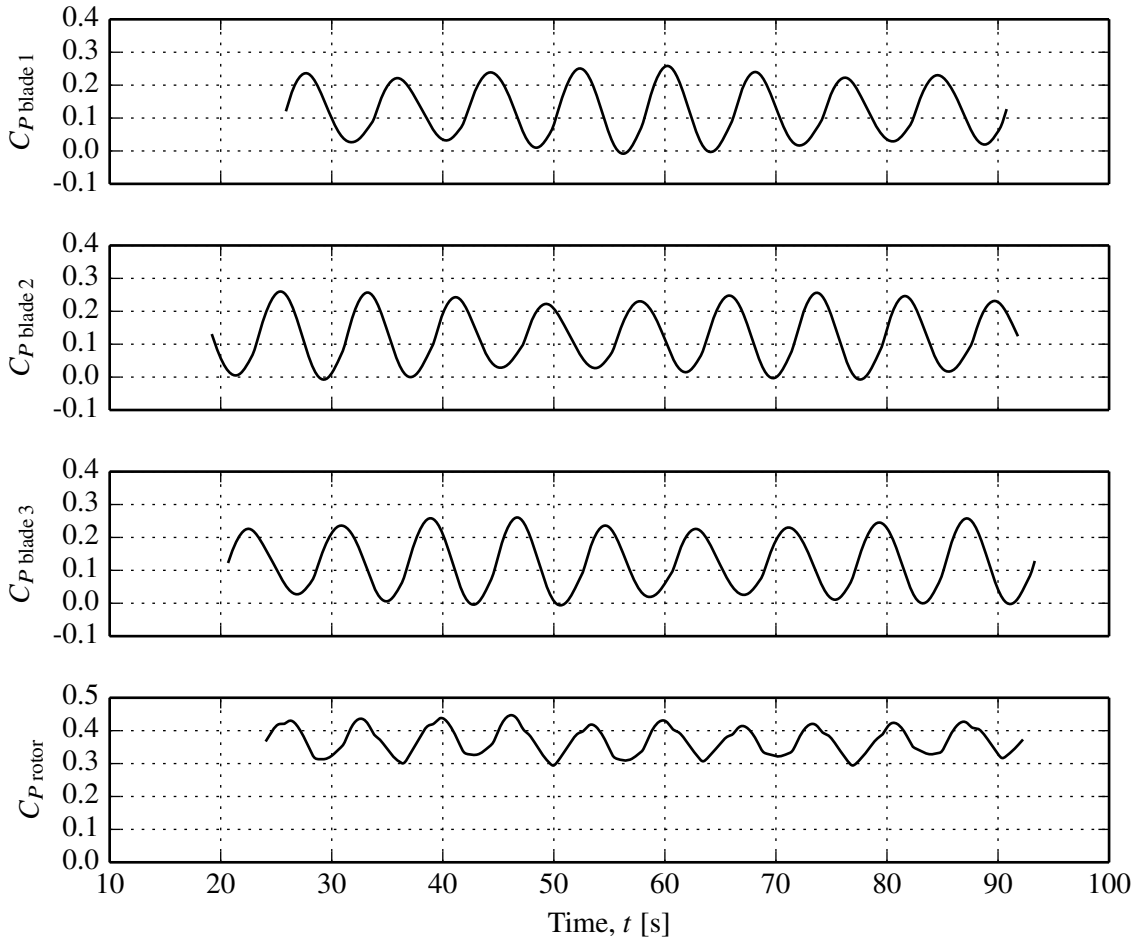

Figure 50: Blade and rotor power histories. Long wave case, λ = 3.5.

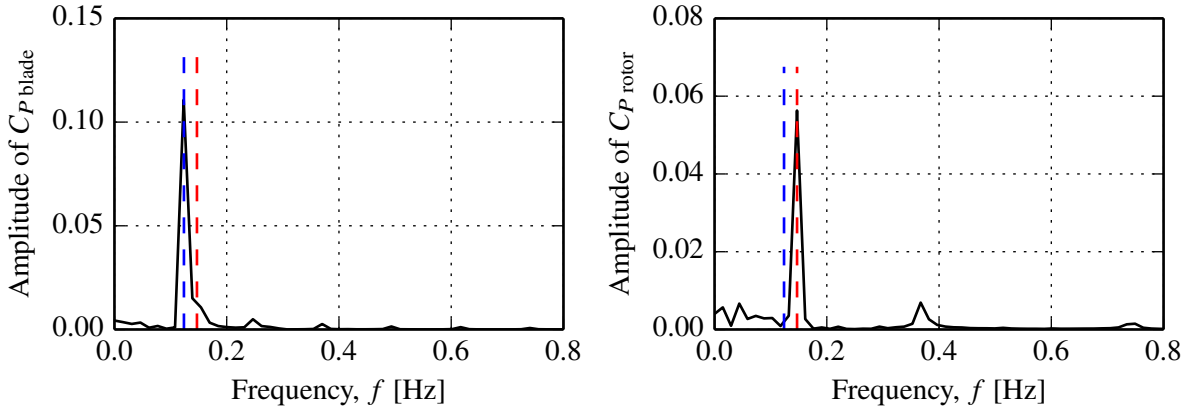

(a) (b)

Figure 51: Power spectra; (a) blade, (b) rotor. Blue - rotor frequency, red - wave frequency. Long wave case, λ = 3.5.

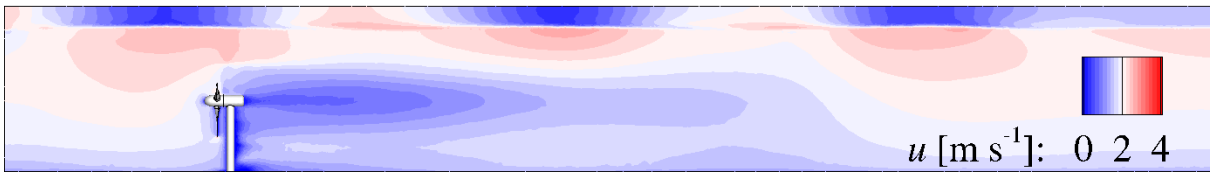

Figure 52: Centre plane velocity field. Long wave case, λ = 3.5.

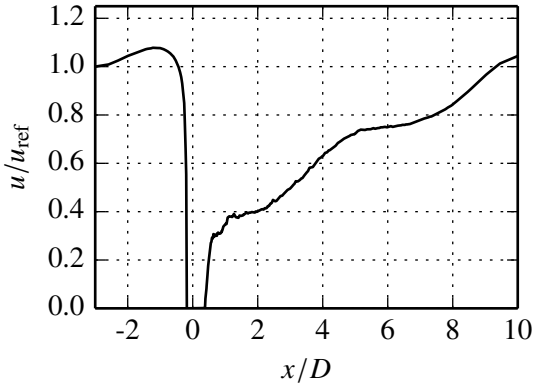

Figure 53: Centre-line streamwise velocity component. Long wave case, λ = 3.5.

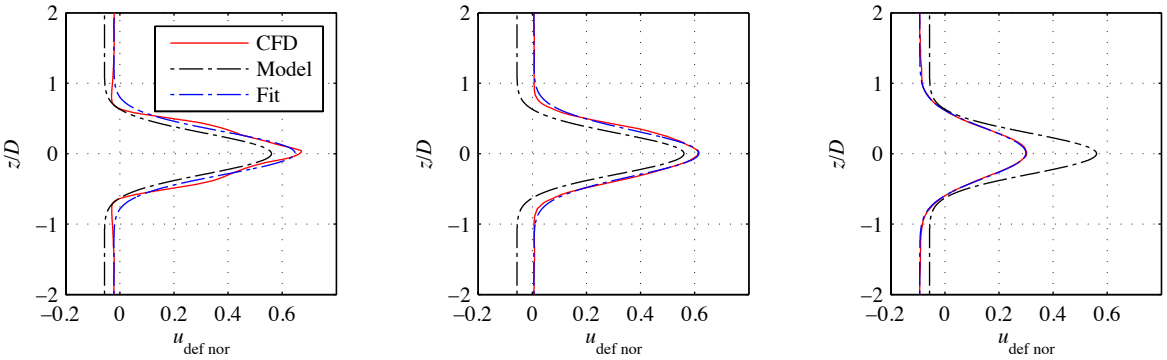

Figure 54: Parametric model of wake velocity deficit (Left to right, x =1D, 2D, 5D). Long wave case, λ = 3.5.

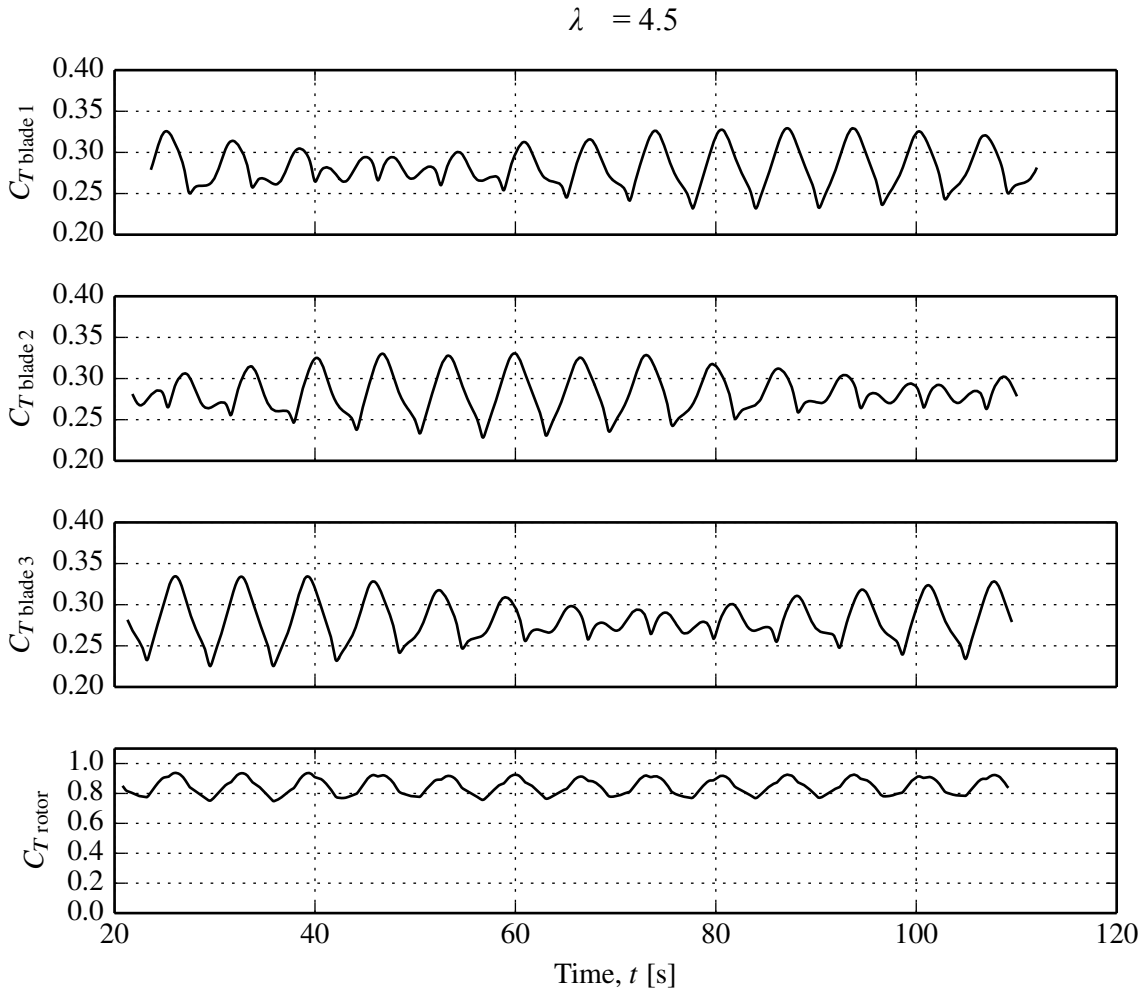

Figure 55: Blade and rotor load histories. Long wave case, λ = 4.5.

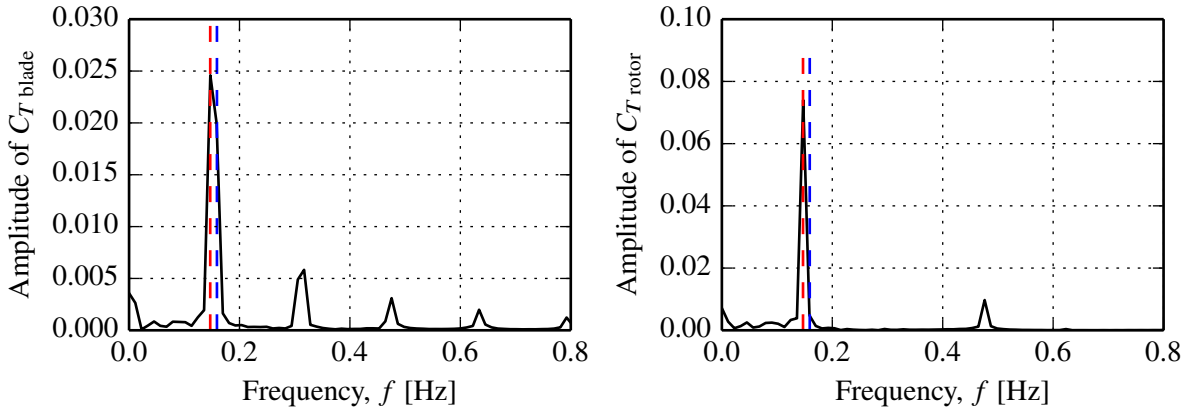

(a) Blade (b) Rotor

Figure 56: Thrust spectra; (a) blade, (b) rotor. Blue - rotor frequency, red - wave frequency. Long wave case, λ = 4.5.

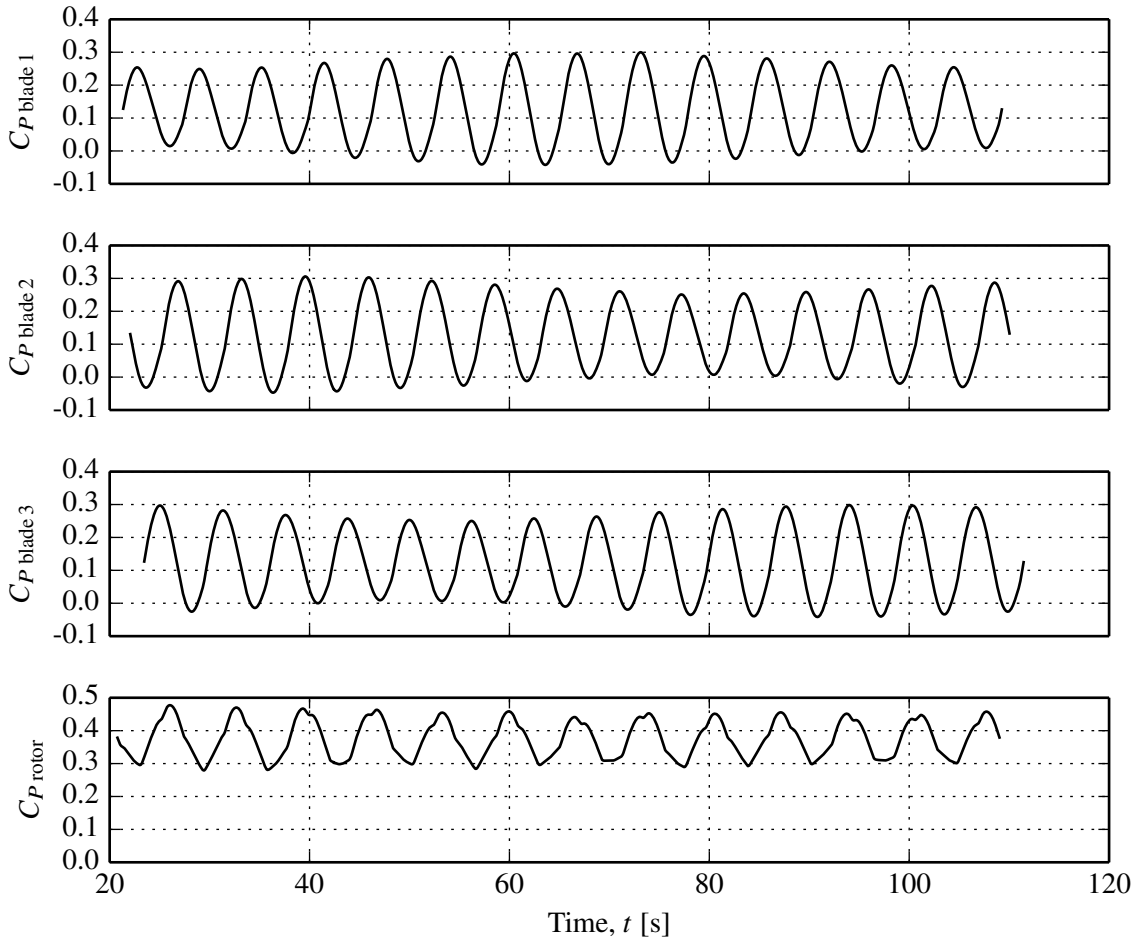

Figure 57: Blade and rotor power histories. Long wave case, λ = 4.5.

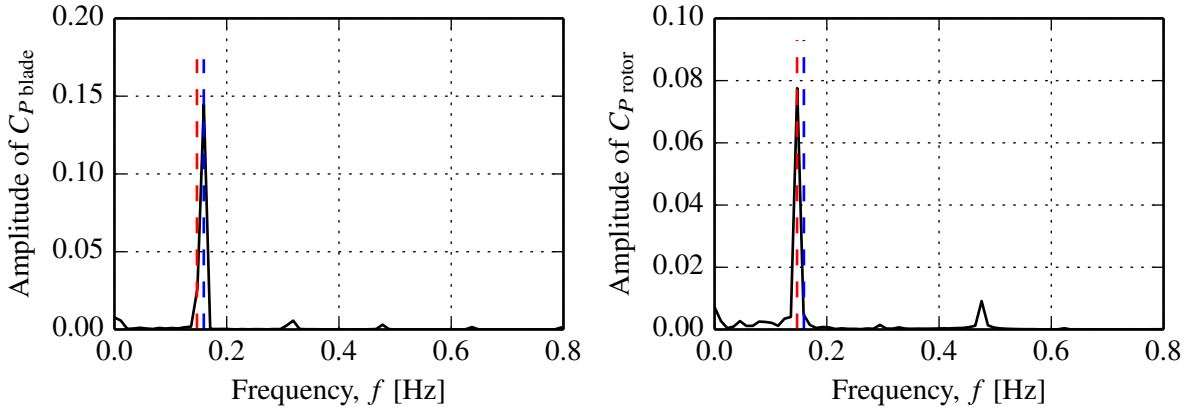

(a) (b)

Figure 58: Power spectra; (a) blade, (b) rotor. Blue - rotor frequency, red - wave frequency. Long wave case, λ = 4.5.

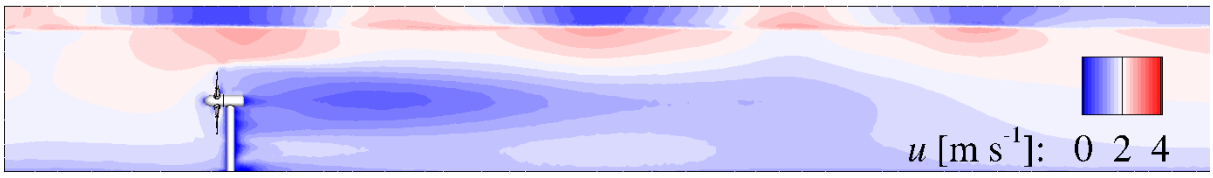

Figure 59: Centre plane velocity field. Long wave case, λ = 4.5.

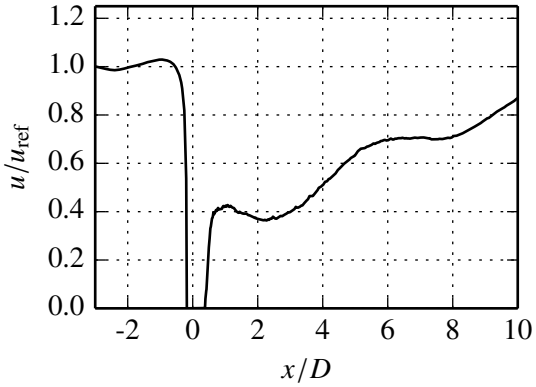

Figure 60: Centre-line streamwise velocity component. Long wave case, λ = 4.5.

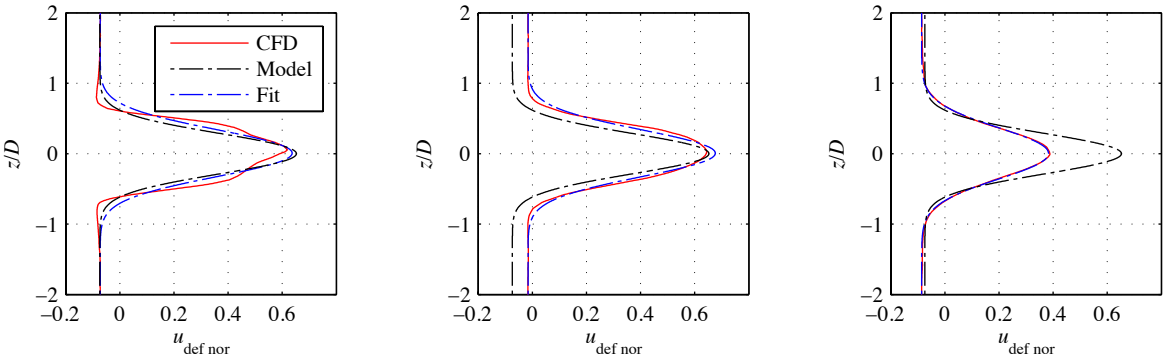

Figure 61: Parametric model of wake velocity deficit (Left to right, x =1D, 2D, 5D). Long wave case, λ = 4.5.

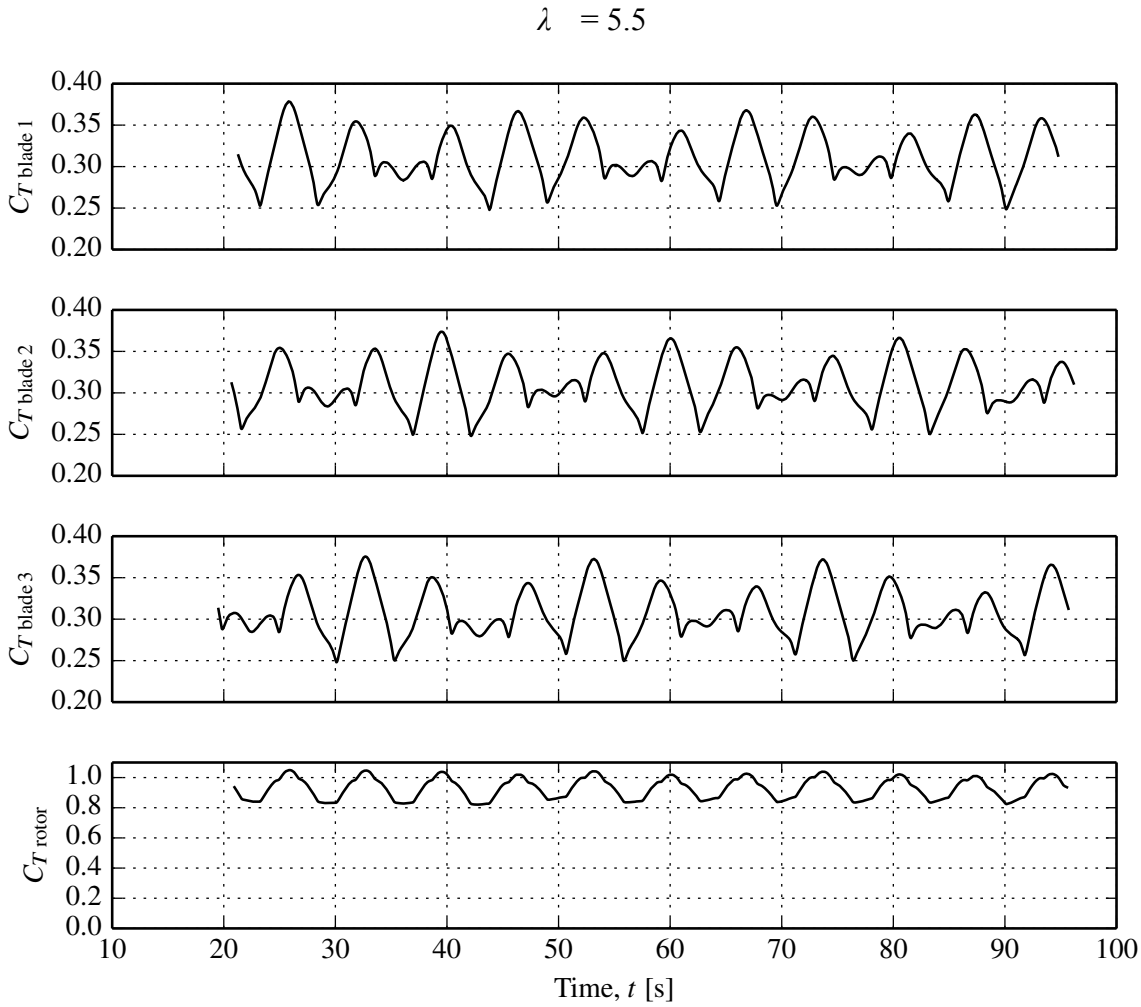

Figure 62: Blade and rotor load histories. Long wave case, λ = 5.5.

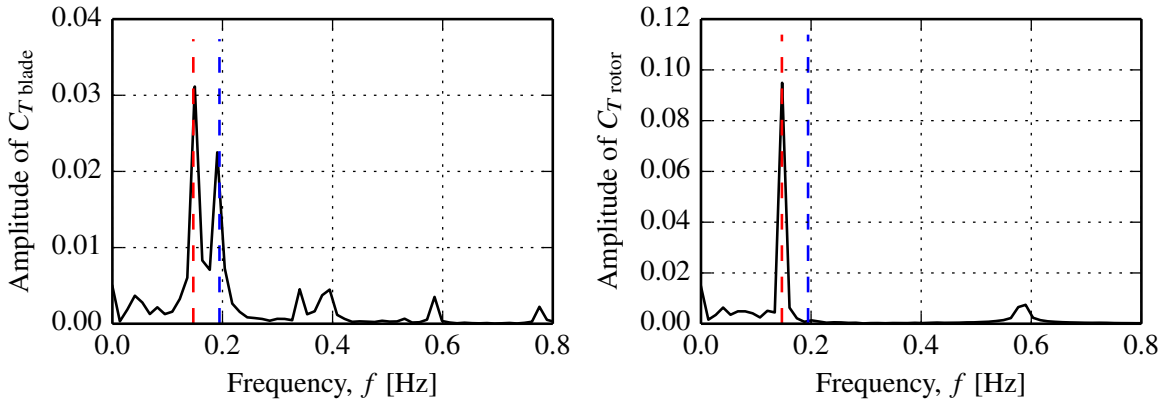

Figure 63: Thrust spectra; (a) blade, (b) rotor. Blue - rotor frequency, red - wave frequency. Long wave case, λ = 5.5.

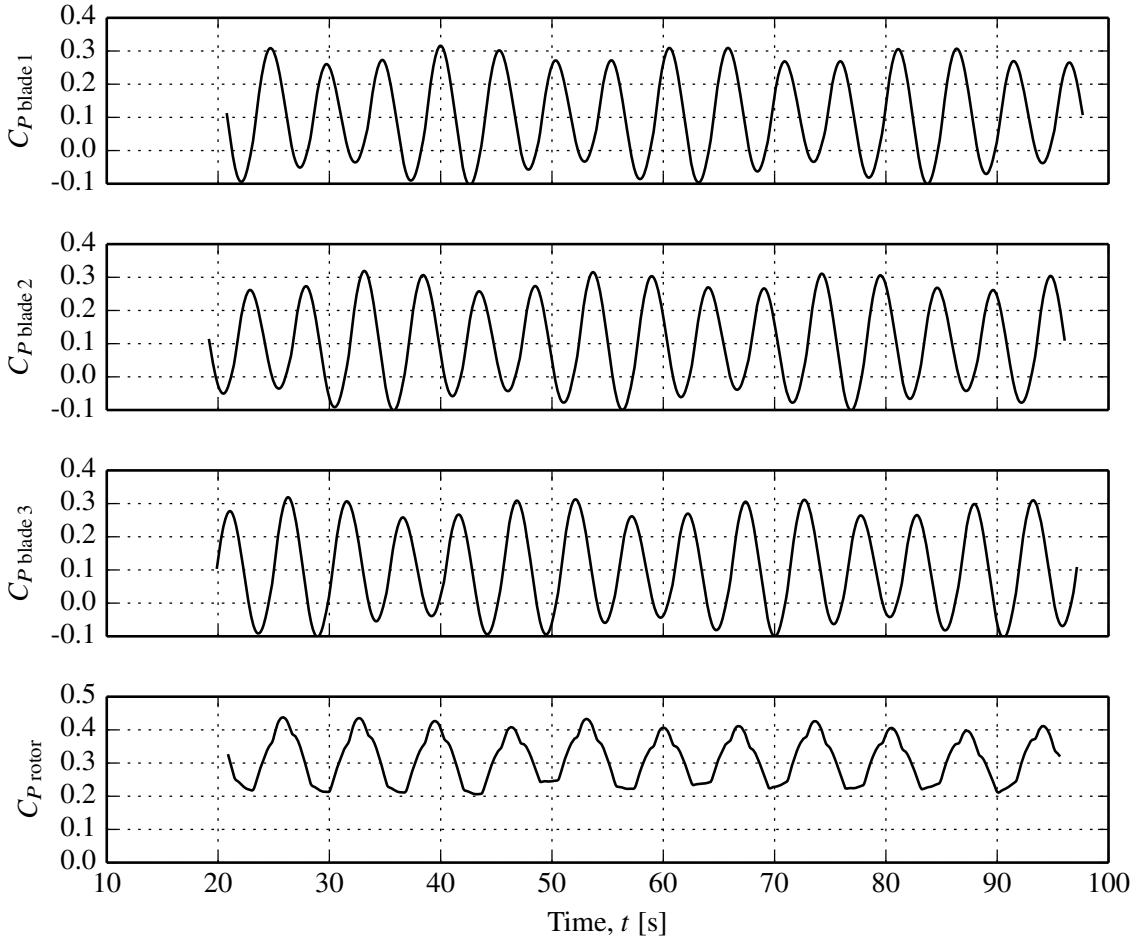

Figure 64: Blade and rotor power histories. Long wave case, λ = 5.5.

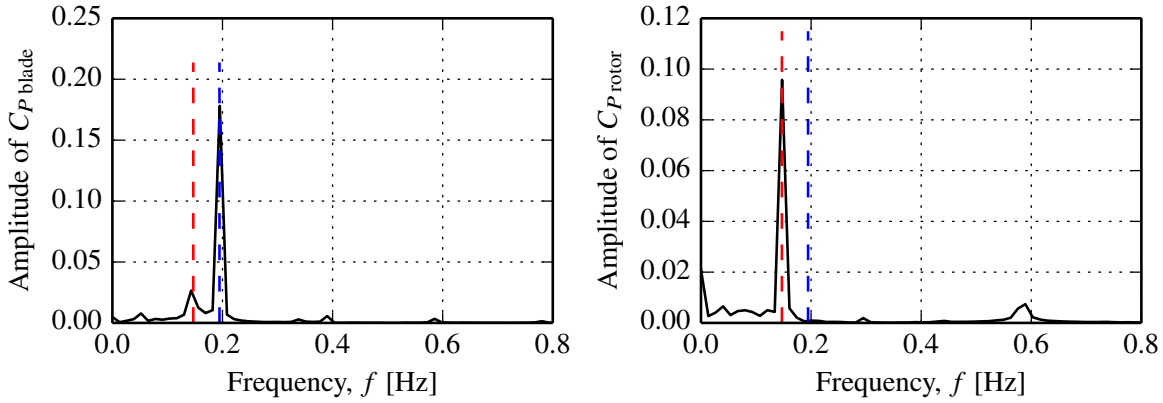

(a) (b)

Figure 65: Power spectra; (a) blade, (b) rotor. Blue - rotor frequency, red - wave frequency. Long wave case, λ = 5.5.

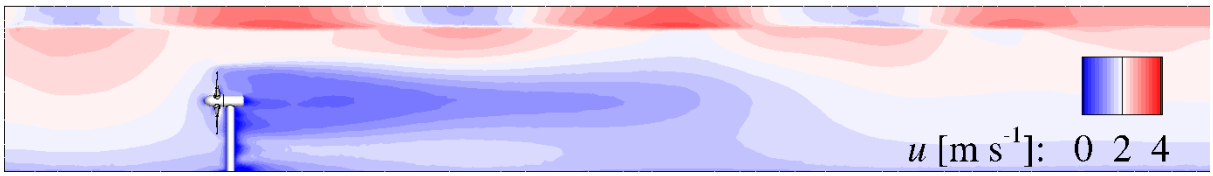

Figure 66: Centre plane velocity field. Long wave case, λ = 5.5.

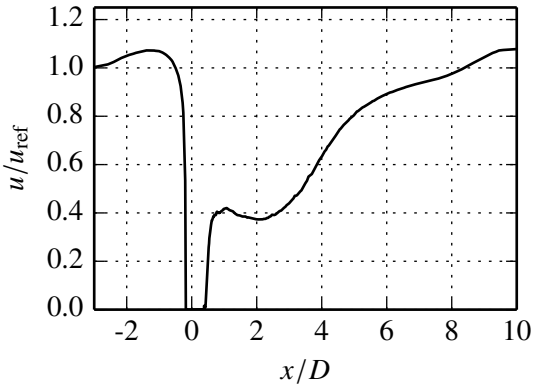

Figure 67: Centre-line streamwise velocity component. Long wave case, λ = 5.5.

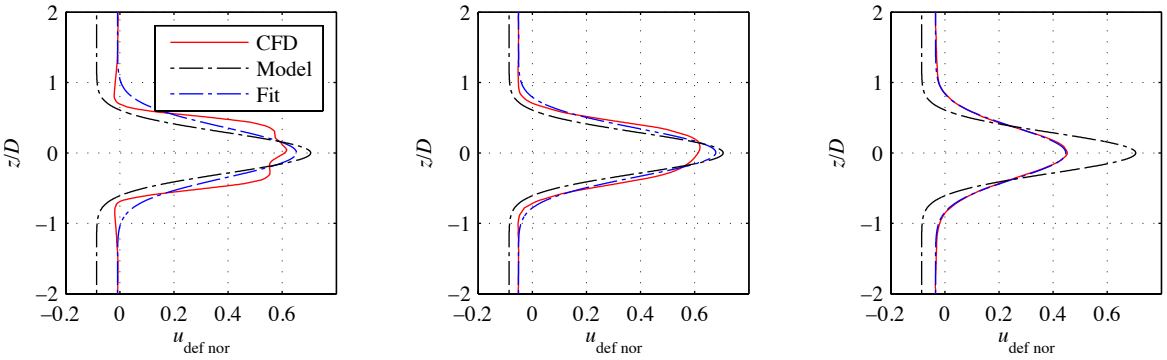

Figure 68: Parametric model of wake velocity deficit (Left to right, x =1D, 2D, 5D). Long wave case, λ = 5.5.

10.3 Case 3 - High wave case

10.3.1 Details

λ_w	55 m
H_w	2 m
ϕ_w	0°

10.3.2 Performance

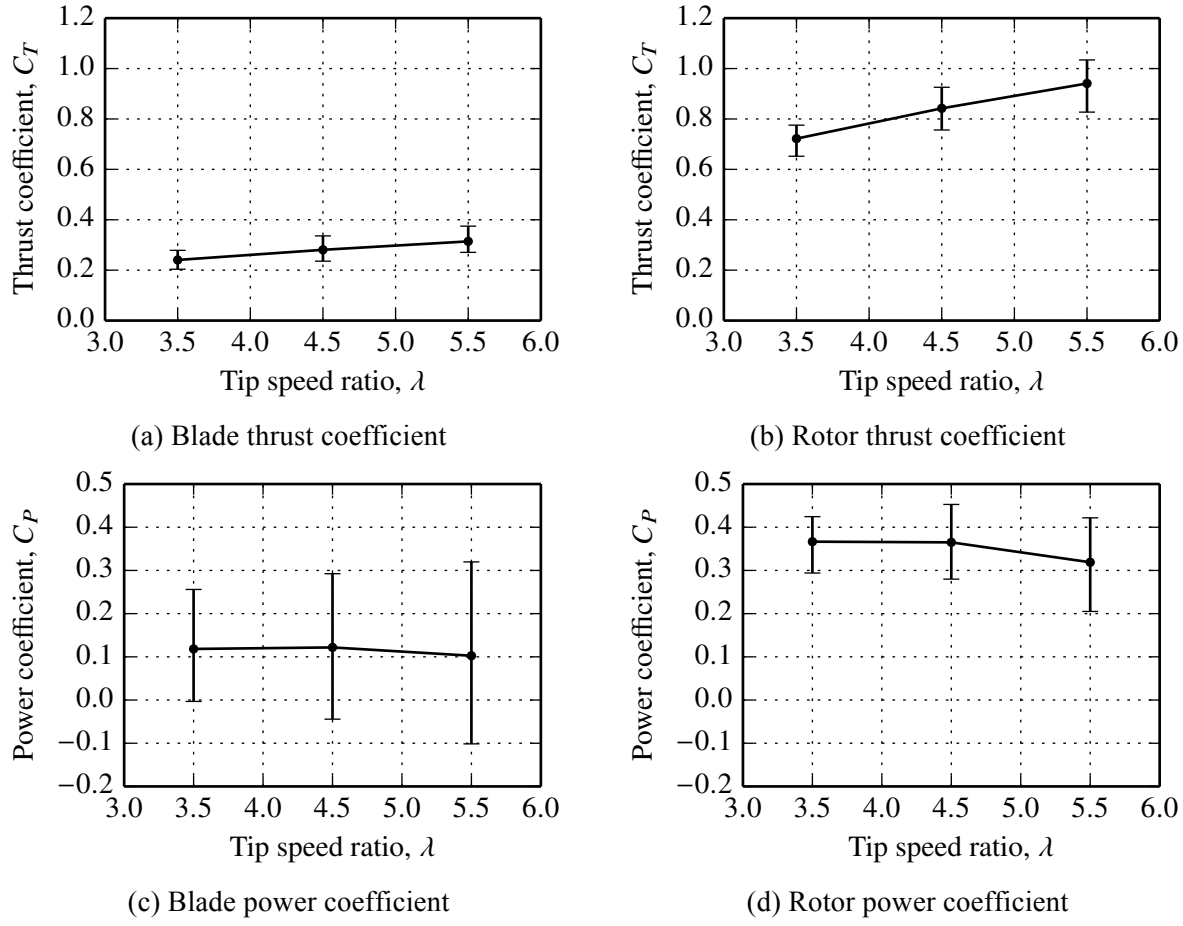

(a) Blade thrust coefficient

(b) Rotor thrust coefficient

(c) Blade power coefficient

(d) Rotor power coefficient

Figure 69: Blade and rotor thrust and power coefficients for the high wave case. Time mean values are displayed as points and vertical bars represent the range of the computed quantity.

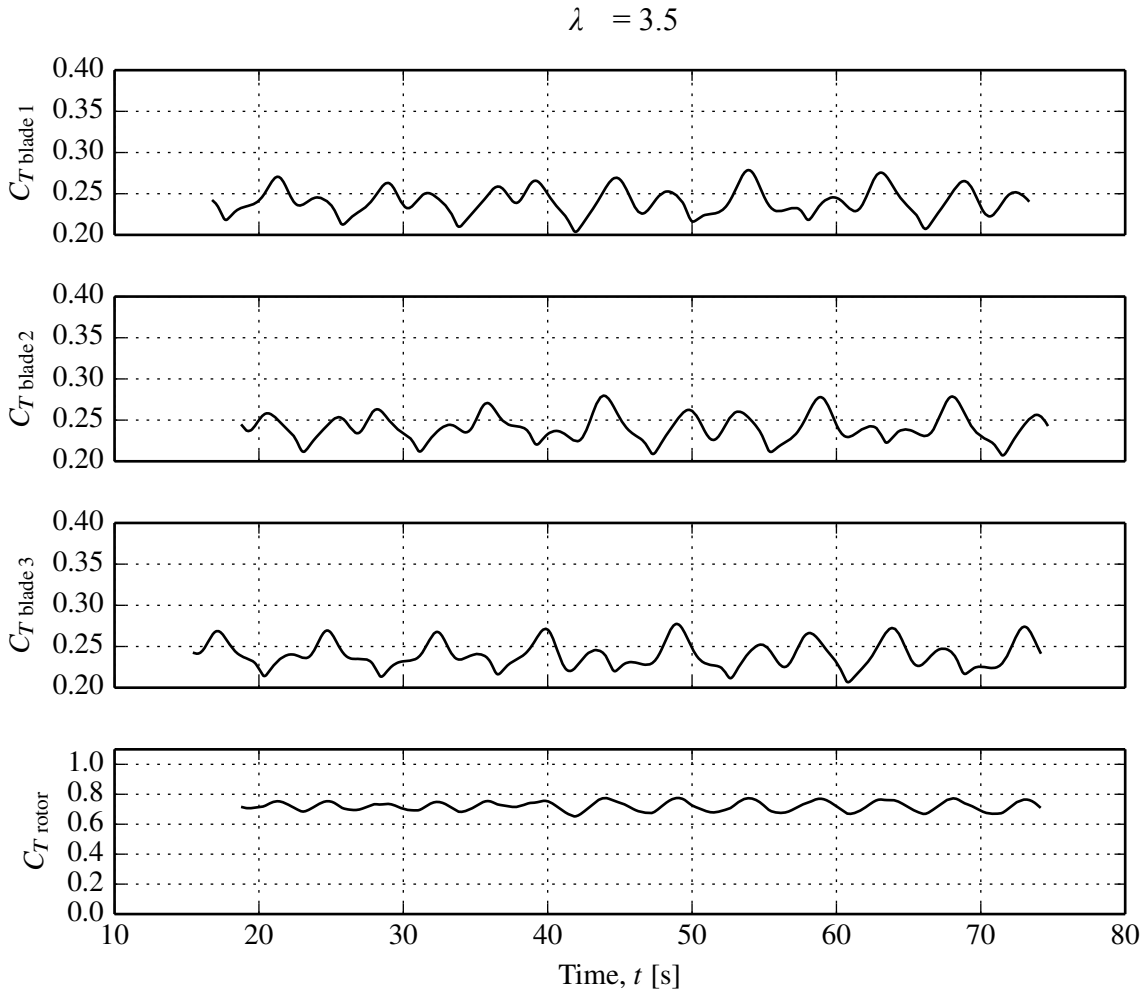

Figure 70: Blade and rotor load histories. High wave case, λ = 3.5.

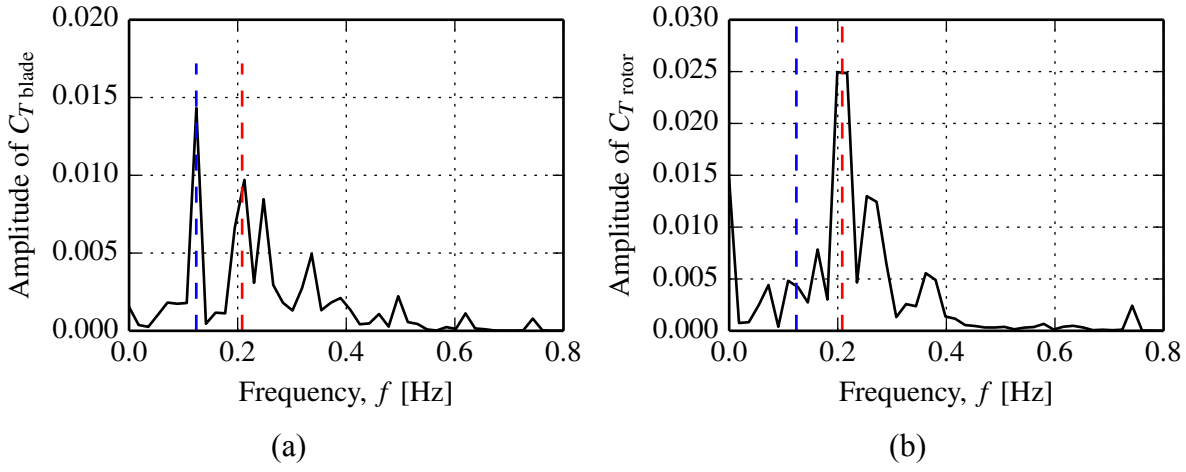

Figure 71: Thrust spectra; (a) blade, (b) rotor. Blue - rotor frequency, red - wave frequency. High wave case, λ = 3.5.

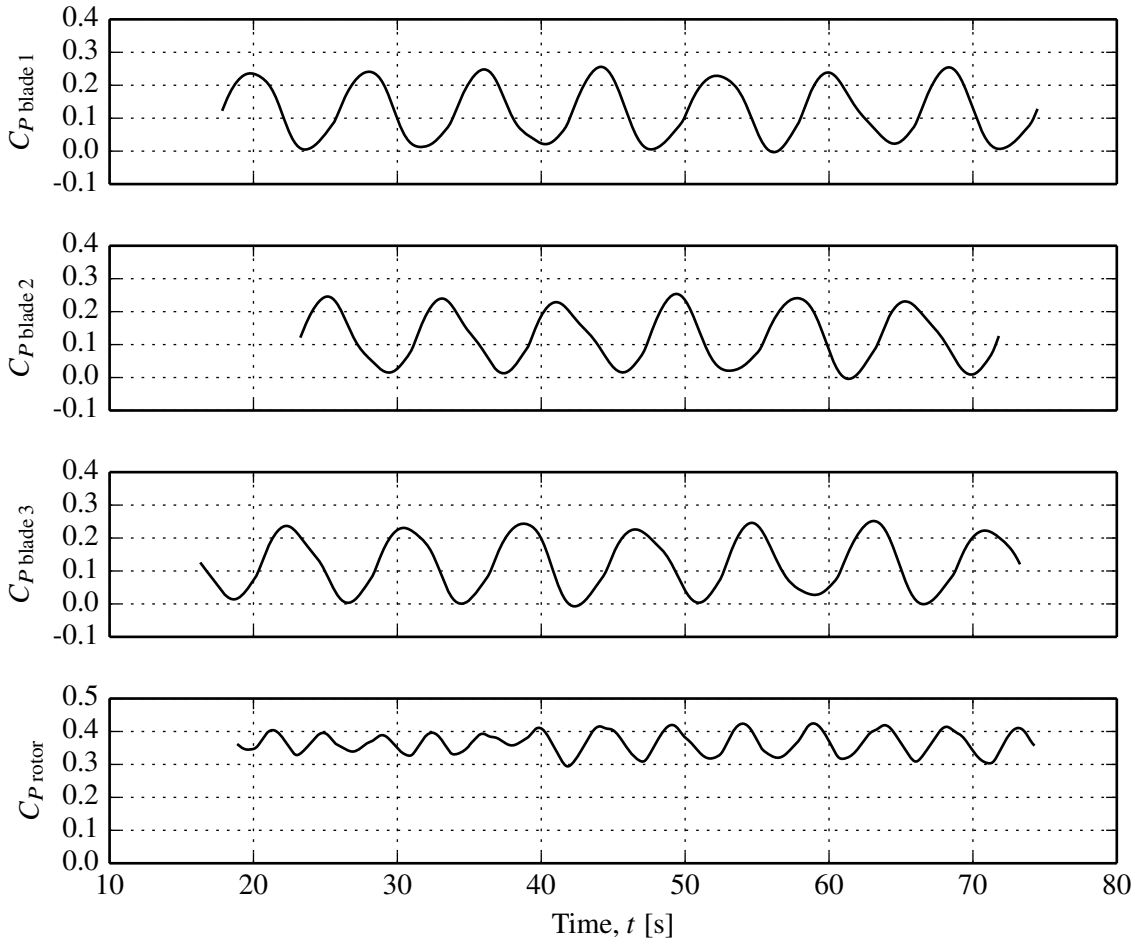

Figure 72: Blade and rotor power histories. High wave case, λ = 3.5.

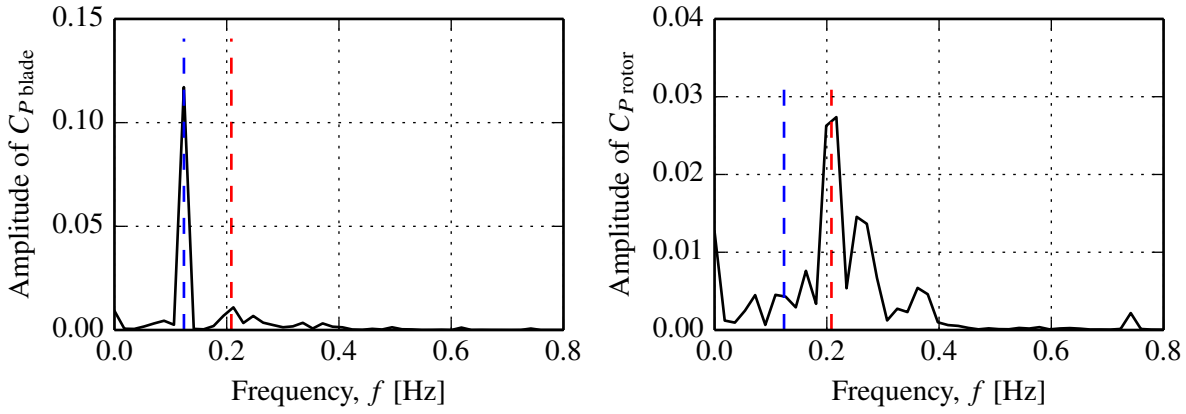

(a) (b)

Figure 73: Power spectra; (a) blade, (b) rotor. Blue - rotor frequency, red - wave frequency. High wave case, λ = 3.5.

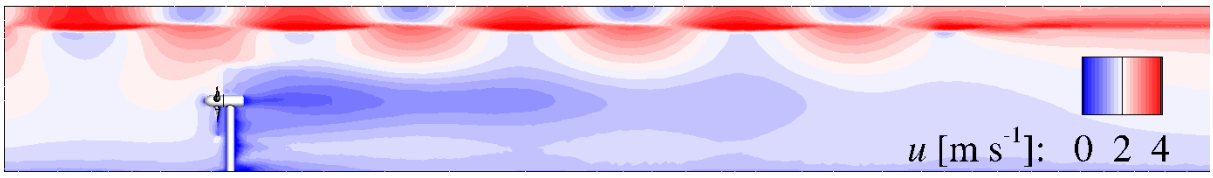

Figure 74: Centre plane velocity field. High wave case, λ = 3.5.

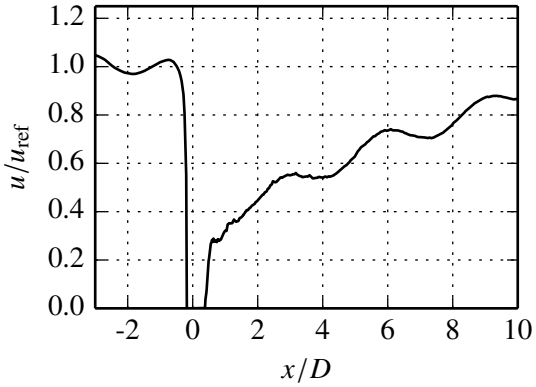

Figure 75: Centre-line streamwise velocity component. High wave case, λ = 3.5.

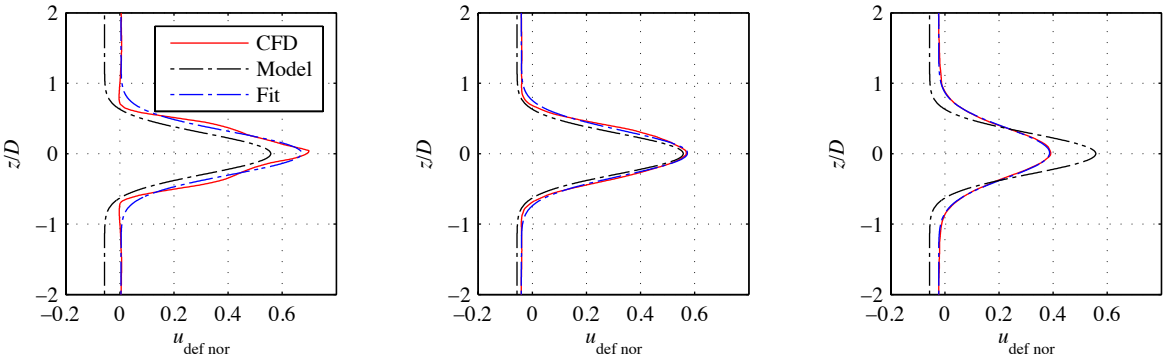

Figure 76: Parametric model of wake velocity deficit (Left to right, x =1D, 2D, 5D). High wave case, λ = 3.5.

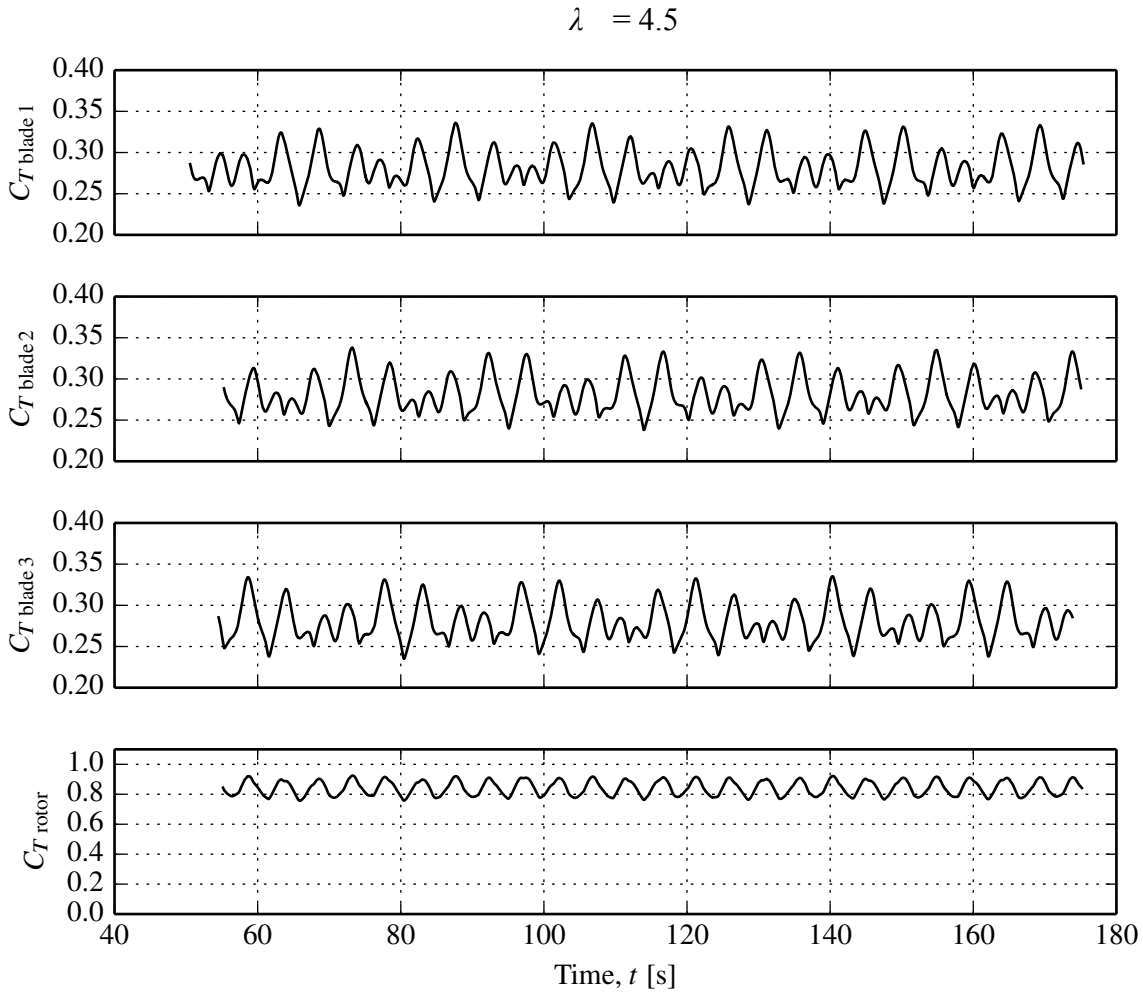

Figure 77: Blade and rotor load histories. High wave case, λ = 4.5.

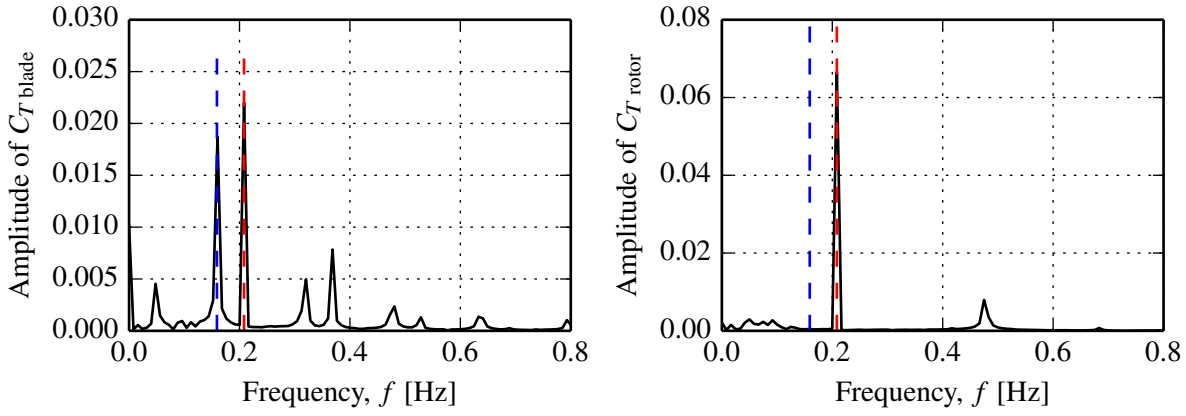

(a) (b)

Figure 78: Thrust spectra; (a) blade, (b) rotor. Blue - rotor frequency, red - wave frequency. High wave case, λ = 4.5.

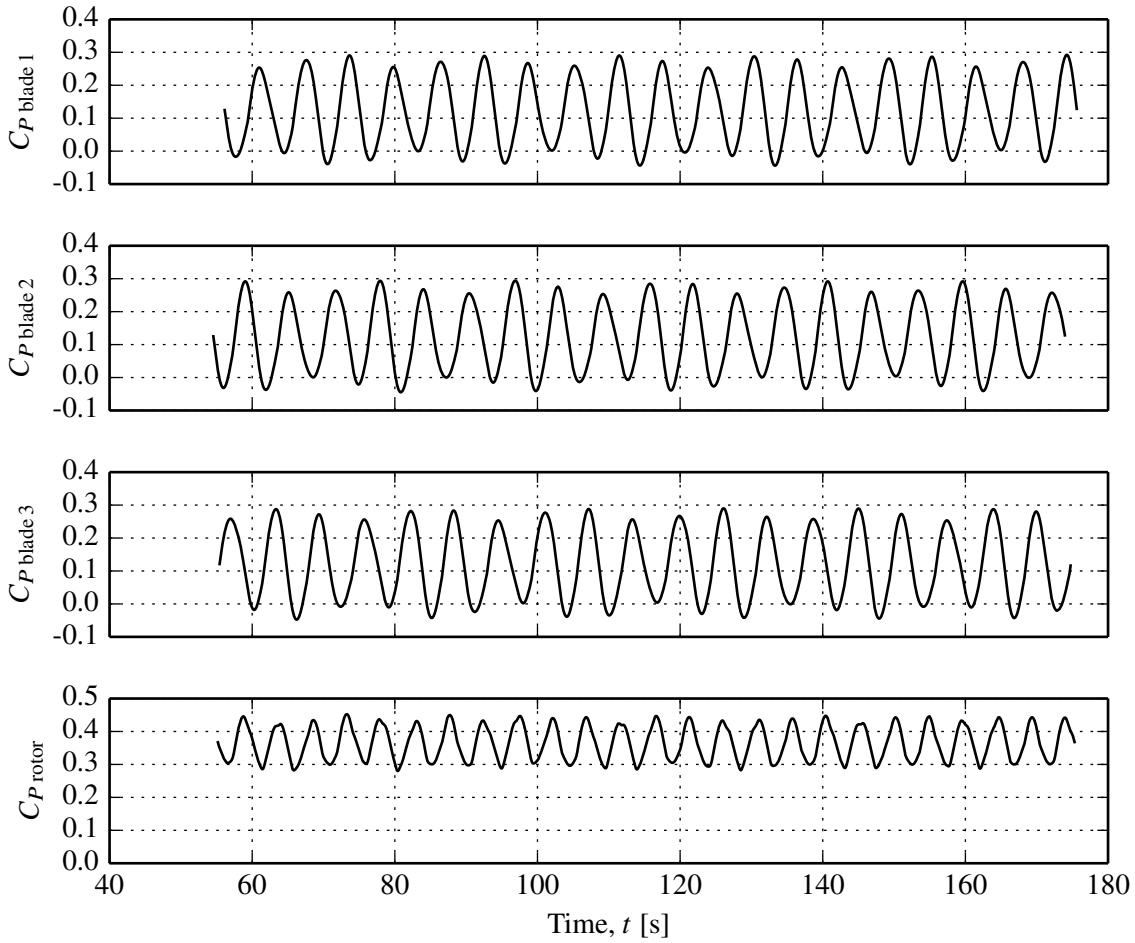

Figure 79: Blade and rotor power histories. High wave case, λ = 4.5.

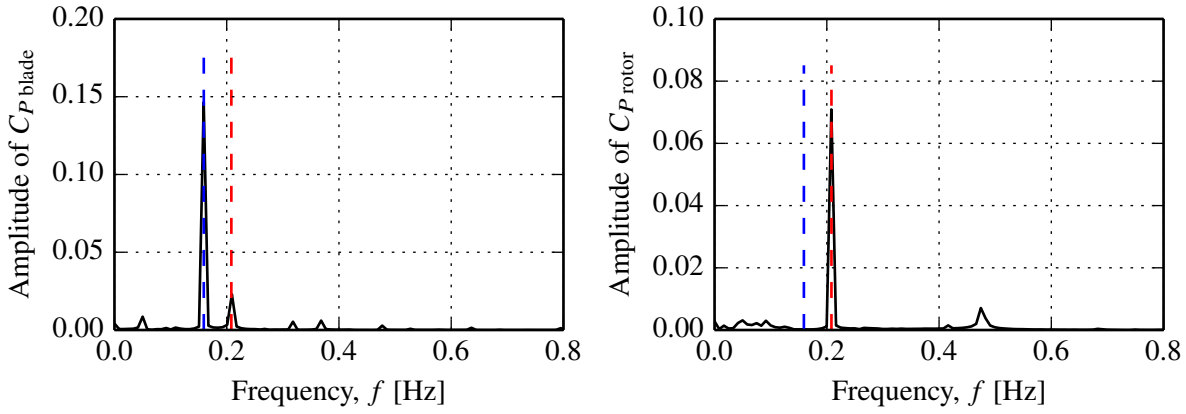

(a) (b)

Figure 80: Power spectra; (a) blade, (b) rotor. Blue - rotor frequency, red - wave frequency. High wave case, λ = 4.5.

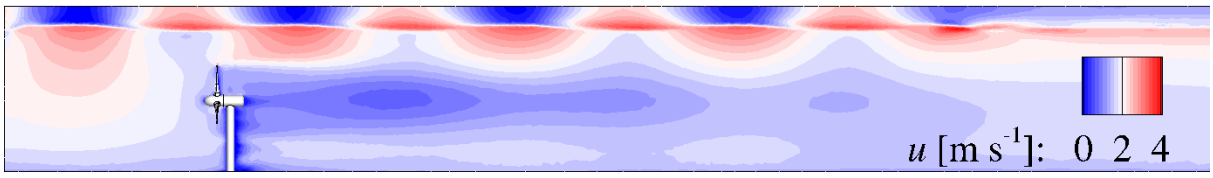

Figure 81: Centre plane velocity field. High wave case, λ = 4.5.

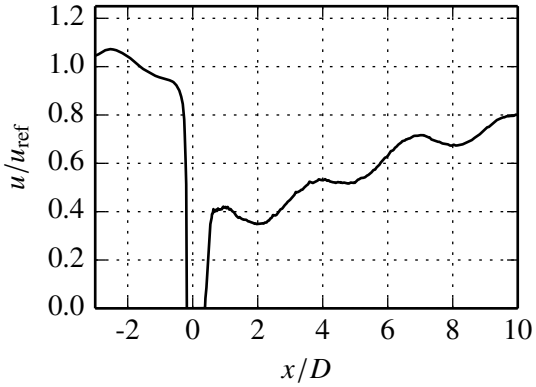

Figure 82: Centre-line streamwise velocity component. High wave case, λ = 4.5.

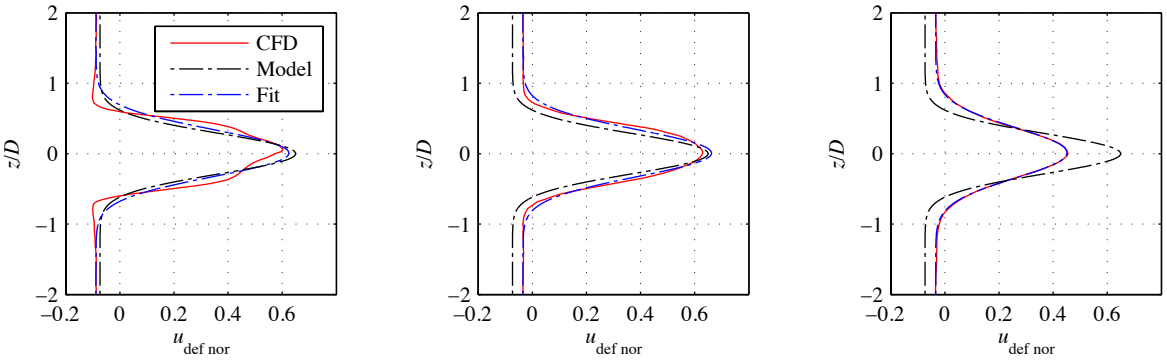

Figure 83: Parametric model of wake velocity deficit (Left to right, x =1D, 2D, 5D). High wave case, λ = 4.5.

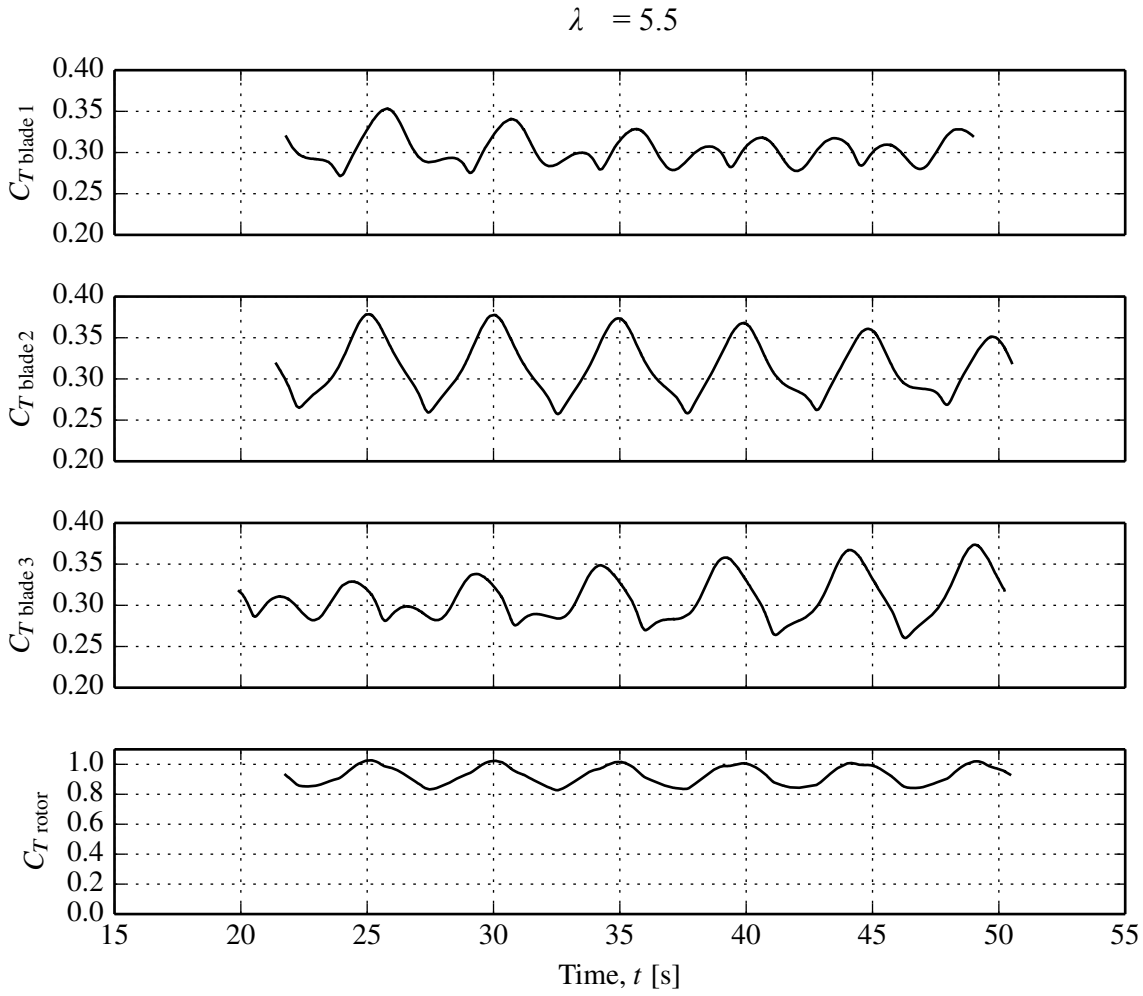

Figure 84: Blade and rotor load histories. High wave case, λ = 5.5.

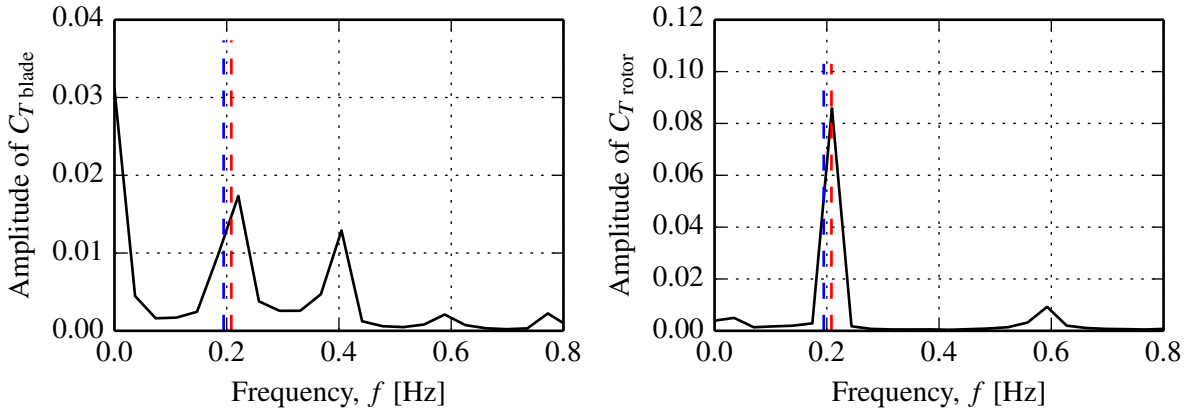

(a) (b)

Figure 85: Thrust spectra; (a) blade, (b) rotor. Blue - rotor frequency, red - wave frequency. High wave case, λ = 5.5.

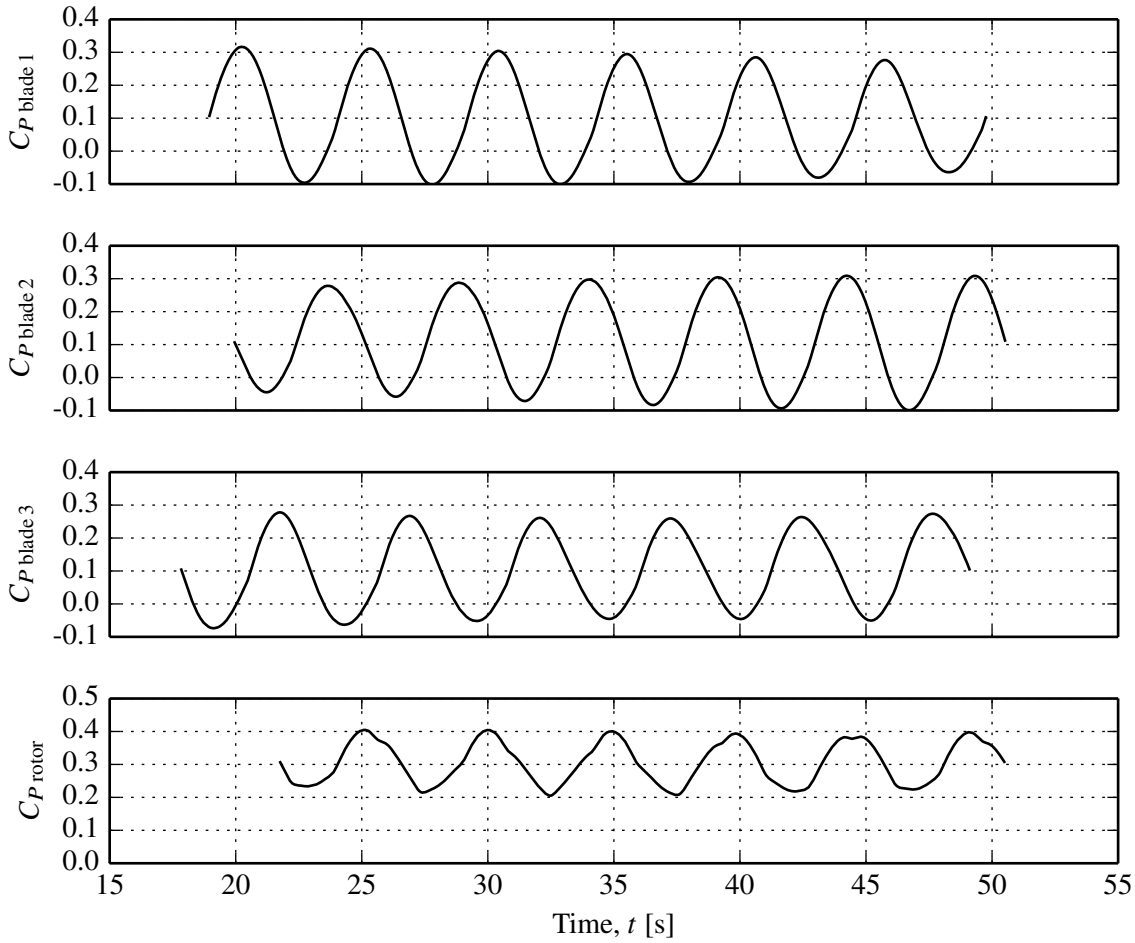

Figure 86: Blade and rotor power histories. High wave case, λ = 5.5.

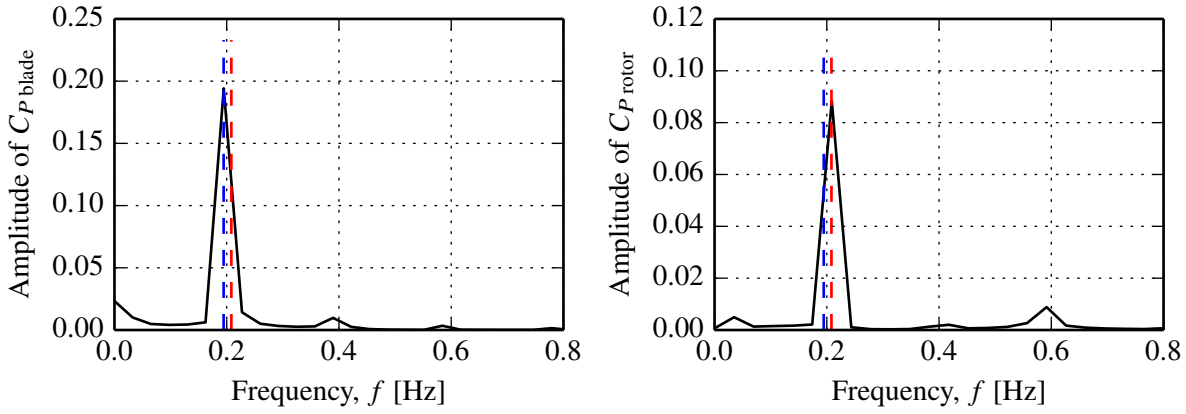

(a) (b)

Figure 87: Power spectra; (a) blade, (b) rotor. Blue - rotor frequency, red - wave frequency. High wave case, λ = 5.5.

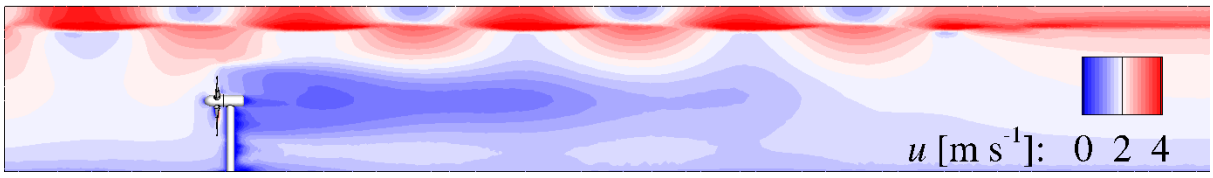

Figure 88: Centre plane velocity field. High wave case, λ = 5.5.

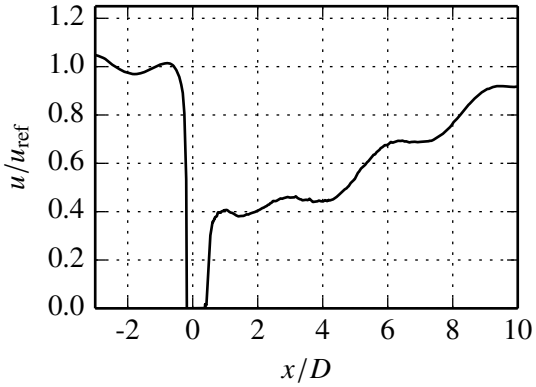

Figure 89: Centre-line streamwise velocity component. High wave case, λ = 5.5.

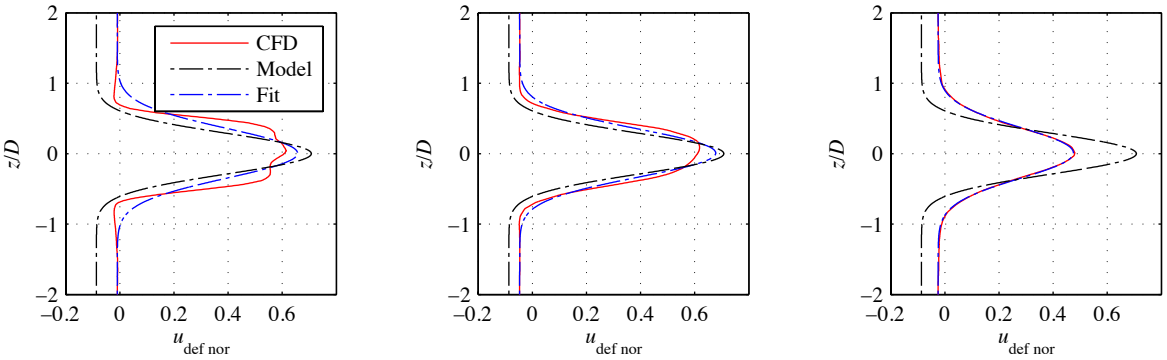

Figure 90: Parametric model of wake velocity deficit (Left to right, x =1D, 2D, 5D). High wave case, λ = 5.5.

10.4 Case 4 - Oblique wave case

10.4.1 Details

λ_w	55 m
H_w	1 m
ϕ_w	30˚

10.4.2 Performance

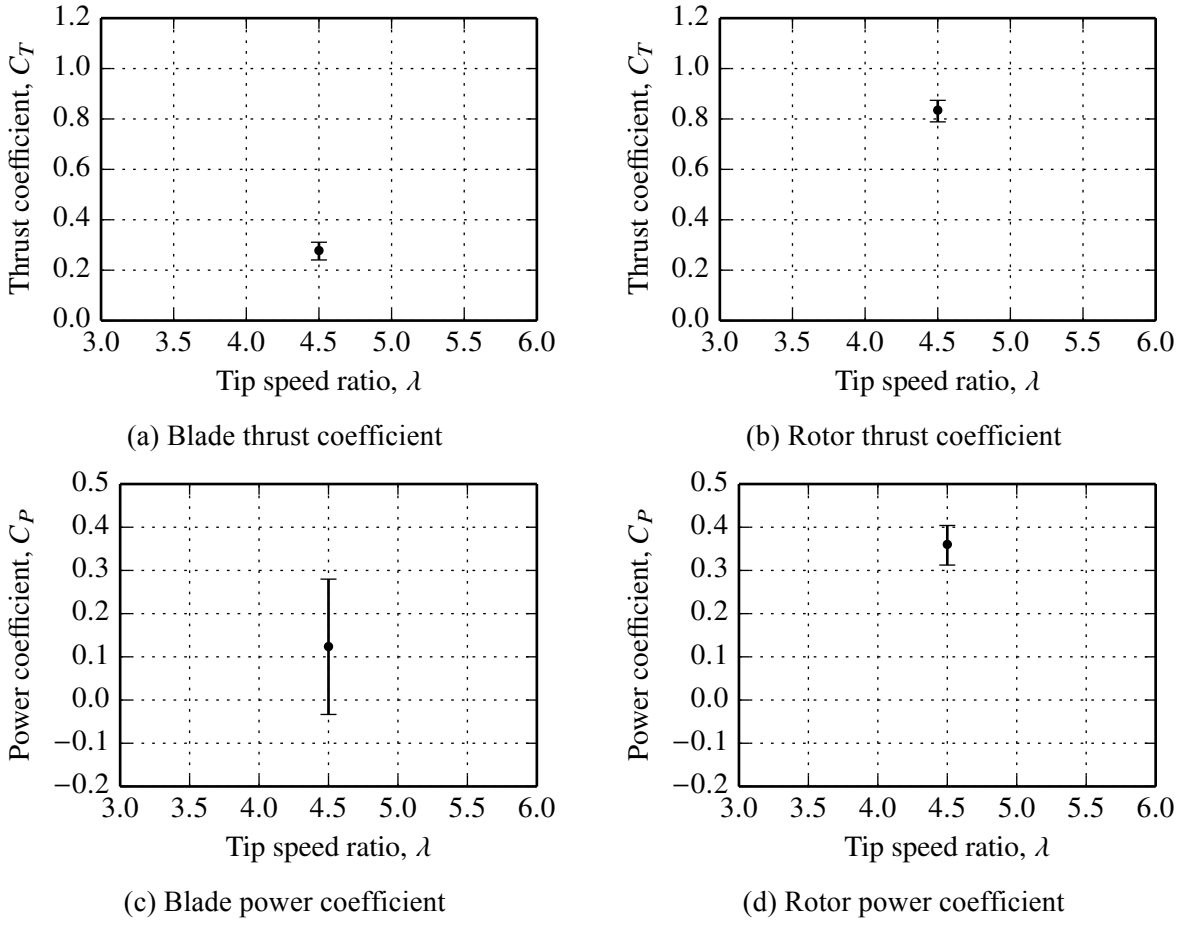

(a) Blade thrust coefficient

(b) Rotor thrust coefficient

(c) Blade power coefficient

(d) Rotor power coefficient

Figure 91: Blade and rotor thrust and power coefficients for the oblique wave case. Time mean values are displayed as points and vertical bars represent the range of the computed quantity.

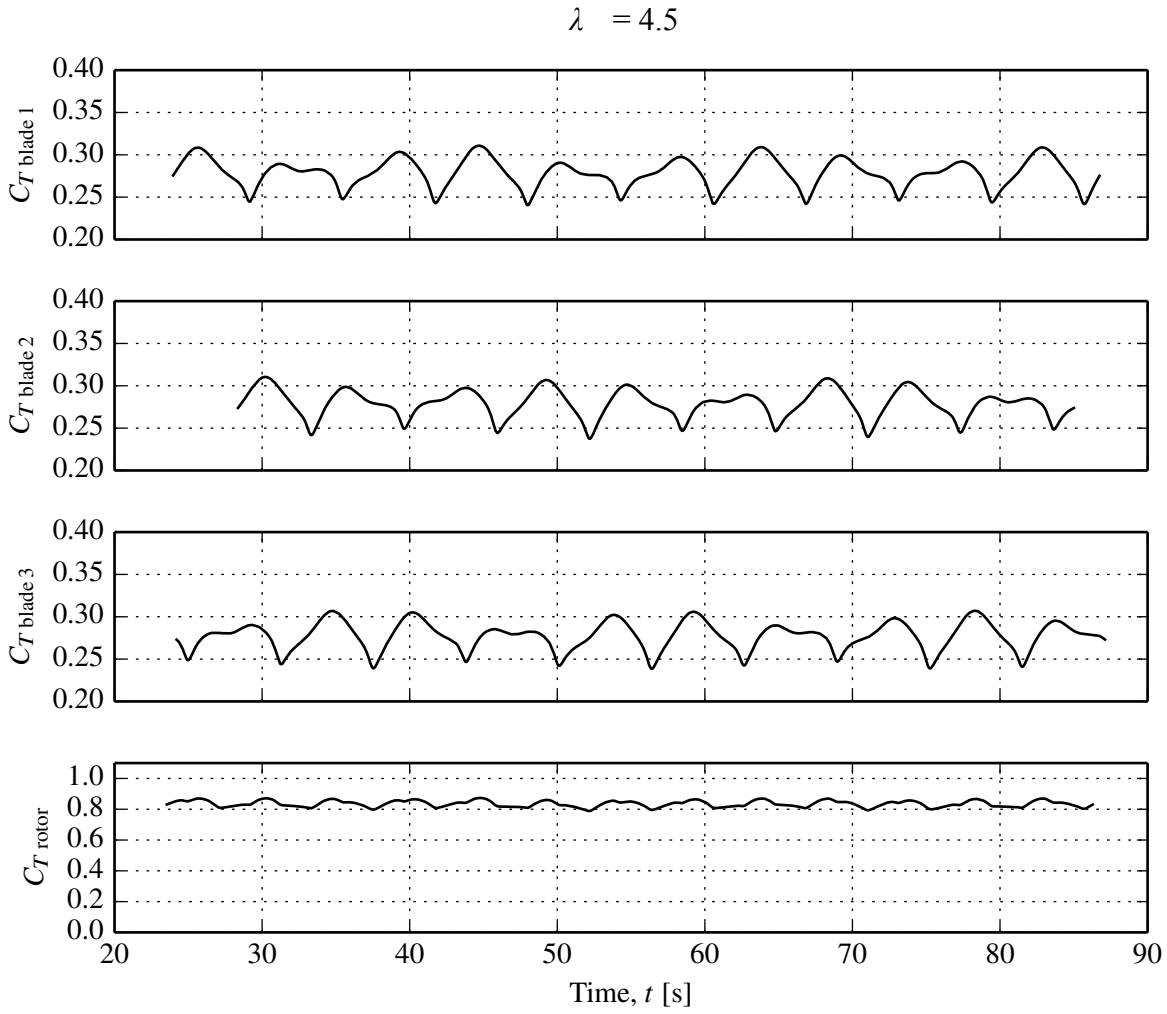

Figure 92: Blade and rotor load histories. Oblique wave case, λ = 4.5.

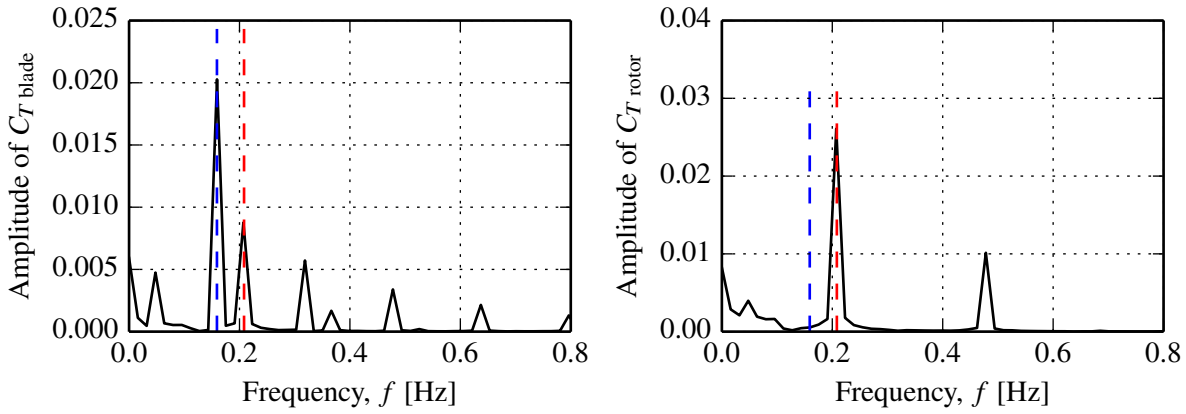

(a) (b)

Figure 93: Thrust spectra; (a) blade, (b) rotor. Blue - rotor frequency, red - wave frequency. Oblique wave case, λ = 4.5.

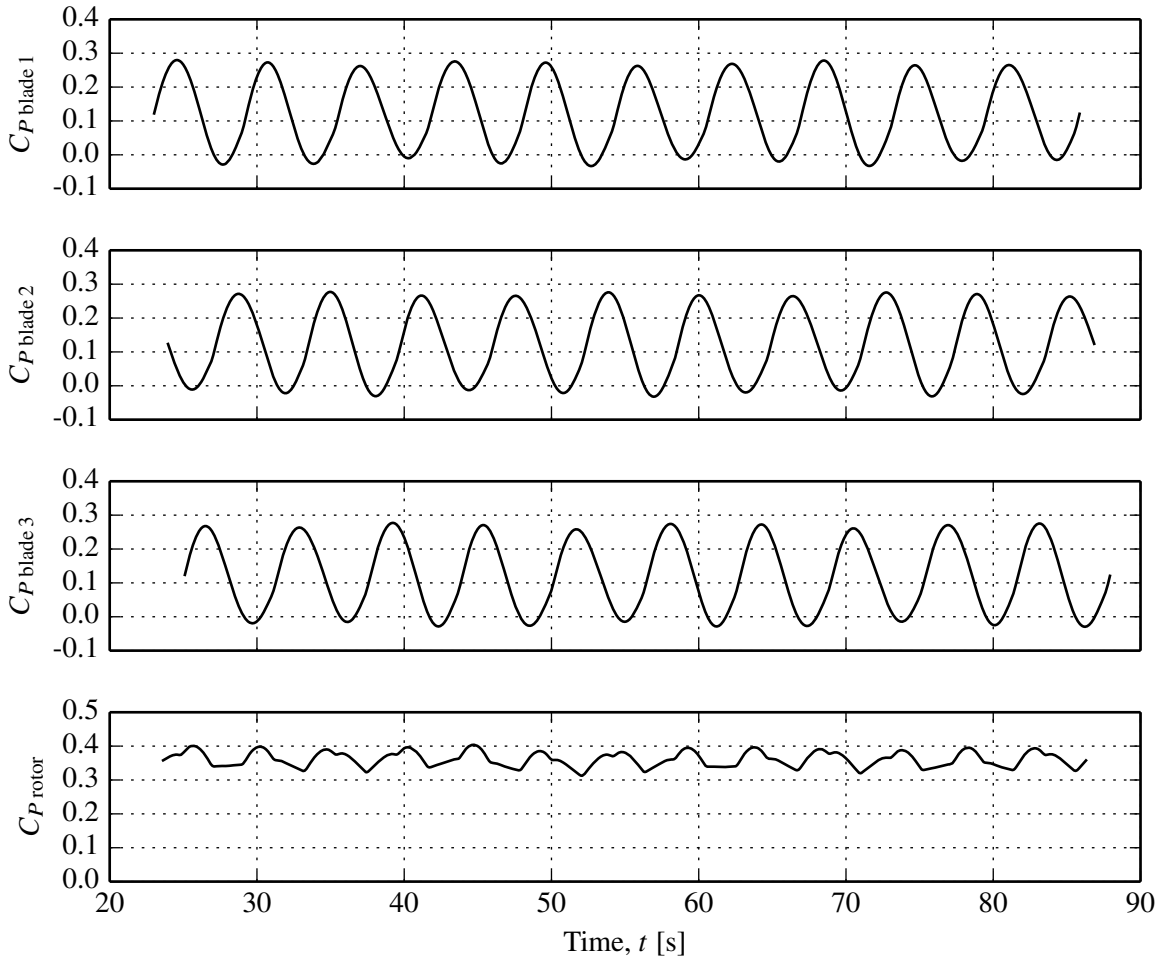

Figure 94: Blade and rotor power histories. Oblique wave case, λ = 4.5.

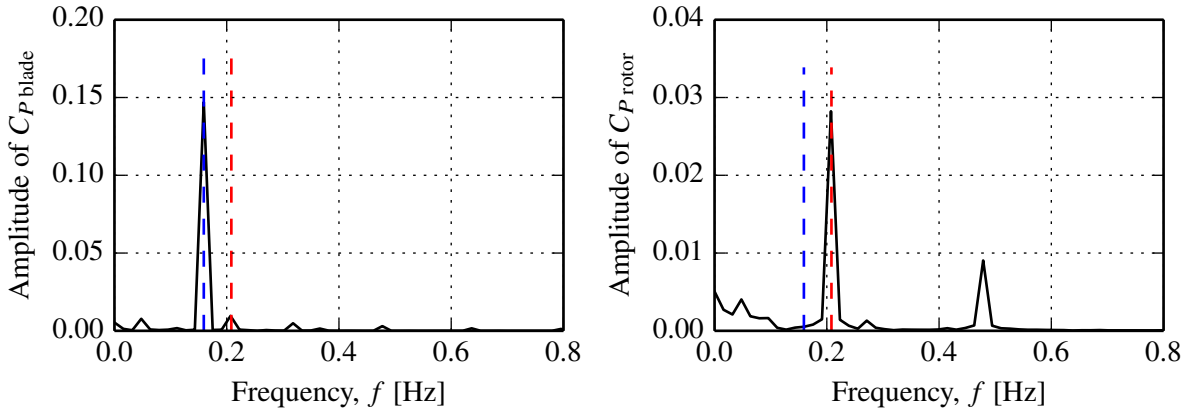

(a) (b)

Figure 95: Power spectra; (a) blade, (b) rotor. Blue - rotor frequency, red - wave frequency. Oblique wave case, λ = 4.5.

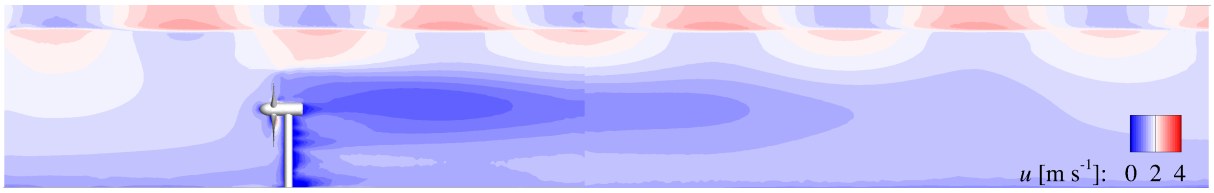

Figure 96: Centre plane velocity field. Oblique wave case, λ = 4.5.

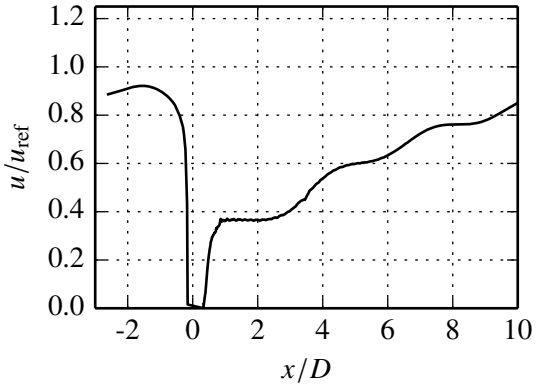

Figure 97: Centre-line streamwise velocity component. Oblique wave case, λ = 4.5.

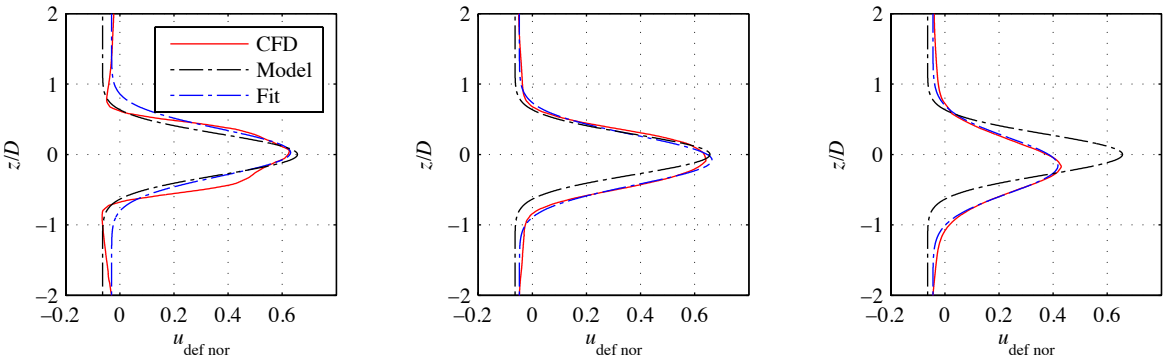

Figure 98: Parametric model of wake velocity deficit (Left to right, x =1D, 2D, 5D). Oblique wave case, λ = 4.5.